NAVAL POSTGRADUATE SCHOOL
Monterey, California

THESIS

A COMPUTATIONAL AND EXPERIMENTAL INVESTIGATION OF A FLUTTER GENERATOR

by

Scott T. Davids

June 1999

Thesis Advisor:	Kevin D. Jones
Co-Advisor:	Max F. Platzer

19990915 075

REPORT DOCUMENTATION PAGE

Form Approved
OMB No. 0704-0188

Public reporting burden for this collection of information is estimated to average 1 hour per response, including the time for reviewing instruction, searching existing data sources, gathering and maintaining the data needed, and completing and reviewing the collection of information. Send comments regarding this burden estimate or any other aspect of this collection of information, including suggestions for reducing this burden, to Washington headquarters Services, Directorate for Information Operations and Reports, 1215 Jefferson Davis Highway, Suite 1204, Arlington, VA 22202-4302, and to the Office of Management and Budget, Paperwork Reduction Project (0704-0188) Washington DC 20503.

1. AGENCY USE ONLY *(Leave blank)*	2. REPORT DATE June 1999	3. REPORT TYPE AND DATES COVERED Master's Thesis

4. TITLE AND SUBTITLE A COMPUTATIONAL AND EXPERIMENTAL INVESTIGATION OF A FLUTTER GENERATOR	5. FUNDING NUMBERS
6. AUTHOR(S) Davids, Scott T.	

7. PERFORMING ORGANIZATION NAME(S) AND ADDRESS(ES) Naval Postgraduate School Monterey, CA 93943-5000	8. PERFORMING ORGANIZATION REPORT NUMBER

9. SPONSORING / MONITORING AGENCY NAME(S) AND ADDRESS(ES)	10. SPONSORING/MONITORING AGENCY REPORT NUMBER

11. SUPPLEMENTARY NOTES
The views expressed in this thesis are those of the author and do not reflect the official policy or position of the Department of Defense or the U.S. Government.

12a. DISTRIBUTION / AVAILABILITY STATEMENT Approved for public release; distribution unlimited.	12b. DISTRIBUTION CODE

13. ABSTRACT *(Maximum 200 words)*

The phenomenon of flutter is well known to aircraft designers. A fluttering wing on an aircraft absorbs a significant amount of energy from the air-stream. In this study, computational and experimental methods are used to investigate the possibility of extracting power from a flow using an oscillating airfoil. A numerical analysis is conducted using an unsteady panel code based on potential flow theory. Through the numerical study the combination of parameters is determined that results in the optimum performance of an oscillating-wing power generator. An experimental oscillating-wing power generator is described and tested in a water tunnel. Power and efficiency measurements from the generator are compared to the numerical results. Similar trends between the results suggest that an oscillating-wing power generator is capable of performance comparable to windmills and is a potential source of alternative power.

14. SUBJECT TERMS Aeroelasticity, Flutter, Flutter Generator, Power generation, UPOT, Wingmill			15. NUMBER OF PAGES 107
			16. PRICE CODE

17. SECURITY CLASSIFICATION OF REPORT Unclassified	18. SECURITY CLASSIFICATION OF THIS PAGE Unclassified	19. SECURITY CLASSIFICATION OF ABSTRACT Unclassified	20. LIMITATION OF ABSTRACT UL

NSN 7540-01-280-5500

Standard Form 298 (Rev. 2-89)
Prescribed by ANSI Std 239-18

i

A COMPUTATIONAL AND EXPERIMENTAL INVESTIGATION OF A FLUTTER GENERATOR

Scott T. Davids
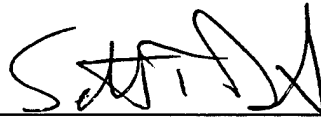Captain, United States Marine Corps
B.S., United States Naval Academy, 1990

Submitted in partial fulfillment of the
requirements for the degree of

MASTER OF SCIENCE IN AERONAUTICAL ENGINEERING

from the
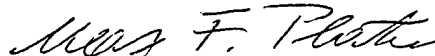
NAVAL POSTGRADUATE SCHOOL
June 1999

Author: _____
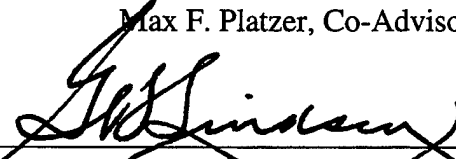
Scott T. Davids

Approved by: _____

Kevin D. Jones, Thesis Advisor

_____

Max F. Platzer, Co-Advisor

_____

Gerald H. Lindsey, Chairman
Department of Aeronautics and Astronautics

iii

ABSTRACT

The phenomenon of flutter is well known to aircraft designers. A fluttering wing on an aircraft absorbs a significant amount of energy from the air-stream. In this study, computational and experimental methods are used to investigate the possibility of extracting power from a flow using an oscillating airfoil. A numerical analysis is conducted using an unsteady panel code based on potential flow theory. Through the numerical study the combination of parameters is determined that results in the optimum performance of an oscillating-wing power generator. An experimental oscillating-wing power generator is described and tested in a water tunnel. Power and efficiency measurements from the generator are compared to the numerical results. Similar trends between the results suggest that an oscillating-wing power generator is capable of performance comparable to windmills and is a potential source of alternative power.

TABLE OF CONTENTS

LIST OF SYMBOLS

A	area swept out by the wing, in terms of c^2
C_D	drag coefficient, drag/($q_\infty S$)
C_L	lift coefficient, lift/($q_\infty S$)
C_M	moment coefficient about x_p, moment/($q_\infty S c$)
C_P	power coefficient, power/($q_\infty S V_\infty$) = $C_L \dot{y} + C_M \dot{\alpha}$
C_{PI}	ideal power coefficient, P_I/($q_\infty S V_\infty$)
C_{PT}	total power coefficient, P_T/($q_\infty S V_\infty$)
c	chord length
f	oscillation frequency in Hz
h	plunge amplitude, in terms of c
h_{LE}	plunge amplitude of the leading edge, in terms of c
h_{TE}	plunge amplitude of the trailing edge, in terms of c
k	reduced frequency, $2\pi f c / V_\infty$
P_I	ideal power, $16/27 P_T$
P_T	total power available, $q_\infty V_\infty A$
q_∞	freestream dynamic pressure, $1/2 \rho_\infty V_\infty^2$
S	wing area
t	time
V_∞	freestream velocity
x_p	pivot location, in terms of c
y	plunge displacement, in terms of c
α	angle of attack (AOA)
α_e	estimated effective angle of attack (magnitude), $\Delta\alpha$-atan(hk)
α_{eff}	effective angle of attack, Eq. 15
α_{ind}	induced angle of attack
$\Delta\alpha$	sinusoidal pitch amplitude
ϕ	phase difference of pitch to plunge
η_{PD}	efficiency based on drag, C_P/C_D
η_{PT}	total efficiency, C_P/C_{PT}
η_{PI}	ideal efficiency, C_P/C_{PI}
ρ_∞	freestream density
τ	non-dimensional time, $tV\infty/c$

ACKNOWLEDGEMENT

I. INTRODUCTION

A. BACKGROUND

The phenomenon of flutter is well known to aeronautical engineers. A wing of an aircraft in a flow permitted to move in two degrees of freedom will oscillate indefinitely given the proper conditions. The wing is absorbing energy from the flow. It follows that if an airfoil is mechanically coupled in pitch and plunge it can extract energy from a flow. It is feasible to construct an oscillating-wing power generator for the purpose of extracting useful power from a flow. McKinney and DeLaurier [Ref. 1] built such a device and called it a wingmill. They tested it in a wind tunnel varying a limited set of parameters and found that the wingmill achieved performance levels comparable with conventional windmills. Since their experiments, it seems little computational or experimental study has been done to further explore more precise parameters which would produce the optimum wingmill performance.

Previous work by Jones and Platzer [Ref. 2] describes the utility of the Unsteady Potential Code (UPOT) to estimate thrust generation and power production from airfoils oscillating in pitch and plunge. Their study showed that power can be extracted from an oscillating airfoil if the phase angle between pitch and plunge is 90 degrees and if the geometric angle of attack exceeds the induced angle of attack. The dependence of performance on angle of attack, phase, pivot location, plunge amplitude, and frequency was briefly considered. No attempt was made to find the optimum parameter configuration for power extraction.

B. OVERVIEW

In the present study UPOT is used to investigate the characteristics of power extraction from an oscillating airfoil. The effect of each parameter through its full range on the performance of the wingmill is explored. The performance is measured by techniques commonly used for wind energy systems. Additionally, the interdependence of the parameters' effects on wingmill performance is described. The numerical study

1

concludes by determining the parameter combination that results in the optimum power-extraction performance by an oscillating airfoil.

The previous experiment by McKinney and DeLaurier was conducted in a wind tunnel. No similar studies are known to have been conducted in a water-flow. A wingmill in water has many practical advantages. It has the potential to extract a large amount of power from a river without stopping the flow. It provides a more environmentally sound alternative to a dam. Additionally, it can be used in slower flowing rivers where dams are not practical due to low terrain and ship traffic. For this study a flutter generator was designed and built to operate in a water tunnel. The device, experiment, and data collection method are described.

The experiment in the water tunnel unfortunately was delayed due to a flood which destroyed the intended facility. Therefore limited time prohibited an in-depth experimental investigation of wingmill performance. However, enough data was collected to make useful comparisons with the numerical study. Additionally, observations made during the experiment resulted in several recommendations to improve the performance of the flutter generator for future experiments.

II. FUNDAMENTALS OF AEROELASTICITY

A. INTRODUCTION TO FLUTTER THEORY

An airfoil placed in a flow is subject to three forces: aerodynamic, elastic, and inertial. Under certain conditions, these forces may interact in such a way as to cause the airfoil to flutter. If an aircraft wing in flight is subjected to a disturbance the three forces mentioned above may interact to cause the wing to oscillate even after the disturbance is removed. Depending on the speed of the flow this oscillation can be divergent, leading rapidly to the destruction of the wing. The aircraft wing is absorbing the energy from the flow. This is prevented in aircraft by changing the wing's stiffness, aerodynamic characteristics, or restricting the flight speed to well below the speed where flutter occurs. When an airfoil in a flow is mechanically coupled in pitch and plunge it can, like an aircraft wing, absorb energy from the flow. As discussed earlier, McKinney and DeLaurier built an oscillating wing power generator reported in a previous study [Ref. 1]. Considering it a combination of a wing and a windmill, they called it a wingmill. The same aerodynamic forces that cause a wing of an aircraft to flutter cause the wingmill to oscillate. The aircraft wing experiencing flutter is subject to elastic forces that govern how the pitching and plunging motions are coupled. With the wingmill, the pitching and plunging motions are coupled mechanically allowing the flow energy to be converted into useful power. Throughout this paper an airfoil in single-mode motion will be referred to as pitching or plunging. An airfoil oscillating in both pitch and plunge will be referred to as flapping.

A significant contributor to the aerodynamic forces acting on an oscillating wing power generator is the phase relationship between pitch and plunge. As described by Platzer [Ref. 3], at an instant in time, the oscillating airfoil sees lift due to its angle of attack to the flow and its plunging motion through the flow. No net work is done on the airfoil when the phase between pitch and plunge is zero as seen in Fig.1a. When the pitch and plunge motion are 90 degrees out of phase, as in Fig. 1b, the lift due to the pitch is in the same direction as the plunging motion throughout the cycle, thus reinforcing the

3

plunging motion. Work is done on the airfoil throughout the cycle. This phase relationship between pitch and plunge allows the oscillating airfoil to be self-excited. This is the basic mechanism that causes flutter. To extract energy from the flow, the phase relationship between pitch and plunge must be around 90 degrees.

a.) Zero phase difference, zero net work.

b.) 90 degree phase difference, work done on the airfoil throughout cycle.
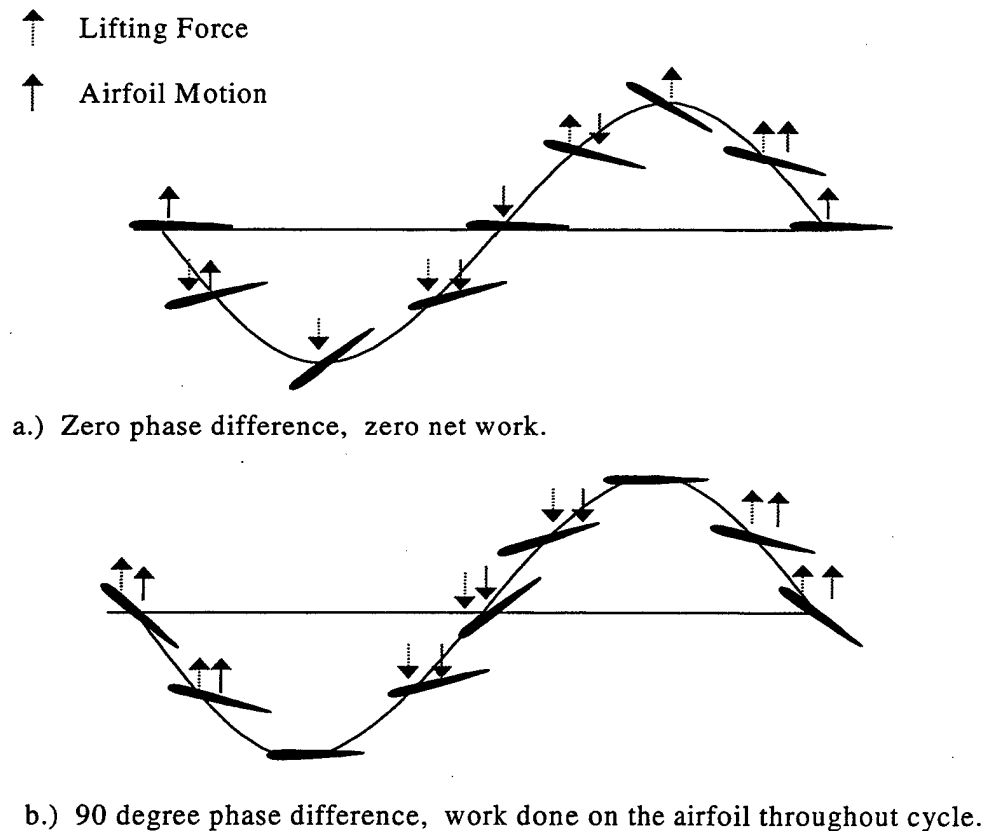
Figure 1. Phase Relationship of a Pitching and Plunging Airfoil. After Ref. 3.

The pitch and plunge phase relationship is not the only mechanism affecting the aerodynamics of a wingmill. There are phase lags and magnitude differences between the true instantaneous lift that the airfoil experiences and the quasi-steady lift. The quasi-steady lift is the lift force induced by the plunging motion of the airfoil if the plunge velocity were constant. An oscillating airfoil does not have a constant plunge velocity

and the lift it experiences differs from the quasi-steady lift. At any instant in time, the difference between the true lift, L, and the quasi-steady lift, L_o, is described by

$$L = L_o r e^{i\psi} \qquad (1)$$

The factor, r, represents the ratio of the absolute value of the instantaneous lift to that of the quasi-steady lift. The actual lift leads the quasi-steady lift by the phase angle, ψ. The quantities ψ and r in general depend on the reduced frequency of oscillation, Mach number, and Reynolds number. The reduced frequency is defined as

$$k = \frac{\omega c}{V_\infty} \qquad (2)$$

where c is the chord length, V_∞ is the freestream velocity, and ω is the circular frequency of oscillation, $\omega = 2\pi f$.

The difference between the true and quasi-steady lift is due to a memory that exists in the flow that stores disturbances. When an airfoil changes orientation, the aerodynamic forces do not change instantaneously. There is always a delay caused by the fact that the vortices shed from the trailing edge move downstream with the finite flow speed. This delay can be described in terms of the change in circulation, Γ. Circulation is defined as the negative of the line integral of velocity around a closed curve in the flow.

$$\Gamma \equiv -\oint_C v \cdot ds \qquad (3)$$

Each time an airfoil changes orientation the circulation around the airfoil changes. When the circulation changes, the Hemholtz Theorem states that there must be an equal and opposite reaction in the flow. This reaction takes the form of a vortex shed into the flow by the airfoil called a starting vortex. When the airfoil is in continuous motion, vortices are shed constantly. These vortices are swept away from the airfoil at a finite speed and in incompressible flow affect the lift on the airfoil until they are far downstream or dissipate. These unsteady flow effects influence the wingmill's performance. Figure 2 is the solution for an airfoil oscillating in plunge only obtained by the linear theory of Theodorsen and Küssner. It shows how the actual lift differs form the quasi-steady lift in magnitude and phase for different oscillating frequencies. [Ref. 3,4,5]

5
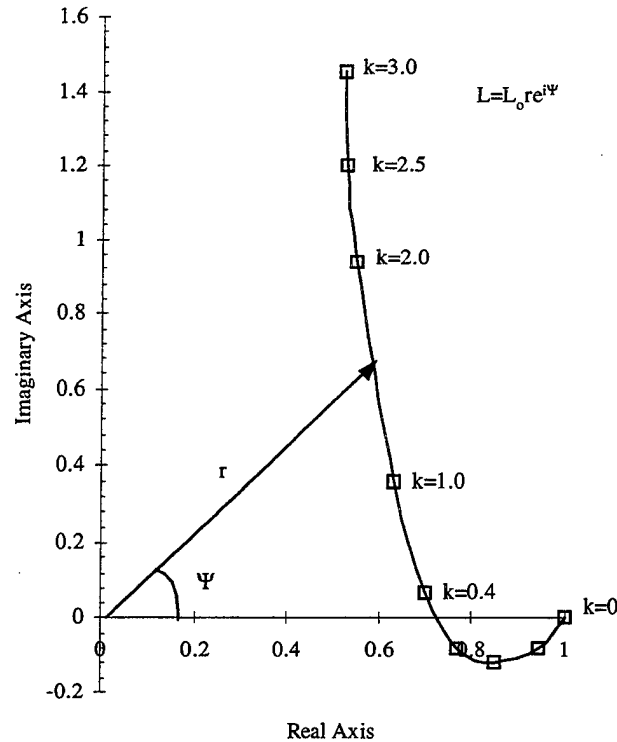
Figure 2. Extraction of Energy from a Flow. After Ref. 1.

B.   METHODS OF ANALYSIS

Since flutter analysis is critical to aircraft design, unsteady aerodynamics has been the subject of intensive study. Areas of interest include prediction of flutter conditions, vibration reduction of airfoils in unsteady flow, lift augmentation, and thrust production. To analyze a flutter problem the equations of motion are formulated as outlined by Platzer [Ref. 3]. The challenge remains to define the unsteady aerodynamic problem in a way that is solvable. The continuity, momentum, and energy equations are combined to produce a non-linear unsteady potential equation. Solutions to the non-linear unsteady potential equation are extremely difficult and only few are known. A small disturbance assumption is introduced to give the linearized unsteady potential equation.

6

$$[1 - M^2]\varphi_{xx} + \varphi_{yy} + \varphi_{zz} - 2\frac{M}{c}\varphi_{xt} - \frac{1}{c^2}\varphi_{tt} = 0 \qquad (4)$$

Equation 4 is the basic equation used to predict oscillatory pressures and aerodynamic forces in most aerodynamic analyses. It is only valid for purely supersonic and purely subsonic flows as well as "sufficiently unsteady" transonic flows. For incompressible flow, Eq. 4 reduces to the Laplace equation. In Chapter III the panel code UPOT developed at the Naval Postgraduate School is briefly described to obtain solutions for incompressible two-dimensional flow past airfoils which execute an arbitrary unsteady motion. [Ref. 3]

III. PANEL CODE

The numerical analysis of the aerodynamics of the wingmill was accomplished using the Unsteady Potential Code (UPOT) at the Naval Postgraduate School. UPOT allowed the wingmill to be analyzed at different oscillating frequencies, plunge amplitudes, pivot locations, phase angles, and angles of attack. UPOT provides wake analysis and time averaged power coefficients, thrust/drag coefficients, and efficiencies of each analyzed case. UPOT also provides instantaneous conditions throughout the cycle so maximum instantaneous conditions can be examined.

A.   PANEL CODE FOR STEADY FLOW

UPOT computes incompressible flow solutions using an unsteady, potential–flow code originally developed by Teng [Ref. 6] with a Graphical User Interface (GUI) developed by Jones and Center [Ref. 7]. The code is based on the work of Hess and Smith [Ref. 8], who originally developed the panel method to solve for the steady flow over an airfoil of finite thickness. The panel method is based on the Laplace equation, which is the governing equation for two-dimensional incompressible flow over an airfoil of arbitrary geometry at an angle of attack. The principle of linear superposition allows for very simple solutions of the Laplace equation to be combined or superimposed to construct more complex solutions. Namely, the superposition of a free-stream solution of the Laplace equation with the vortex solution produces the solution for flow over a lifting airfoil. Airfoils of a finite thickness are accounted for by the addition of the source solution;

$$\Phi = \varphi_\infty + \varphi_v + \varphi_s \qquad (5)$$

The panel method divides the airfoil into n panels and places a uniform source distribution and a uniform vorticity distribution on each panel. The source distribution varies from panel to panel and the vorticity distribution is the same for each panel. This gives n+1 unknowns: n source distributions and one vorticity distribution. The boundary

conditions that need to be satisfied are the flow tangency condition and the Kutta trailing edge condition. The flow tangency condition requires that the normal component of the total velocity at the midpoint of each panel due to the free-stream and the velocities induced by the source and vorticity distributions be zero. The Kutta condition requires that the pressures on the upper and lower surfaces of the airfoil are equal at the trailing edge. There are n equations for the flow tangency conditions on each panel and one equation for the Kutta condition giving n+1 equations for n+1 unknowns. A computer easily solves this system of linearly independent equations. [Ref. 3]

B.   PANEL CODE FOR UNSTEADY FLOW

The unsteady panel code adopts the procedure of Basu and Hancock [Ref. 9]. Recall the discussion in Chapter II about the influences of the angle of attack, plunging motion, and phase lags due to unsteady flow effects on the aerodynamics of an oscillating airfoil. To take all these into account, UPOT uses the Hemoltz Theorem which requires that a change in circulation around an airfoil must be matched by an equal counter vortex, the starting vortex. The airfoil is modeled as in the steady case by source and vortex distributions. The range of motion of pitch and plunge is divided into step changes. Each time a step change occurs, a starting vortex is shed into the wake in the form of a point vortex. A new vortex is formed on the wake panel at each time-step to replace the one that was shed into the flow. There are three additional unknowns added to the steady case: the starting vortex strength, the length of the wake panel, and the orientation of the wake panel from which the starting vortex originates. These three unknowns are solved by adding three equations that satisfy the following conditions:

1) The Hemholtz Theorem that says the vortex strength on the wake panel must be equal and opposite to the circulation change of the airfoil.

2) The wake panel is oriented in the direction of the local resultant velocity at the panel's midpoint.

3) The length of the wake panel is proportional to the magnitude of the local resultant velocity and to the time-step.

In the unsteady case, the Kutta condition and the wake panel orientation and length conditions are non-linear and require an iterative solution procedure. Figure 3 summarizes the essential elements of the panel-code wake model. Δ is the wake panel length, γ_w is the distributed vorticity strength on the wake panel, θ is the wake panel orientation, and Γ is the circulation about the airfoil. The subscript k is the current time step and k-1 is the previous time step. The instantaneous and time averaged values for lift, drag, and moment forces on the airfoil are displayed in graphical and numerical format.
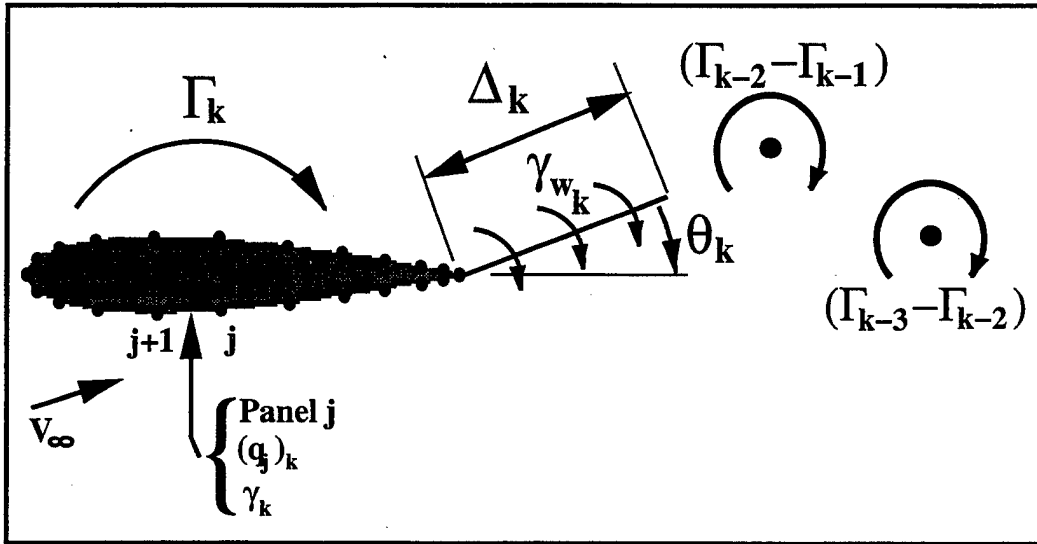
Figure 3. Schematic of the Panel-Code Wake-Model. From Ref. 2.

The accuracy of the Unsteady Potential Code was examined by Riester [Ref. 10] who found it to predict the linear theory of Theodorsen accurately, differing only at high frequencies with some dependence on plunge amplitude. Jones and Platzer [Ref. 2] also found differences between UPOT and linear theory at higher frequencies. They attributed them to UPOT's greater accuracy due to the deforming wake used in the panel code.

The solution by Theodorsen and Küssner for L/L_0 in a plunging airfoil was compared to UPOT and is shown in Figure 4. Note that Theodorsen and Küssner analyzed a flat plate while the UPOT analysis was conducted for a NACA 0012 airfoil.
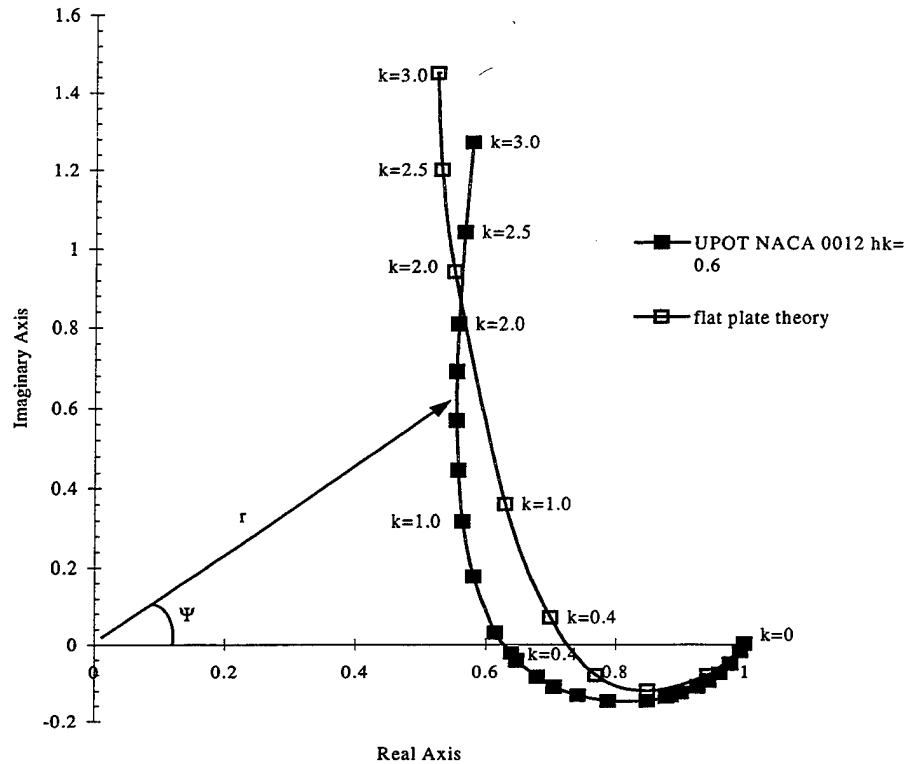
Figure 4. UPOT Compared to Flat Plate Theory of Theordorsen and Küssner.

C.   LIMITATIONS OF NUMERICAL SIMULATION

UPOT is based on the solution of the Laplace equation. Therefore it cannot evaluate any kind of separated flow. This becomes critical for evaluations at high angles of attack. The results will be valid only for incompressible flow and therefore are limited to low-speed calculations. Results are generally considered accurate to a Mach number of around 0.3 for steady flow. The accuracy of unsteady flow solutions may be limited to a lower Mach number. In the numerical analysis, all inertial effects of the mechanical system are ignored. Additionally, the influence of the displaced fluid, the so-called apparent mass, may not be fully addressed. There is some question as to whether or not apparent mass effects are included in UPOT given that the code is based on potential-

12

flow. The apparent mass may have a significant effect on the flow solution at high amplitudes or high frequencies of oscillation in dense fluids, such as water.

IV.   EQUATIONS OF MOTION AND PERFORMANCE

A.   EQUATIONS OF MOTION

The motion of a flapping airfoil in the numerical model is sinusoidal and described by the following equations:

$$\alpha(\tau) = \Delta\alpha \sin(k\tau) \quad (6)$$

$$y(\tau) = h\sin(k\tau + \phi) \quad (7)$$

Here τ is the non-dimensional time, h is the maximum plunge amplitude, $\Delta\alpha$ is the range of geometric angle of attack, and k is a non-dimensional frequency called the reduced frequency. Plunge amplitude, reduced frequency, and phase are parameters of the wingmill that can be varied in the numerical analysis and are described later. [Ref. 8]

B.   EQUATIONS OF PERFORMANCE

1.   Power Coefficient

The power generated by the wingmill is measured by UPOT in terms of the power coefficient:

$$C_P = power/(q_\infty S V_\infty) = C_L \dot{y} + C_M \dot{\alpha} \quad (8)$$

Where q_∞ is the freestream dynamic pressure, S is the airfoil surface area, and V_∞ is the freestream velocity. The power coefficient is also equal to the product of the lift coefficient, C_L, and the plunge rate, $\dot{y}$, added to the product of the moment coefficient, C_M, and the pitch rate, $\dot{\alpha}$. The instantaneous C_P is of interest to determine which portions of the cycle are negative power producers. The magnitude of the negative power production has an effect on the performance of the wingmill.

A more useful measure of power is the mean power coefficient, $\overline{C_P}$, which is obtained by averaging the C_P over one or more cycles. The $\overline{C_P}$ calculated by UPOT becomes constant within about three cycles for low frequencies and high plunge amplitudes. At higher frequencies and low plunge amplitudes non-linearities in the wake

cause the $\overline{C_P}$ to change over time, requiring several cycles to become constant. The non-linearities become noticeable when the point vortices in the wake become strong and start to impinge on each other. For frequencies approaching $k = 2.0$, the non-linearities in the wake become so extreme that the $\overline{C_P}$ solution does not converge to a periodic solution for a long time, if ever. The effect of increasing the reduced frequency for a constant plunge amplitude on $\overline{C_P}$ is shown in Fig. 5. The corresponding wakes as depicted by UPOT are shown in Fig. 6. UPOT does not allow the strength of the point vortices within the wake to dissipate with time as they would in an actual flow. Although they become less influential as their distance from the airfoil increases, each point vortex has a finite effect on the lift of the airfoil. As the wake becomes asymmetric about the mean plunge position, the numerical results become irregular. An attempt was made to determine the average deviation of $\overline{C_P}$ based on the value of k. It was found that once the numerical values for $\overline{C_P}$ stopped converging to a steady value, the average deviation of $\overline{C_P}$ did not depend on k for the range of time-steps investigated. With run times approaching eight hours per data point, the effort was abandoned. It was assumed that the non-linearities in the solution indicated conditions where flow separation would be highly likely.
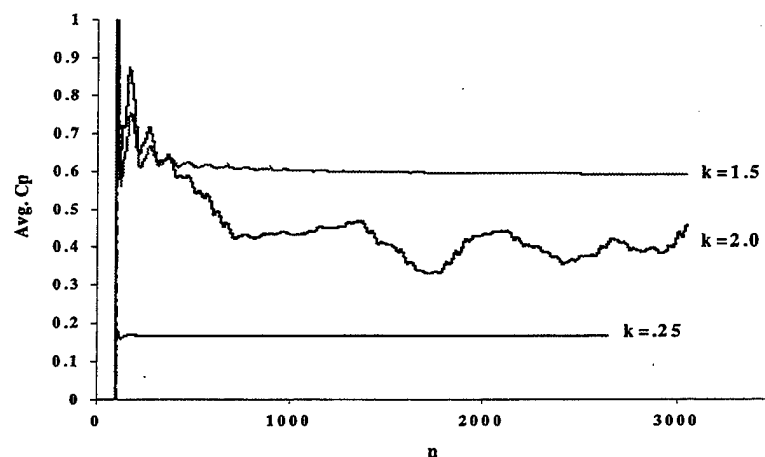
Figure 5. UPOT Power Coefficient Output for Various Reduced Frequencies.
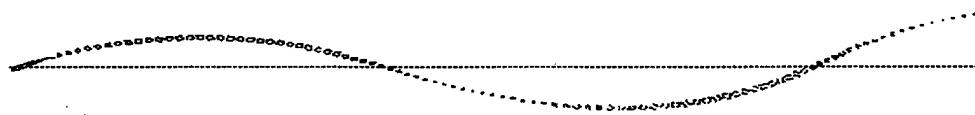
k = 0.25
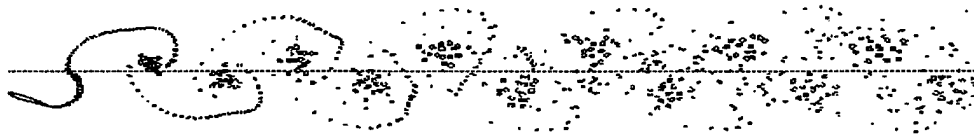
k = 1.5
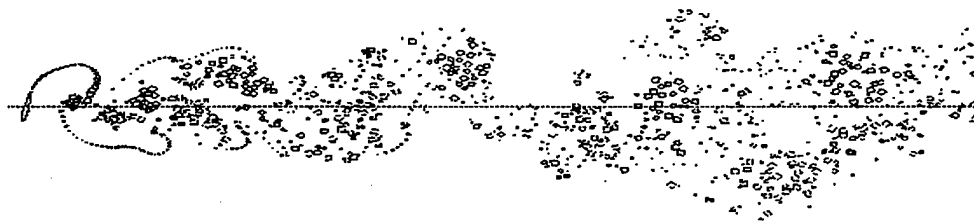
k = 2.0

Figure 6. UPOT Wake Structure Output for Various Reduced Frequencies.

2. Efficiency Based on Drag

Performance is generally measured in terms of efficiency. There are several definitions of efficiency in aerodynamics. In propulsion studies, efficiency is commonly defined as the ratio of propulsive power, or thrust times velocity compared to the power put into the system. When considering this efficiency in terms of power extraction, the reciprocal is taken. The result is the ratio of power extracted compared to drag times velocity. This efficiency based on drag, η_{PD}, is optimized when the most power is extracted from the flow for the least amount of drag. A high η_{PD} will maximize the power extracted while minimizing the disturbance to the flow. Efficiency based on drag would be an appropriate performance measurement if flutter generators were placed in series, each extracting a small portion of the energy remaining in the flow. [Ref. 11]

3.   Efficiency Based on Total Power in the Flow

For a single stage generator, the highest performance is achieved when all the energy is extracted from the flow, theoretically leaving the flow at a standstill behind the generator. This performance can be measured by the ratio of the power extracted by the generator to the power available to the generator. The result is an efficiency based on total power, η_{PT}; also called total efficiency.

Total efficiency is derived from the Rankine-Froude actuator disk theory. Actuator disk theory is commonly used to describe windmill power absorption. It calculates the amount of energy available to the windmill by replacing the windmill rotor with an actuator disk. Actuator disk theory assumes the following:

1. Steady flow with no obstructions upstream or downstream.
2. Uniform flow velocity at the disc.
3. Flow passing through the disc is separable from remaining flow by well-defined stream tubes.
4. No rotation of flow is produced by the disk. [Ref. 12]

The total efficiency can be given as the ratio of the time averaged power coefficient of the wingmill, $\overline{C}_P$, to the total power coefficient, C_{PT}.

$$\eta_{P_T} = \frac{\overline{C}_P}{C_{PT}} \quad (9)$$

The total power coefficient, C_{PT}, is similarly defined as

$$C_{PT} = \frac{P_T}{q_\infty S V_\infty} \quad (10)$$

The time averaged power coefficient of the wingmill is defined from Eq. 8 as

$$\overline{C}_P = \frac{\text{avg. power output}}{q_\infty S V_\infty} \quad (11)$$

where P_T is the power in the flow that passes through the cross-sectional area normal to the flow direction that is swept out by the airfoil.

18

$$P_T = q_\infty V_\infty A \quad (12)$$

Therefore, the total efficiency becomes

$$\eta_{PT} = \frac{\overline{C_P} S}{A} \quad (13)$$

Since UPOT considers the chord to be equal to one and its results are in terms of unit span, the total efficiency is found by dividing the $\overline{C_P}$ as given by UPOT by the swept area, A.

The swept area varies with phase, pivot position, angle of attack, and plunge amplitude. Assuming the airfoil is thin, the maximum swept area will be bracketed by the motion of the leading or trailing edge or both, depending on the parameter combination. The vertical position of the leading and trailing edges of the airfoil are given by:

$$
\begin{aligned}
y_{LE} &= h\cos(\omega t - \phi) + x_p \sin(\Delta\alpha \cos(\omega t)) \\
y_{TE} &= h\cos(\omega t - \phi) + (x_p - 1)\sin(\Delta\alpha \cos(\omega t))
\end{aligned}
\quad (14)
$$

A Matlab routine (located in App. A) was written to determine the vertical position of the leading and trailing edges throughout the cycle. The code compared the two motions and determined the maximum area swept by the airfoil normal to the flow. The vertical position of the leading and trailing edges of a flapping airfoil with different phase relationships between pitch and plunge is shown in Fig. 7.
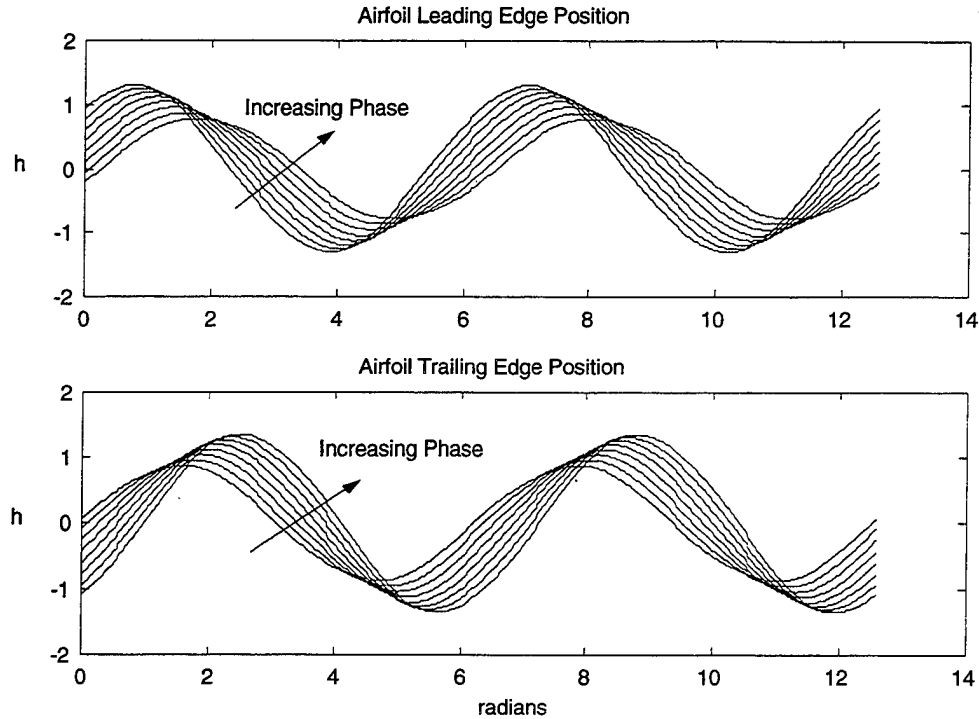
Figure 7. Vertical positions of leading and trailing edge of a flapping airfoil with varying phase. $\Delta\alpha = 60°$ ($\alpha_e = 15°$), $k = 1.0$, $h = 1.0$, $\phi = 60°$-$130°$, $x_p = 0.5$.

Obtaining a total efficiency of 100% would mean extracting all the energy from the flow bringing the flow immediately behind the airfoil to a stop. Since without flow through the disk no energy can be extracted, a limit of extractable energy exists. Actuator disk theory predicts that at most 16/27 of the power flowing through the disk can be extracted. This is known as the Betz limit after Albert Betz, the German aerodynamicist. [Ref. 12]

Since the physical flutter generator is configured with a single airfoil, this study will emphasize total efficiency rather than efficiency based on drag. Additionally, the study of total efficiency provides a helpful way of comparing wingmill performance with windmill performance.

C.   DESCRIPTION OF WINGMILL PARAMETERS

There are five wingmill parameters studied in the numerical analysis: pitch amplitude, reduced frequency, phase angle, plunge amplitude, and pivot location. With the exception of the pitch amplitude and the phase angle, the parameters are entered into UPOT in a non-dimensional form. The plunge amplitude and pivot location is given in terms of chord length. A plunge amplitude, h, of 0.5 means the airfoil will plunge ±0.5 chord lengths from neutral. An airfoil with a pivot location, x_p, of 0.5 pitches about the half-chord point. The plunge amplitude is defined at the pivot location so it does not represent the vertical distance swept by the airfoil. As seen in Fig. 7 and Eq. 14, the vertical distance swept by the airfoil depends on the extreme positions of the leading and trailing edges. The phase angle, ϕ, is the phase angle between pitch and plunge with pitch leading plunge.

The angle between the airfoil chordline and the incident flow is the effective angle of attack, α_{eff}. The induced angle of attack, α_i, is dependent on the sinusoidal pitch amplitude, $\Delta\alpha$, and also h, k, ϕ, and x_p. The induced angle of attack and the geometric angle of attack determine the effective angle of attack as shown in Fig. 8.
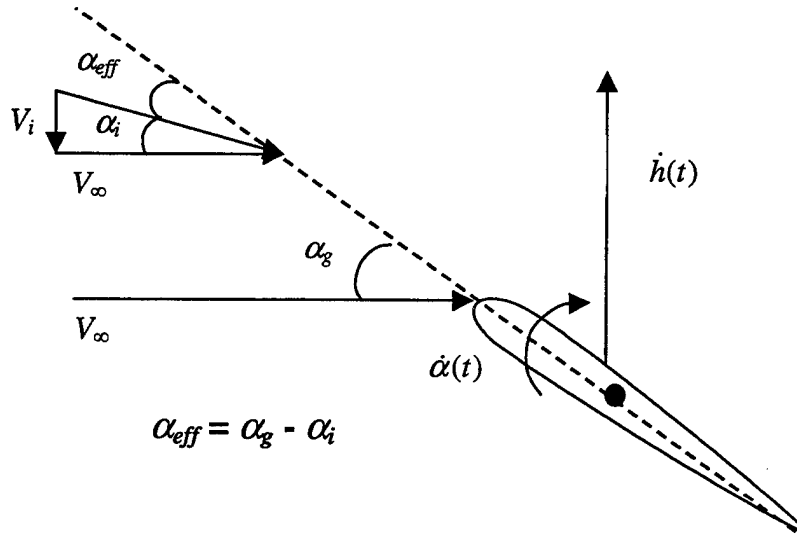
Figure 8. Effective Angle of Attack.

Figure 9 is used to explain how varying the airfoil's parameters change the effective angle of attack. In Fig. 9a, the airfoil is in pure plunging motion with zero geometric angle of attack. Its motion through the flow induces an angle of attack dependent on its plunge rate. If the airfoil is assumed to be thin, $\alpha_{eff} = \alpha_i$ everywhere on the surface of the airfoil. The airfoil in pure pitching motion is shown in Fig. 9b. The airfoil's α_{eff} is equal to its geometric angle of attack minus the angle of attack induced by the pitch rate. The pitch rate varies along the chord and is dependent on the frequency of oscillation and the pivot position. Therefore α_{eff} is not constant along the airfoil's chord. Since dynamic flow separation often starts near the leading edge in part due to the airfoil shape, the effective angle of attack is usually defined at the leading edge. The airfoil in coupled motion is shown in Fig. 9c. The geometric angle of attack appears to match the induced angle of attack making $\alpha_{eff} = 0$. However there is a small induced angle of attack due to the pitch rate. At higher frequencies and lower plunge amplitudes the pitch rate can be the dominating contributor to the effective angle of attack.
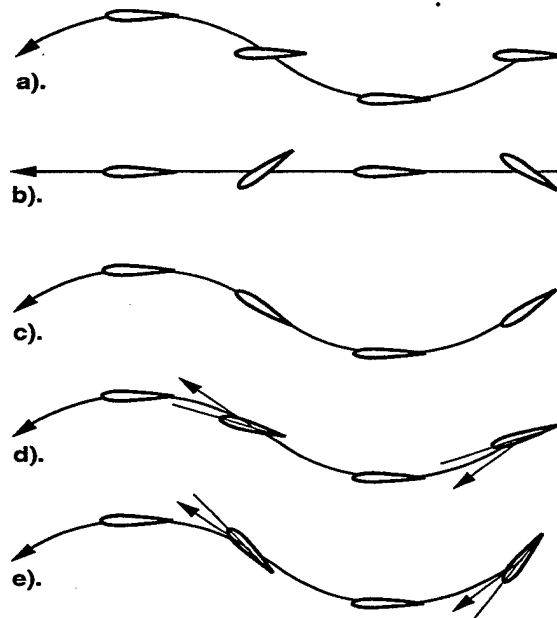
Figure 9. Effective Versus Geometric Angle of Attack. From Ref. 2.

Figure 10 shows the effective angle of attack seen by a flapping airfoil at the leading edge. The effective angle of attack at the leading edge is no longer sinusoidal and is dominated by the high pitch rate. The effective angle of attack at the leading edge is given by

$$\alpha_{eff} = \alpha(t) - \tan^{-1} \left[\frac{h'(t) - \alpha'(t)x_p \cos(\alpha(t))}{U_\infty - \alpha'(t)x_p \sin(\alpha(t))} \right] \quad (15)$$

The key to power extraction or thrust production is to have a positive effective angle of attack. When the pitch amplitude is lower than that of the feathering case, as shown in Fig. 9d, the oscillating airfoil produces thrust. When the pitch amplitude exceeds that of the feathering airfoil as shown in Fig. 9e, power is extracted from the flow.
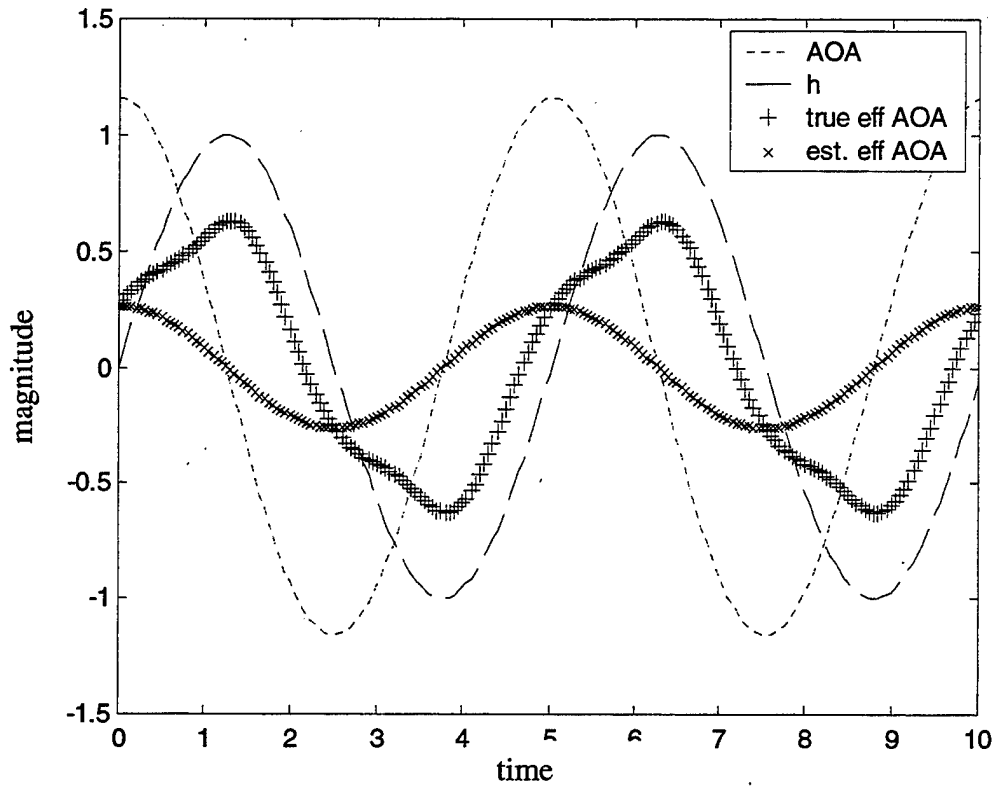
Figure 10. Leading Edge Effective Angle of Attack. $\Delta\alpha = 66.3°$, $k = 1.25$, $h = 1.0$, $\phi = 90°$, $x_p = 0.5$.

23

When analyzing the ability of a flapping airfoil to extract power from a flow, the effective angle of attack is of more interest as a parameter than the geometric angle of attack. It is desirable to evaluate the influence of the parameters of the wingmill keeping the maximum effective angle of attack constant. However this is impractical since the maximum α_{eff} varies with all the other parameters as well as position on the airfoil. The approach used in the numerical analysis was to define an estimated effective angle of attack in terms of the plunge velocity hk. The induced angle of attack due to the maximum plunge velocity is atan(hk), therefore the estimated effective angle of attack is given by

$$\alpha_e = \Delta\alpha - \text{atan}(hk) \qquad (16)$$

The estimated effective angle of attack is the maximum effective angle of attack based on the plunge velocity. It does not account for effects caused by pitch rate and is only valid at the pivot position and at the point in the cycle where hk is maximum. The maximum value of the estimated effective angle of attack may be much less than the actual effective angle of attack seen by various locations of the airfoil as seen in Fig. 10. At a given point in the cycle, some type of flow separation is bound to occur at locally high effective angles of attack at certain locations on the airfoil. It is not known if this will have an adverse or beneficial effect on the performance of the wingmill.

V.   NUMERICAL ANALYSIS

Different wingmill cases were explored to determine trends in the wingmill's response to parameter variations. The goal of the numerical analysis was to determine how each parameter variation individually affected the wingmill's performance and the dependence of one parameter on another. The numerical analysis also sought to find the overall parameter combination that would produce the optimum efficiency.

A.   NUMERICAL ANALYSIS RESULTS

1.   Effective Angle of Attack

Increasing the magnitude of the effective angle of attack increases the power output linearly. It is shown in Fig. 11a how varying the effective angle of attack varies the power output for selected reduced frequencies. At high frequencies, the smaller effective angles of attack do not perform as well. Since the plunge velocity is used to calculate the effective angle of attack, the reduction in performance is due to the higher pitch rates that occur at high frequency. Figure 11a is also an indication of where the effective angle of attack based on plunge velocity differs from the true effective angle of attack. If the airfoil had a true effective angle of attack of zero, all the curves in Figs. 11a and 11b would pass through the origin, producing no work for zero true effective angle of attack. Note how the curves based on estimated effective angle of attack tend to pass through the origin except when the reduced frequency gets large. At reduced frequencies of $k = 1.5$, zero estimated effective angle of attack results in negative power. In Fig. 11b, the maximum instantaneous negative power in the cycle is shown to be relatively constant for the range of effective angles of attack. Higher frequencies require a much greater power input to pitch the airfoil through the flow. The efficiency based on total power in the flow varies as the $\overline{C}_P$ (Fig. 11c) since the swept area is related to the angle of attack linearly. The efficiency based on drag reaches an optimum where the effective angle of attack produces the most amount of lift for the least amount of drag. This

optimum occurs at different angles of attack dependent on the frequency; higher

frequencies achieving optimum η_{PD} at higher effective angles of attack. (Fig. 11d)
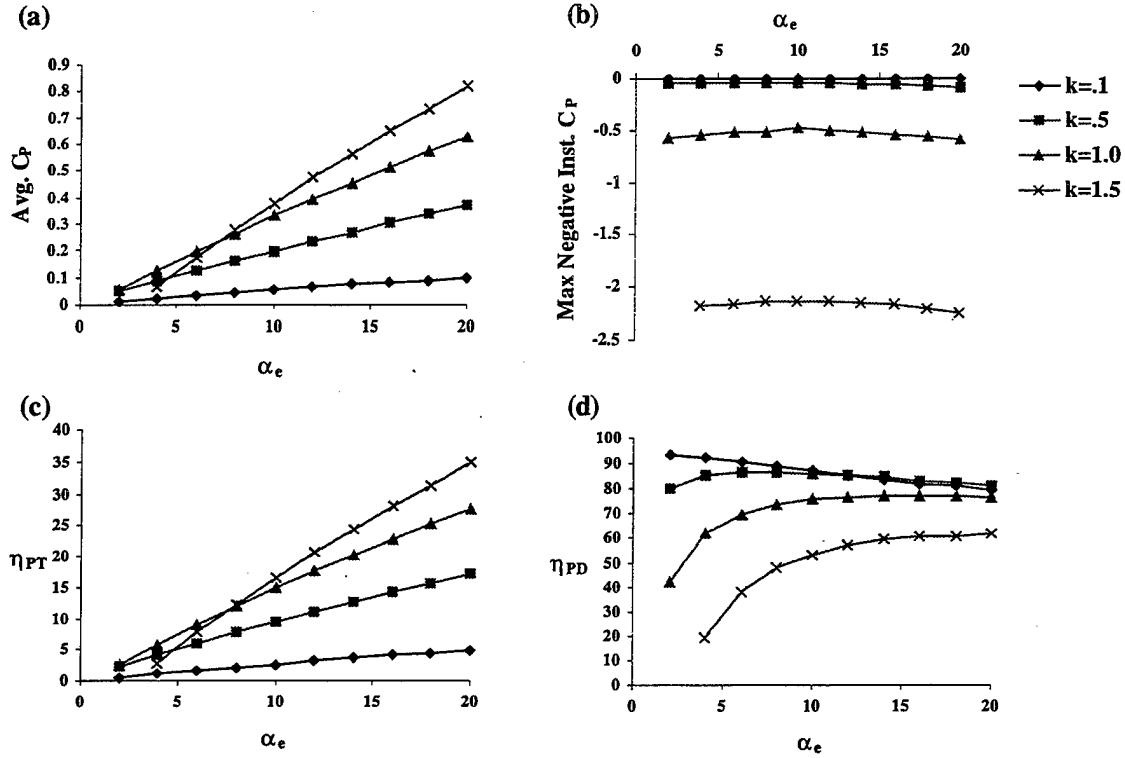
Figure 11. Effect of Effective Angle of Attack on Wingmill Performance for Various
Reduced Frequencies. $h = 1.0$, $\phi = 90°$, $x_p = 0.5$.

The effect of increasing the angle of attack for different plunge amplitudes is

shown in Fig. 12. Higher plunge amplitudes increase the slope of the $\overline{C}_P$ versus α_e curve

as the higher frequency values did. The effect of low plunge amplitude on the total

efficiency is interesting. There is an optimum effective angle of attack around 18

degrees. As the pitch amplitude increases on a wingmill with a very small plunge

amplitude, the pitch becomes the most significant contributor to the swept area. The

wingmill starts to behave like a purely pitching airfoil and efficiency decreases. The

sharp increase of maximum negative power into the system shown in Fig. 12b is another

example of the effective angle of attack based on the plunge velocity diverging from the

true effective angle of attack. At high plunge amplitudes the angle of attack the airfoil

26

actually sees is less than predicted by the effective angle of attack based on plunge velocity. Varying the plunge amplitude significantly alters the relationship of efficiency based on drag with the effective angle of attack as shown in Fig. 12d. When the reduced frequency is fixed, a high plunge amplitude means that the airfoil is moving faster through the flow. There is an optimum angle of attack that produces the most lifting force for the least amount of aerodynamic drag.
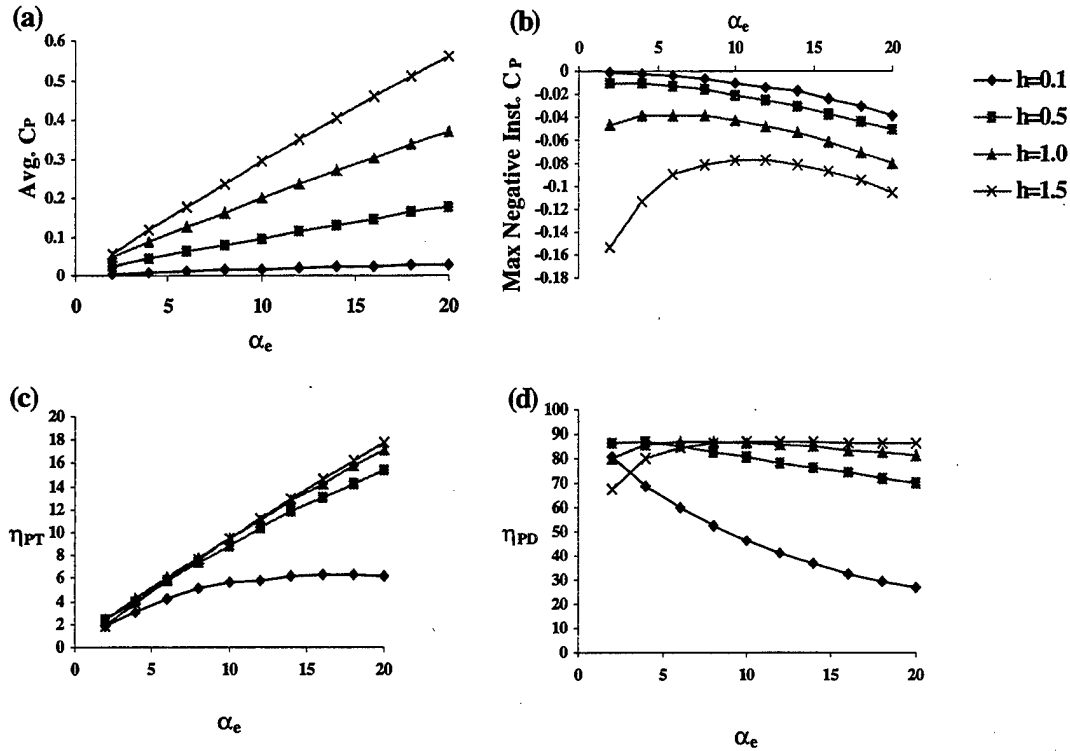
Figure 12. Effect of Effective Angle of Attack on Wingmill Performance for Various Plunge Amplitudes. $k = 0.5$, $\phi = 90°$, $x_p = 0.5$.

2. Reduced Frequency

The performance variation with reduced frequency for different effective angles of attack is shown in Fig. 13. As seen in the angle of attack analysis, there is an optimum power and total efficiency based on energy in the flow for a range of frequencies. This optimum occurs at a relatively high reduced frequency. Lower effective angles of attack

27

reach the optimum at a lower frequency. The instantaneous negative power increases rapidly with frequency since the pitch velocity is increasing, but it is interesting to note that the magnitude of pitch angle has no influence (Fig. 13b). The efficiency based on drag is highest at low frequencies and small effective angles of attack. As frequency is increased, higher angles of attack provide better performance.
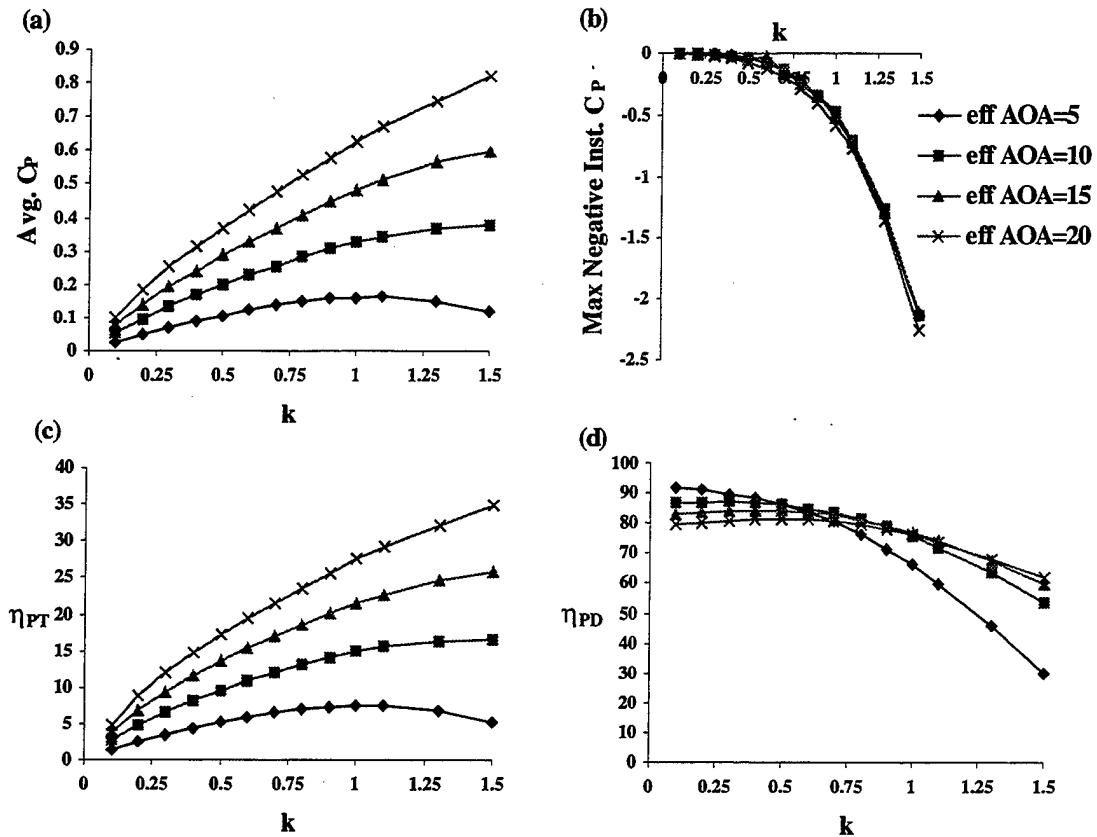
Figure 13. Effect of Reduced Frequency on Wingmill Performance for Various Effective Angles of Attack. $h = 1.0$, $\phi = 90°$, $x_p = 0.5$.

28

The effect of the reduced frequency on wingmill performance for various pivot locations is shown in Fig. 14. At low reduced frequencies, the pivot position has no effect on performance. As the frequency increases, the performance varies with pivot location. The amount of power absorbed by a wingmill with a pivot forward of half chord starts to decay first as frequency increases. Forward pivot positions have a greater maximum negative power than aft pivot positions. The reason for this difference is that since the aerodynamic center of the airfoil is near the quarter chord point, it is beneficial to pivot aft of the quarter chord. As the pivot position moves aft along the chord the center of lift has a greater moment to help move the pitch the airfoil.
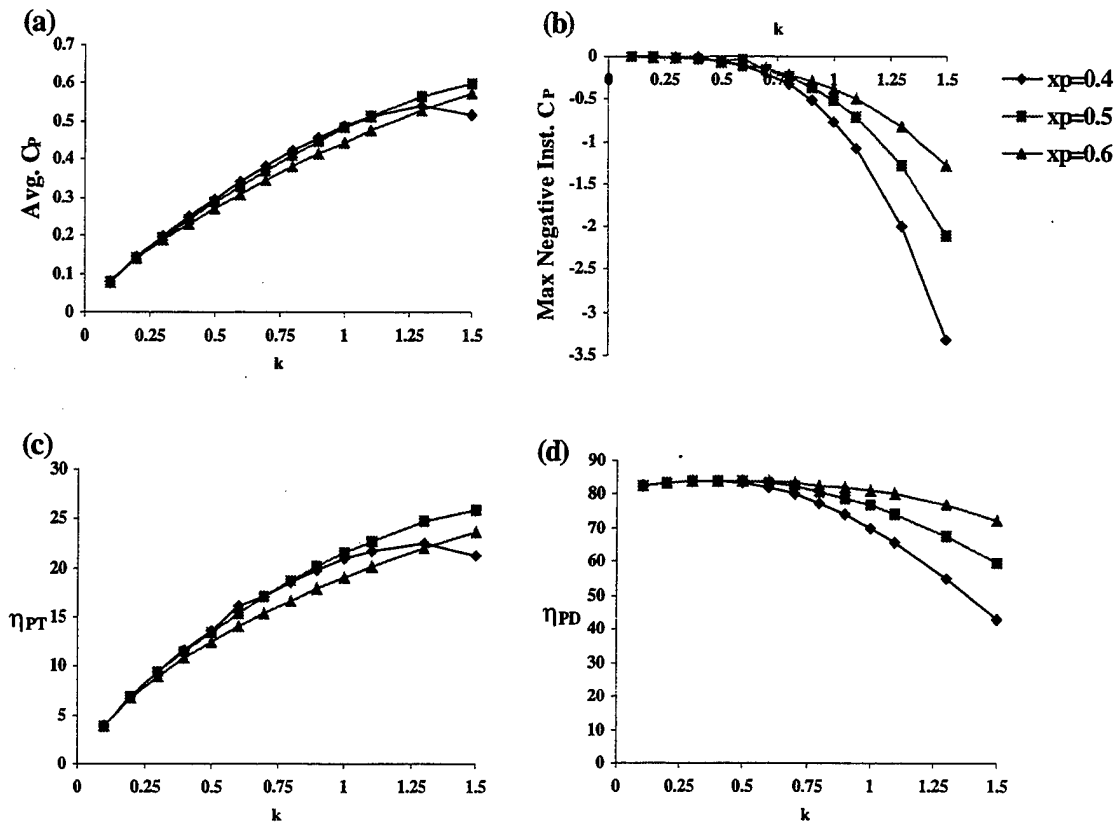
Figure 14. Effect of Reduced Frequency on Wingmill Performance for Various Pivot Locations. $\alpha_e = 15°$, $h = 1.0$, $\phi = 90°$.

3. Plunge Amplitude

The effect of plunge amplitude on wingmill performance is shown in Fig. 15. As plunge amplitude increases, power increases linearly as seen in Fig. 15a. The maximum negative power required in a cycle also increases linearly through the lower plunge amplitudes as seen in Fig. 15b. The lower effective angles of attack diverge at the high plunge amplitudes indicating that the effective angle of attack based on plunge velocity no longer reflects the angle of attack the airfoil sees. Initially, plunge amplitude has a significant effect on the efficiency of the wingmill. Once the plunge amplitude reaches one chord length, efficiency levels drop off since the swept area continues to grow. As plunge amplitude increases, there are portions of the swept area that are not supplying energy to the wingmill. The highest efficiencies based on drag are achievable at high plunge amplitudes as seen in Fig. 15d. At the highest plunge amplitudes, quasi-steady effects are much larger than oscillatory effects. However, for a fixed frequency, an increasing plunge amplitude results in an increased plunge rate. Higher plunge velocity reduces the angle of attack seen by the airfoil at certain parts of the cycle.
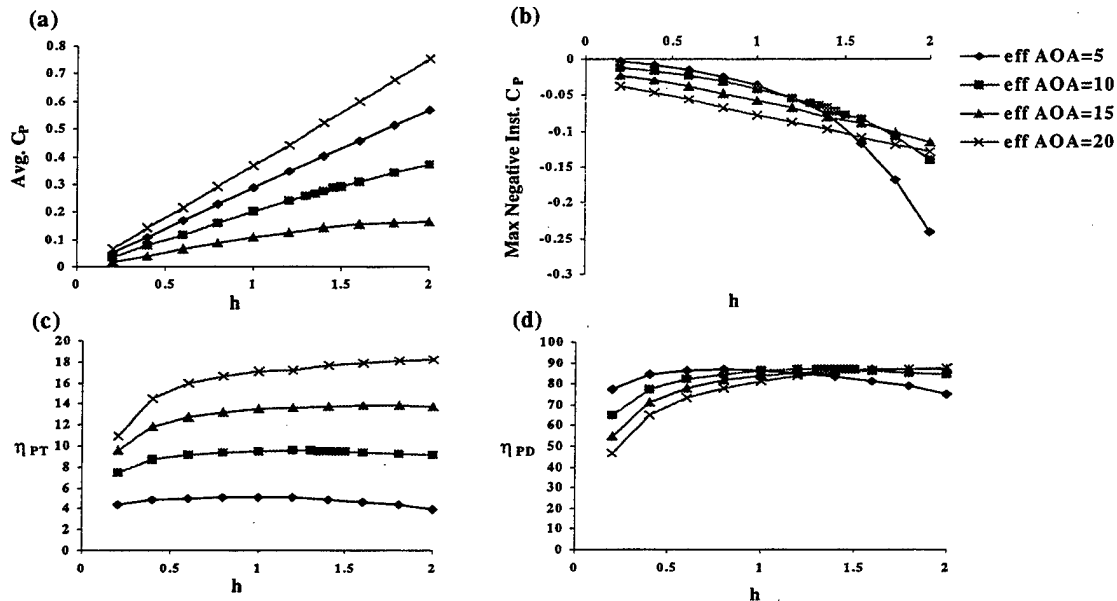
Figure 15. Effect of Plunge Amplitude on Wingmill Performance for Various Effective Angles of Attack. $k = 0.5$, $\phi = 90°$, $x_p = 0.5$.

4. Phase

The effect of phase variation on wingmill performance for different effective angles of attack is shown in Fig. 16. For the range of effective angles of attack, the most power is extracted when the pitch and plunge motions are 90 degrees out of phase. The efficiency based on energy in the flow directly corresponds to the power extracted since the swept area is minimum at 90 degrees phase. The efficiency based on drag peaks just over 100 degrees phase due primarily to the airfoil shape.
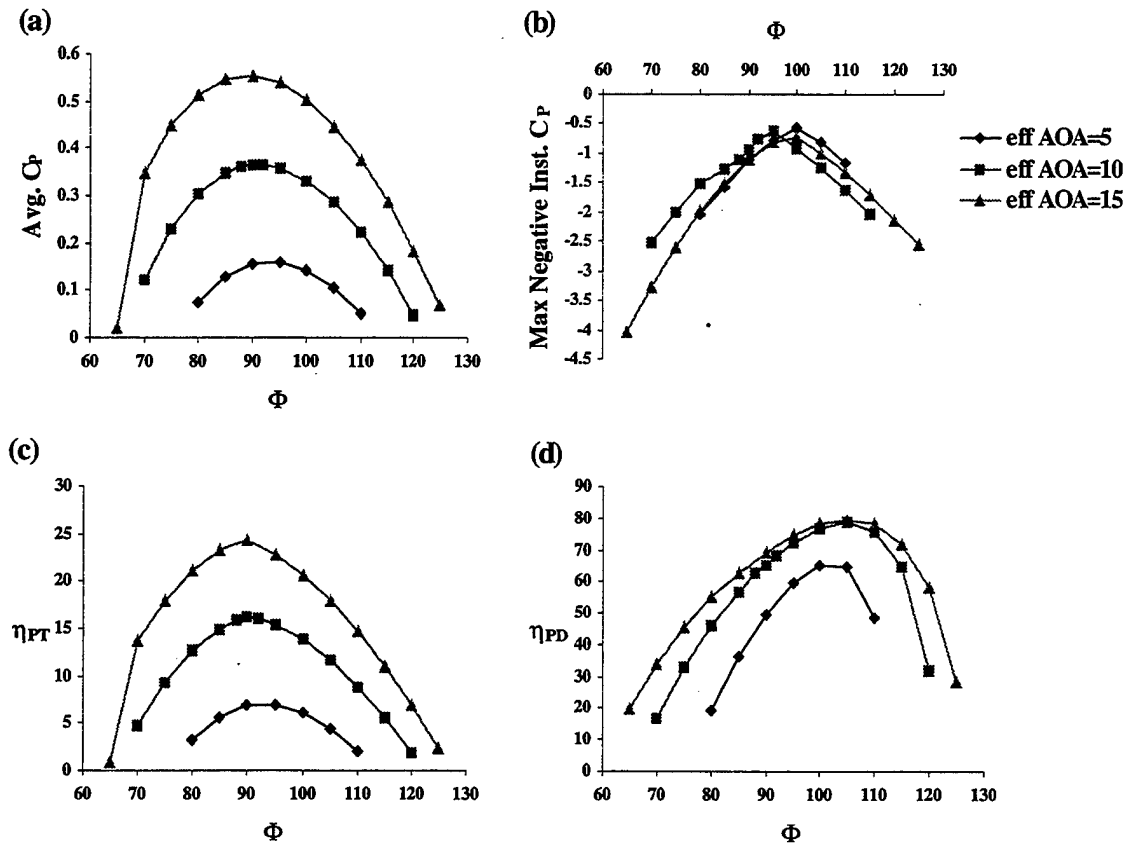
Figure 16. Effect of Phase Angle on Wingmill Performance for Various Effective Angles of Attack. $k = 0.5, h = 1.0, x_p = 0.5$.

The effect of phase variation on the wingmill performance is also plotted for different pivot locations in Fig. 17. An airfoil pivoting at midchord extracts the most power when the phase angle is 80 degrees as seen in Fig. 17a. The highest power output was at 60 degrees phase pivoting at the trailing edge. This corresponds to a low negative power requirement (Fig. 17b). However, the efficiency based on total power maintains an optimum at 90 degrees phase (Fig. 17c) since the swept area is still a minimum there. The efficiency based on drag is not dependent on swept area so its optimum can be reached at a range of phase angles by varying the pivot location.
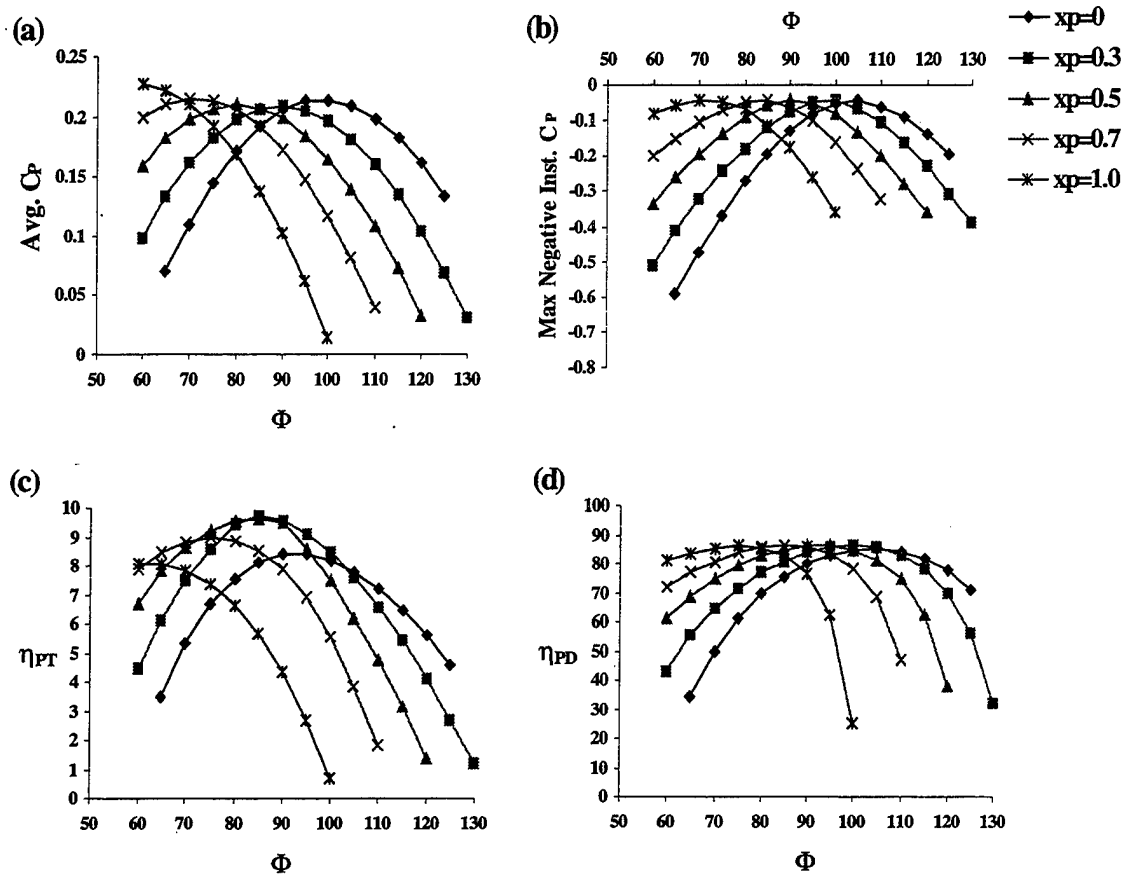
Figure 17. Effect of Phase Variation on Wingmill Performance for Various Pivot Positions. $\alpha_e = 10°$, $k = 0.5$, $h = 1.0$.

The effect of phase variation on performance for different reduced frequencies is shown in Fig. 18. The optimum phase relationship for power output shifts from just under 90 degrees to just over 90 degrees with increasing frequency as shown in Fig. 18a. Although lower frequencies result in lower power output, they are less affected by less than optimum phase relationships. The amount of negative power grows sharply for higher frequencies when the phase angle varies from 100 degrees as shown in Fig. 18b. The total efficiency is optimum at 90 degrees phase for all frequencies above $k = 0.25$ as shown in Fig. 18c. The similarity between the $\overline{C}_P$ and total efficiency plots is due to the fact that the frequency has no effect on the total swept area. The efficiencies due to drag reach an optimum at 90 degrees for lower frequencies, but shift to 108 degrees for higher frequencies with a resulting loss of efficiency. As shown in Fig. 18, the wingmill performance effects due to the phase relationship between pitch and plunge are for the most part independent of the effects due to reduced frequency.
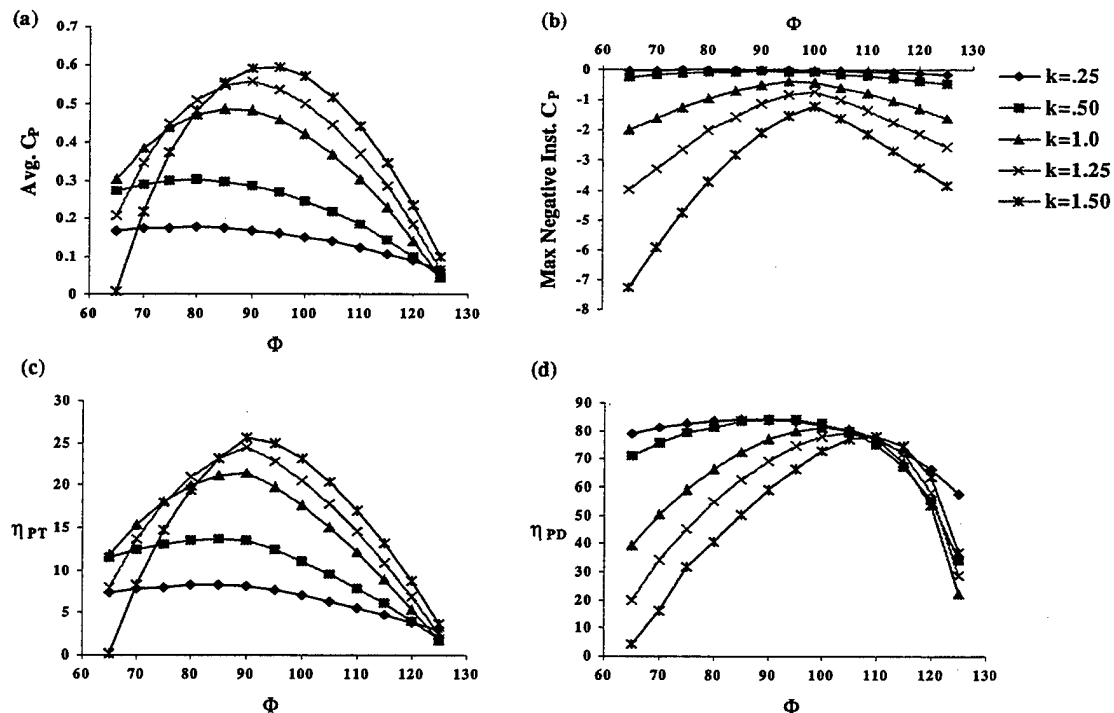
Figure 18. Effect of Phase Angle on Wingmill Performance for Various Reduced Frequencies. $\alpha_e = 15°$, $h = 1.0$, $x_p = 0.5$.

33

5.   Pivot Location

The effect of varying the pivot position on wingmill performance is shown in Fig. 19. Adjusting the pivot location of the wingmill is similar to changing the phase. The maximum power is extracted for ϕ = 90 degrees when the pivot is at 0.3 chord. For phase angles less than 90 degrees the pivot point for optimum $\overline{C}_P$ moves aft of mid-chord. For phase angles greater than 90 degrees, the optimum pivot location moves forward of the leading edge as seen in Fig. 19a. The maximum negative power reaches minimum values when the airfoil comes close to feathering through the flow. For 90 degrees phase this is at the mid-chord. The highest efficiency occurs when the pivot is just before the mid-chord position that can be attributed to the airfoil's thickness. The airfoil's thickness probably also plays a role in the fact that phases under 90 degrees perform better than those over 90 degrees. Efficiencies based on drag reflect the same trends but drop off faster at the aft pivot positions since there the aerodynamic drag of moving the thickest part of the airfoil is higher.
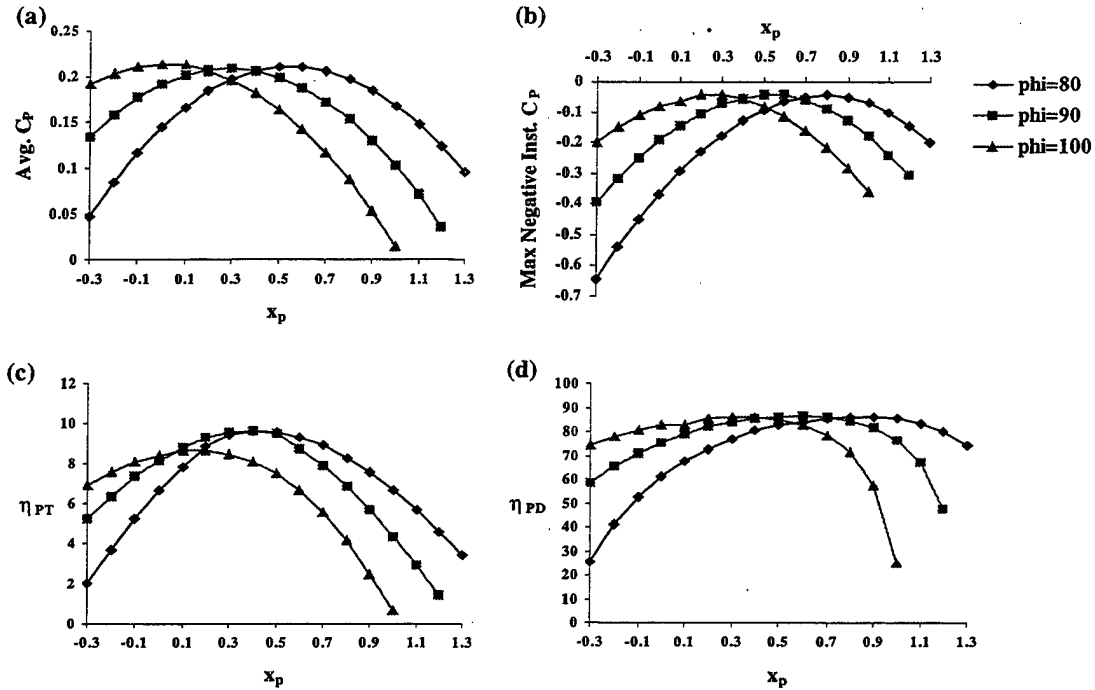
Figure 19. Effect of Pivot Location on Wingmill Performance for Various Phase Angles.
α_e = 10°, k = 0.5, h = 1.0.

B. NUMERICAL ANALYSIS DISCUSSION

1. Parameter Relationships

As is evident from the results, each of the five variable wingmill parameters affects another's ability to influence the performance of the wingmill. An obvious interdependency occurs between the pivot position and the phase angle. Moving the pivot from the leading edge effectively alters the phase. This relationship is shown in Fig. 20 for different pivot positions by plotting the phase angle versus total swept area. For pivot positions forward of the half-chord, phase angles greater than 90 degrees result in the lowest swept area. However, the lowest swept area values do not correspond to optimum performance. This is because the optimum power output occurs with phase angles greater than 90 degrees as shown in Fig 17a.

The minimum swept area is reduced for combinations of phase and pivot position away from 90 degrees phase. This implies that greater efficiency is possible at phase angles other than 90 degrees. However, as seen from Fig. 17, the power extracted is small where the swept area is minimum for phase angles different from 90 degrees. This keeps the optimum efficiency near 90 degrees phase.
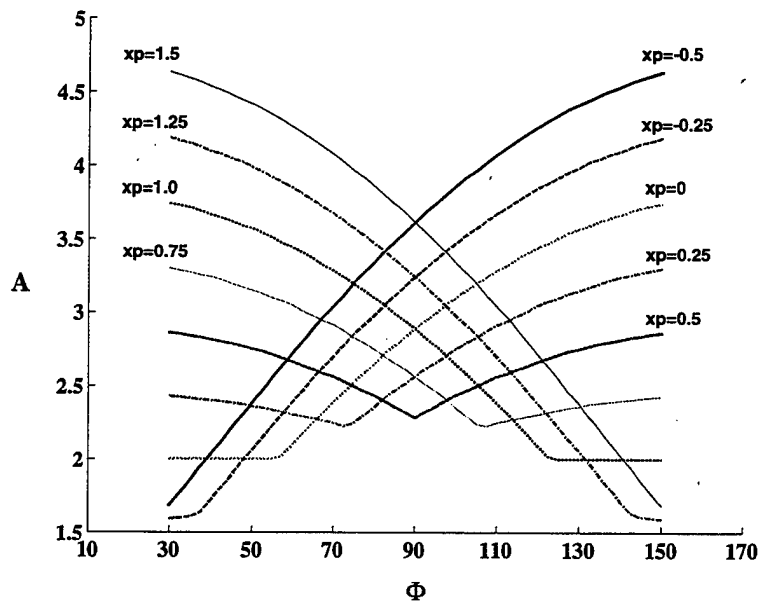
Figure 20. Total Swept Area for Various Phase Angles.

While wingmill performance due to phase is strongly dependent on pivot position, it is independent of the estimated effective angle of attack. An optimum phase setting will remain so at any angle of attack. Therefore, according to the panel code, a wingmill could vary its effective angle of attack according to the power demand without having to adjust the phase angle.

As seen earlier, the wingmill performance due to the pivot position is dependent on the reduced frequency at $k > 0.5$. This is due to the shape of the airfoil and the fact that the center of lift is roughly at the quarter chord point. The maximum performance is generally obtained when the airfoil is pivoting about the half-chord and has about a 90 degree phase relationship between pitch and plunge. This is because the total swept area is minimum at these settings and this holds true at lower reduced frequencies. However, as the reduced frequency is increased, the pitch rate becomes a significant factor in the amount of power transferred between the airfoil and the flow through a cycle. At high frequencies, the pitch rate is faster. Since the center of lift is near the quarter-chord point, airfoils with pivot positions further aft experience a greater moment that helps the airfoil through the pitch change. This is evident by the difference in the maximum negative $\overline{C_P}$ in the cycle dependent on pivot position. At high frequencies, wingmills with pivot positions forward of mid-chord require significantly greater power to pitch through the flow (Fig. 19b).

As described earlier, the effective angle of attack is the key to the ability of an oscillating airfoil to generate power. The angle of attack drives the wingmill. Its influence is critical to the performance of the wingmill but it is difficult to determine the angle of attack's true influence since the effective angle of attack varies throughout the cycle and across the airfoil. The estimated effective angle of attack in this study was generally limited to 15 degrees, near the static stall value of the NACA 0012. The numerical results show that the true effective angle of attack varies significantly from the effective angle of attack based on the plunge velocity. Further, the results show that this variation has significant effects on the performance that are not intuitive. The panel code

36

is able to accurately describe the forces on the airfoil accounting for the true effective angle of attack at all locations on the airfoil. These numerical results are valid only if the flow remains attached. The possibility of detached flow is described in more detail later.

The numerical results show that while the performance characteristics resulting from phase and pivot position are independent of the angle of attack, the performance curves based on reduced frequency and plunge amplitude are dependent on the angle of attack and each other. The numerical results show how the optimum performance of the wingmill varies significantly depending on how the reduced frequency, plunge amplitude, and angle of attack are combined. The significance of the interaction between the frequency, flow speed, and plunge amplitude to unsteady aerodynamics has long been recognized and has been consolidated into a parameter called the Strouhal Number.

2. Strouhal Number

The Strouhal Number is given as

$$St = \frac{h_{TE}\omega c}{2\pi U_\infty} \quad (17)$$

where h_{TE} is the plunge amplitude of the trailing edge of the airfoil. The Strouhal number is generally considered to be the defining parameter in wake dominated flows. The Strouhal number is a measure of the parameters that most affect the wake: flow speed, frequency, and plunge amplitude at the trailing edge. Since the wingmill exhibits high performance when subjected to wake-dominated flows, an analysis of different Strouhal numbers is instructive. To conduct a numerical analysis of wingmill performance variation for a constant Strouhal number using the panel code, the plunge amplitude had to be determined from the desired Strouhal number. Since h_{TE} depends on h, the determination of h requires an iterative process for each data point. To avoid this time-consuming process, values of plunge velocity, hk, were evaluated instead of the Strouhal number. The difference being only that the plunge amplitude at the pivot point defines the parameter rather than the value of h at the trailing edge. A comparison of wingmill efficiency versus k curve for constant $St = 0.5$ with one for constant $hk=0.5$ is plotted in Fig. 21. Note that equal St and hk do not mean equal wingmill parameters, therefore

37

performance magnitudes will vary. The figure shows a relative similarity in shape between *St* and *hk* and therefore the utility of *hk* as a useful performance parameter. The parameter *hk* has an additional benefit to the analysis in that lines of constant *hk* are also lines of constant angle of attack when defined by Eq. 16.

The effect of the reduced frequency on the power coefficient for different lines of constant *hk* is shown in Fig. 22. As the reduced frequency is increased, the plunge amplitude is decreased. More power is produced at high *hk* and high plunge amplitudes. High plunge amplitudes have a detrimental effect on the efficiency as shown in Fig. 22b. Here there is a clear optimal efficiency for a particular *hk* value. The effect of *hk* on both the efficiency and the power coefficient is shown in Fig. 22c. High efficiency and high power are desired, and as seen in Figure 22c, both are improved at higher values of *hk*. The panel code indicates that although increasing values of *hk* continue to provide more power, the efficiency starts to suffer.
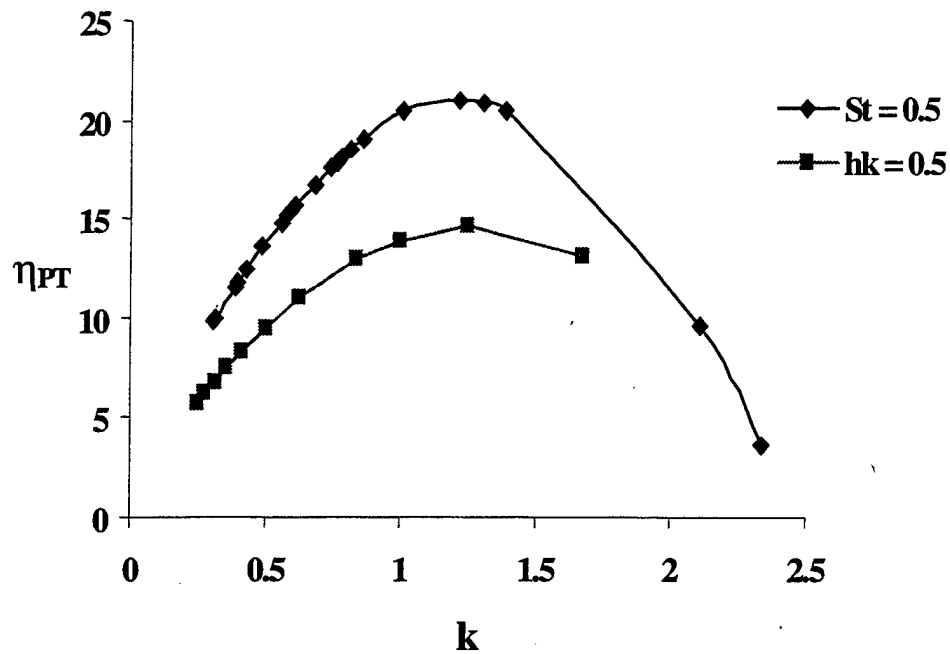
Figure 21. Comparison of *hk* = 0.5 with Strouhal Number of 0.5.
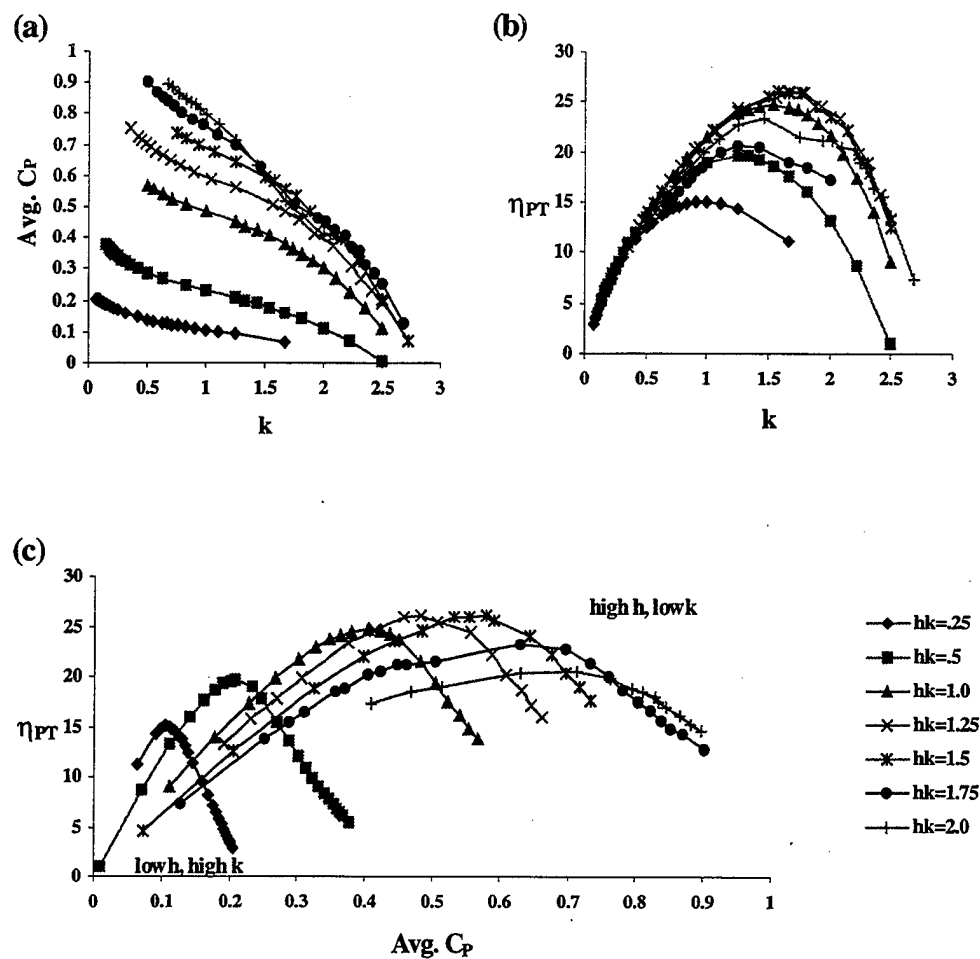
Figure 22. Effect of *hk* on Wingmill Performance.
$\alpha_e = 15°$, $\phi = 90°$, $x_p = 0.5$.

Figure 23 is a contour plot of h versus k. The contour lines are lines of constant total efficiency. A clear optimum efficiency occurs for $h \approx 0.8$ and $k \approx 1.7$. At the lower frequencies, efficiency varies little with h. At higher frequencies, optimum efficiency is highly dependent on h. An increasing frequency results in a greater pitch and plunge acceleration that results in a large negative power input at the plunge extremes if h is big. If h is too small, the airfoil extracts little power from the flow. It is shown on the plot how, as h is varied to either side of the optimum, the efficiency rapidly decreases to zero, eventually putting power into the flow. Thus at optimum conditions, the plunge amplitude is critical. Below optimum conditions the frequency is more critical than plunge amplitude.
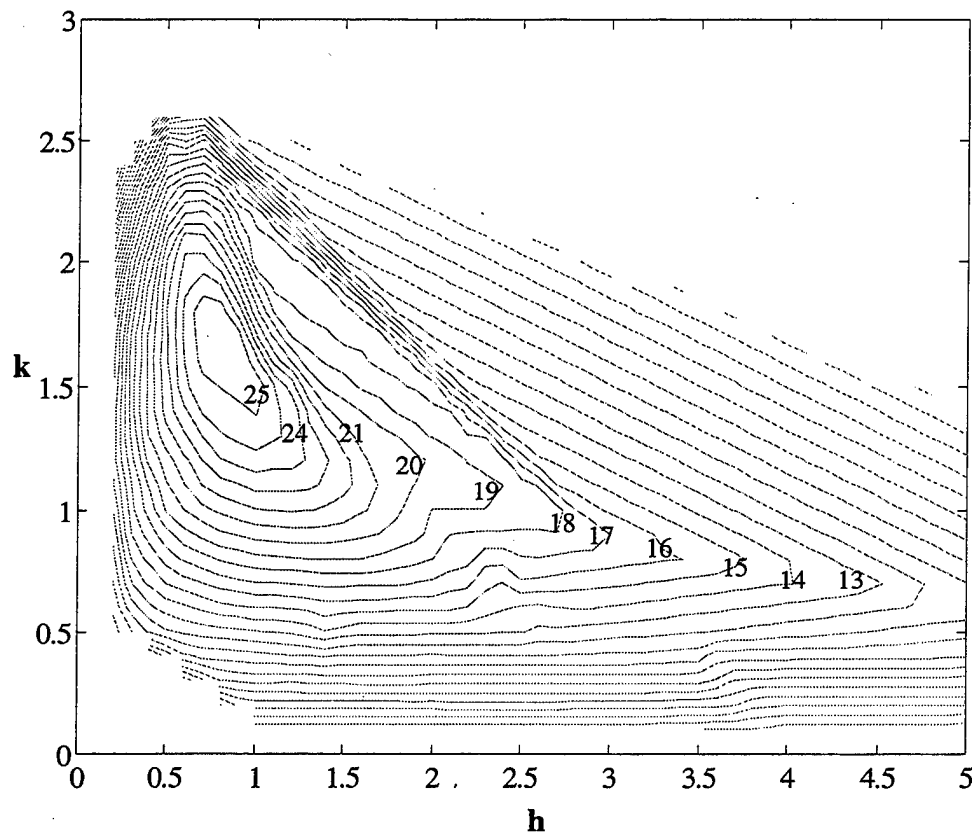
Figure 23. Contour Plot of Wingmill Efficiency for Varying h and k.
$\alpha_e = 15°$, $\phi = 90°$, $x_p = 0.5$.

The analysis of the parameter hk was conducted using an estimated effective angle of attack based on an hk of 15 degrees. The results therefore contain the effects of the true effective angle of attack. As hk gets bigger, the assumption that the effective angle of attack reflects the angle of attack the airfoil sees becomes less valid. Flow separation might occur which would not be modeled by the panel code. Since it is not known if the flow becomes separated at these extreme angles of attack, wingmill performance at high hk will have to be validated by experimental results.

3.   Optimum Wingmill Conditions

A manual optimization technique was conducted using the panel code to find the optimum efficiency based on total power in the flow. The process was started with parameters corresponding to the optimum efficiency from the contour plot in Fig. 23. A baseline configuration was established and each parameter was varied separately a small amount greater and less than the baseline. When the direction that provided an improved efficiency from each parameter was determined, the parameters were changed at once and a new baseline was established. The process was repeated until changing the parameters in either direction offered no improvement. The results are shown in Table 1.

Reduced Frequency (k)	1.975
Plunge Amplitude (h)	0.625
Pivot Location (x_p)	0.55
Phase (ϕ)	94°
Efficiency (η_{PT})	30.01%

Table 1. Optimal Wingmill Conditions from the Panel Code

These optimum conditions were determined using a constant estimated effective angle of attack of 15 degrees. The true effective angle of attack and the likelihood of flow separation will increase at these high frequencies due to high pitch rates. The pivot position and phase angle will further increase the difference between the true and

41

estimated effective angle of attack. This difference means that the wingmill at optimum conditions may see different effective angles of attack than predicted. It is not known if the airfoil will experience static or dynamic stall or if its performance will suffer or benefit.

In general, the optimum wingmill conditions occur around 90 degrees phase with a pivot location around mid-chord. This is where the airfoil extracts the most power for the least amount of swept area. Optimal conditions also occur when the plunge amplitude is just under a chord length, also providing a small swept area. It is intuitive that values for the parameters that provide the least amount of swept area also provide the most efficiency. However, the idea of an optimum reduced frequency and hk value is not intuitive and must be determined through investigation. These frequency parameters have much to do with the wake structure and its influence on the oscillating airfoil. As the values for k are increased from zero, the wake structure improves the performance of the wingmill. But as k values are increased, the wake structure becomes large and the flow velocity small. The most benefit of the wake structure on the performance of the wingmill is realized at frequencies just below those at which the wake structure destroys the wingmill's performance.

4. Limitations and Errors

a. *Comparison to Garrick's Linear Theory*

The comparison of the Unsteady Potential Code to linear theory is well documented for oscillating airfoil propulsion by Jones and Platzer [Ref. 2] and Riester [Ref. 10]. The linear approach of Garrick [Ref. 13] assumes a non-deforming, planar wake and a flat airfoil. UPOT agrees with Garrick's linear theory at low reduced frequencies, but the agreement diminishes as k is increased. This is primarily due to the ability of UPOT to calculate the effects of wake deformation. Referring back to Fig. 6 the wakes at different frequencies are illustrated. It is evident that as the frequency grows, so does the non-linearity of the wake. As discussed by Jones and Platzer [Ref. 2], the wake behind an oscillating airfoil takes the form of a row of vortices of clockwise

rotation above the symmetry plane, and a row of vortices of counter-clockwise rotation below the symmetry plane. This vortex roll-up produces stream-wise and cross-stream forces that are not considered by linear theory. Comparison of UPOT with Garrick's linear theory for the power extraction case is shown in Fig 24. This comparison confirms the same differences from linear theory for the propulsive case exist for the power extraction case. Figure 24 shows that UPOT diverges even more from linear theory with increasing angle of attack. Considering that high angles of attack result in increased power production, the significance of the contribution of vortex roll-up to the performance of the wingmill is apparent in the comparison.
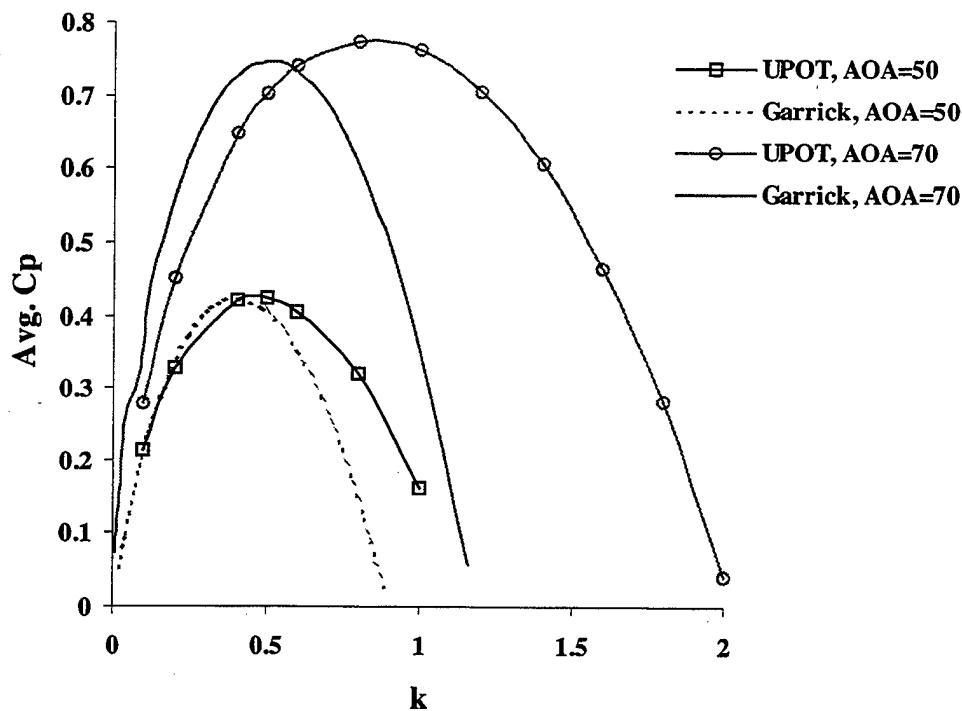
Figure 24. Comparison of UPOT with Garrick's Linear Theory.
$h = 1.0$, $\phi = 90°$, $x_p = 0.5$.

b.   Dynamic stall effects

The numerical analysis was conducted assuming the flow remains attached to the airfoil throughout the cycle. UPOT cannot model detached flow. At the angles of attack analyzed, it cannot be assumed that the flow will remain attached. It is likely that the flow will undergo some sort of dynamic stall. The effect the dynamic stall has on the lift and moment of the airfoil is significant and strongly dependent on the reduced frequency.

Dynamic stall on an airfoil can produce lift and pitching moment values that are much higher than static values. The difference between static and dynamic normal and pitching moments for a NACA 0012 airfoil for $k = 0.3$ is shown in Fig. 25. As seen in the figure, dynamic stall is brought on by a rapid increase in angle of attack past the static stall value. A strong vortex formed at the leading edge is swept over the airfoil and into the wake. At the beginning of this event there is a rapid increase in forces and concludes with an abrupt loss of lift. When the airfoil pitches back to neutral, the forces do not follow the same path since there is a delay for the flow to reattach. [Ref. 12]

The reduced frequency can be thought of as the non-dimensional time needed to convect the disturbance across the airfoil and into the wake. The higher the reduced frequency, the stronger the effects of dynamic stall. The panel code does not consider impending dynamic stall effects when calculating the power of the wingmill. Most of the numerical analysis was conducted keeping the effective angle of attack based on plunge velocity under the static stall values. Since the actual effective angle of attack reaches values well above the static stall value, dynamic stall may occur. If dynamic stall is not reached, the airfoil may still exhibit performance influenced by impending dynamic stall, recovering before the flow completely separates. If dynamic stall occurs, its presence will be evident in the experimental results and flow visualization.

44
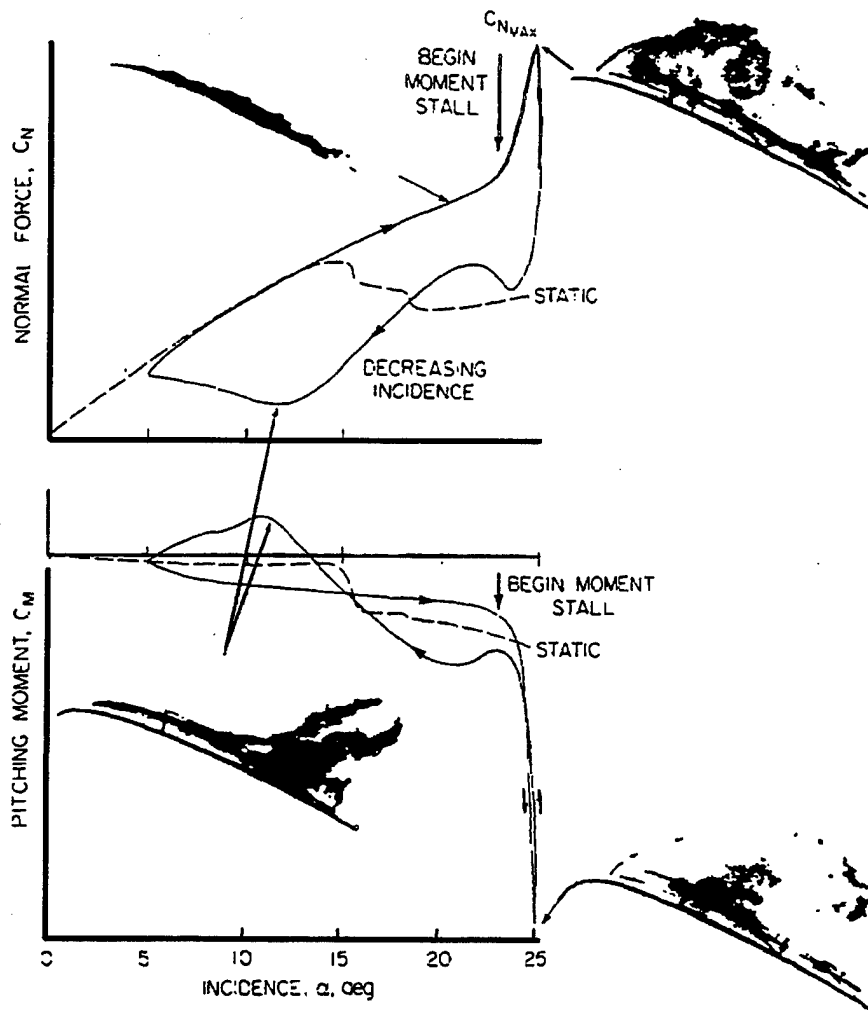
Figure 25. Typical static and dynamic variation of normal force and pitching moment as a function of α for NACA 0012 airfoil. $k = 0.3$, Re = 2.5×10^6. From Ref. 14.

45

VI. EXPERIMENTAL APPARATUS

A. OSCILLATING WING POWER GENERATOR

Experimental data was obtained from an oscillating wing flutter generator designed at the Naval Postgraduate School by Dr. Kevin Jones. Figure 26 is a schematic and Fig. 27 is a photograph of the flutter generator. The mechanism consists of an airfoil that is able to move in a coupled pitch and plunge motion. The airfoil is a section of a model helicopter rotor blade that has a smooth graphite-epoxy skin over a light foam core. The symmetric airfoil with a cusped trailing edge is approximately 14% thick, with the maximum thickness at about $0.35c$. The chord length is 62mm and the span is 350 mm, resulting in an aspect ratio of about 5.6 and a wing area of 0.0217 m^2. Attached to each tip of the airfoil are aluminum blocks that contain mounting points for bearings that fit into slots in rails mounted to the tunnel wall. These bearings can be adjusted from $-0.1c$ to $1.0c$ to allow the pivot position to vary. The aluminum blocks provide a place to connect the airfoil to the rest of the mechanism. Thin, airfoiled push-rods attach the airfoil via ball-joints to the swing arm of the mechanism. An aluminum plate mounted on the opposite side of the swing arm pivot counterbalances the swing arm and airfoil. Through a push-rod and an intermediate swing arm, the rocking swing arm rotates a phasing gear which through another gear, rotates the main shaft. Since the power-stroke is sinusoidal, the model will not have a fixed angular velocity. The main shaft has a flywheel to smooth out the cycle at the extremes of the plunge amplitude. On one end of the shaft is the pitch arm which through a linkage drives a bell-crank back and forth. The bell-crank is located on the end of the swing arm above the airfoil. A thin airfoiled push-rod connects the trailing edge of the airfoil with the bell-crank. When the airfoil plunges up and down, the swing arm moves with it, turning the main shaft and the pitch arm. The pitch arm moves the bell-crank back and forth, which in turn pitches the airfoil. Springs are used to conserve energy at the plunge extremes. Adjustment screws on the springs allow the system to be tuned. There is also a spring over-ride coupling installed on the push-rod that attaches the intermediate swing arm to the phasing gear. This allows the

flutter generator to under/overshoot the prescribed value slightly, relieving the stress on the push-rods. [Ref. 13]
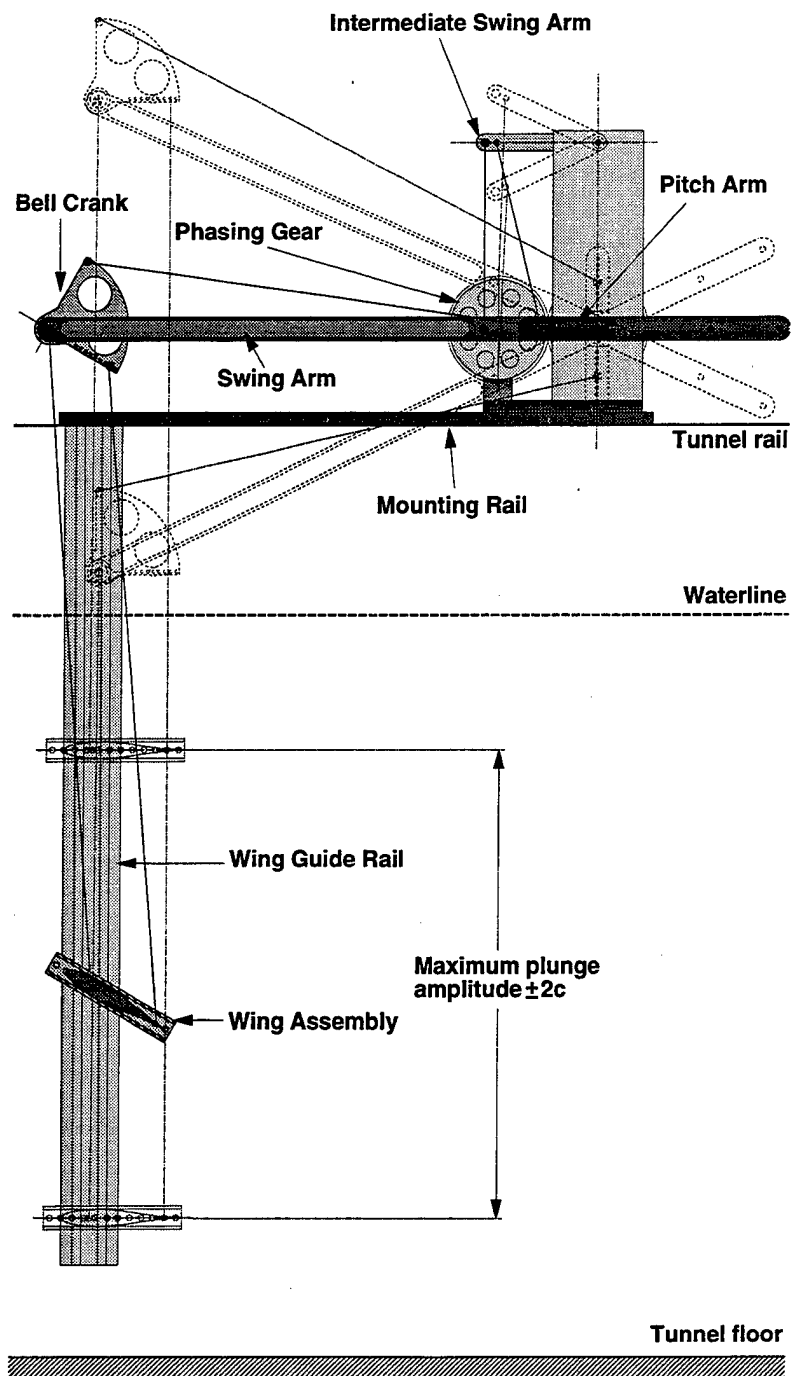
Figure 26. Schematic of the Flutter Generator. From Ref. 11.
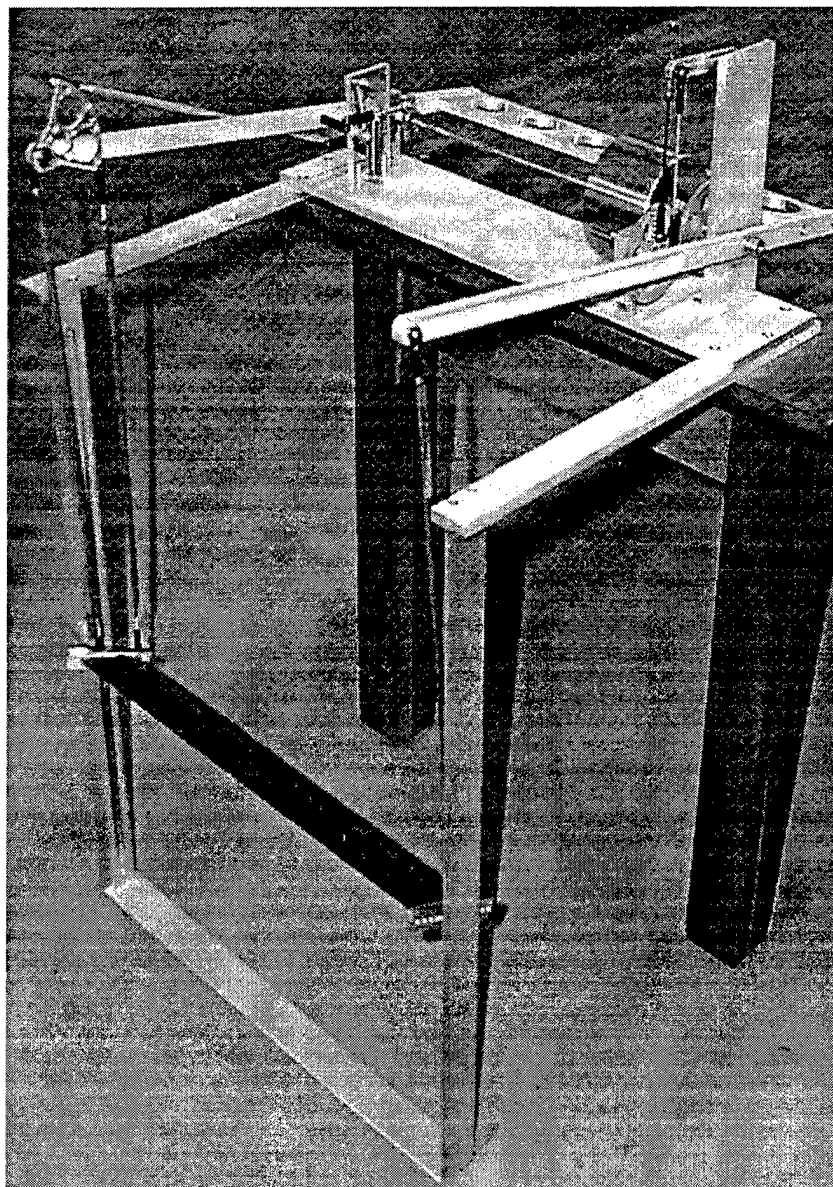
Figure 27. Photograph of the Flutter Generator. From Ref. 11.

The airfoil on the flutter generator is capable of pitch amplitudes of ±65 degrees and plunge amplitudes of ±125mm. The pivot position can be adjusted between −0.1c to 1.0c. The phase can be adjusted incrementally by shifting teeth between the phasing gear and the gear on the main shaft; and infinitesimally by adjusting the pitch arm with a set screw.

While the plunging motion of the flutter generator is sinusoidal, the pitching motion is not. The translation of the pitch arm to the bell-crank via a push-rod introduces non-linear motion. This causes a different phase relationship between the pitch and plunge motions at the top of the cycle from the bottom of the cycle. By adjusting the linkages, the phase relationships can be made the same, but this causes a difference in pitch between the upstroke and the downstroke.

B. WATER TUNNEL

The flutter generator was operated in the water tunnel in the Hydrodynamics Laboratory at the Naval Postgraduate School. The water tunnel is a continuous flow, closed circuit system with horizontal orientation. The test section is 38 cm wide and 127 cm long, with a nominal water depth of 30.5 cm. The walls and bottom are made of plexiglass and the top is open. The rails that guide the airfoil are mounted to the test section walls and the flutter generator is mounted to the top of the walls. To remove large scale disturbances, the flow passes through two honeycomb screens; one within the converging section and one just upstream of the test section . The flow speed is controlled by a handle on the drive motor enabling the flow velocity to be varied from zero to over 3 ft/s. Figure 28 is a photograph of the water tunnel with the flutter generator installed.
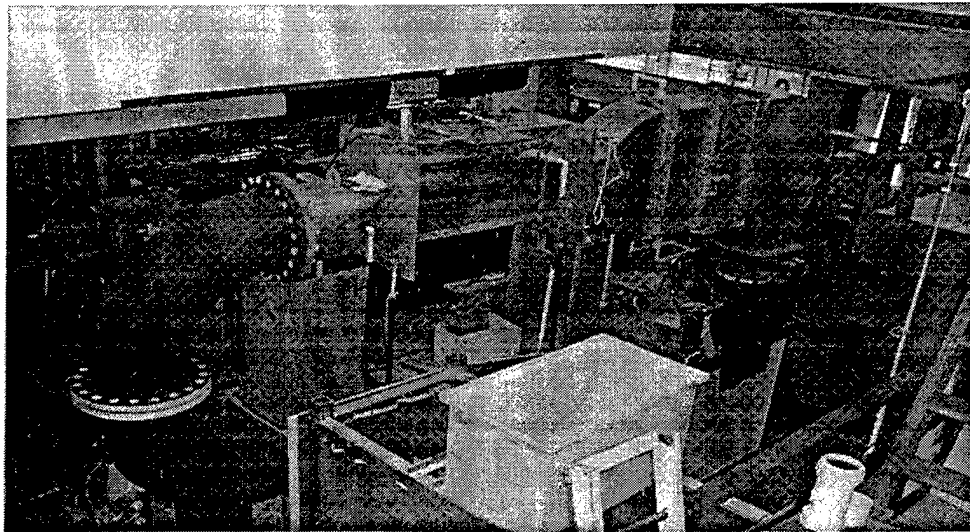
Figure 28. Naval Postgraduate School Hydrodynamics Laboratory Water Tunnel.

50

C.   PERFORMANCE MEASUREMENT

The power output of the oscillating flutter generator is determined as follows: The main shaft of the flutter generator is connected via gearing to a three pole electric motor which is driven as a generator. Two different resistances can be applied to load the motor, 0.011 ohm and 0.02 ohm. The voltage produced by the generator is read by a DSO-2102 digital storage oscilloscope and stored in a file. The root mean square voltage is evaluated over several cycles. The total efficiency is determined by dividing the product of the power coefficient and the chord length by the total swept area as given by Eq. 13. The total swept area is measured with a ruler and a protractor from direct examination of the motion of the airfoil.

The motor was calibrated using a direct torque measurement method. The flutter generator was partially disassembled to isolate the motor. Weights of known mass were attached to a lightweight nylon line which was wrapped around the flywheel. The different weights were dropped and allowed to reach terminal velocity with each of the resistances applied. A magnetic reed switch was mounted to the flywheel and connected to a power source and the oscilloscope, sending a signal to the oscilloscope at each rotation. The digital oscilloscope recorded the voltage signal from the motor and measured the rotation speed of the flywheel. The rotation and motor output signals were obtained for several different weights and used to plot a calibration curve. Figure 29 is the motor calibration curve plotted for each resistance using the following expressions:

$$P_{IN} = (\text{Torque})(\text{rotation speed})$$
$$= (\text{mass})(\text{gravitational constant of Earth})(\text{radius})(\text{frequency})(2\pi) \quad (18)$$
$$P_{OUT} = (\text{Volts})^2/\text{resistance} \quad (19)$$

The error bars indicate the average deviation of the signal recorded by the digital oscilloscope.
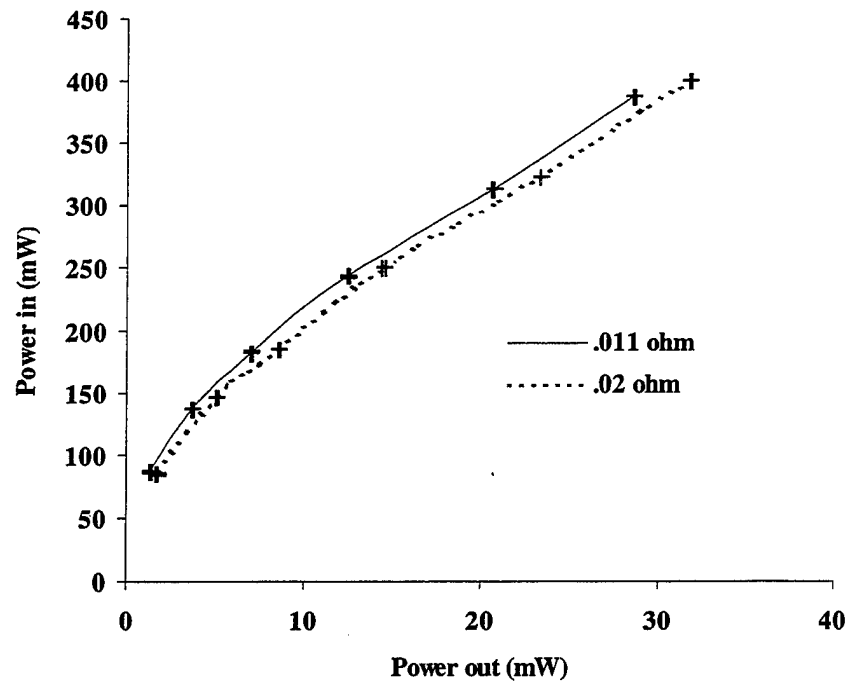
Figure 29. Motor Calibration Curves for Resistances of 0.011 Ω and 0.02 Ω.

The flow speed was determined using a Model 512 OEM electromagnetic water current meter made by Marsh-McBirney, Inc. The current meter generates a magnetic field in the flow. The flowing water acts as a conductor in the magnetic field and produces a voltage which is proportional to its velocity. The voltage is recorded by the digital oscilloscope. The electromagnetic water current meter is accurate to within ±0.07 ft/sec.

The performance of the flutter generator was determined from the signal of typically 40 cycles recorded by the digital oscilloscope. The time-averaged power output from the motor was found from the root mean square of the voltage output. The power that the flutter generator delivered to the motor was determined using the calibration curve. The time-averaged power coefficient, $\overline{C_P}$, was found from the time-averaged power output, the surface area of the airfoil, S, and the flow velocity, V_∞, using Eq. 11. The total efficiency was determined from $\overline{C_P}$, measured A, and the surface area of the airfoil, S, using Eq. 13.

52

VII. EXPERIMENTAL RESULTS

Due to a flood that damaged the water tunnel where the experiment was to originally take place, the experiment was delayed. When an alternate water tunnel was found and the necessary model modifications were made, time permitted obtaining only a sampling of experimental data for each parameter. The plots show experimental points of the wingmill at various configurations under two loads. The error bars indicate the average deviation of the output signal added to the average deviation of the motor calibration.

A. ANGLE OF ATTACK

For the experiment, $\Delta\alpha$ was defined as the angle of attack of the airfoil to the flow at the zero plunge position. The angle of attack was adjusted by changing the pitch-rod attachment point on the bell-crank and the pitch arm. Due to the non-sinusoidal pitch motion, the angle of attack measured on the upstroke was often different from that measured on the downstroke. As a result, the push-rod linkages themselves were adjusted until the angle of attack on the upstroke and downstroke were within one degree of each other. This method allowed the angle of attack to be varied while leaving the phase angle relatively constant. The angle of attack is expressed as the effective angle of attack based on plunge velocity as given by Eq. 16. The power coefficient and total efficiency are plotted for various effective angles of attack in Figs. 30a and 30b. The power and total efficiency generally increase as angle of attack increases. The plots of $\overline{C}_P$ and η_{PT} are similar due to the linear change in swept area with change in angle of attack. Since the load on the motor cannot vary infinitesimally, it was not possible to keep the reduced frequency constant while varying other parameters. The reduced frequency increased from $k \approx 0.62$ to $k \approx 1.5$ causing the effective angle of attack to change. The total efficiency for various estimated effective angles of attack is plotted in Fig. 30c. At $\alpha_e \approx 23$ degrees, total efficiency decreases. Notice that this α_e is well above the static stall limit of 15 degrees. It is probable that the airfoil is experiencing a

53
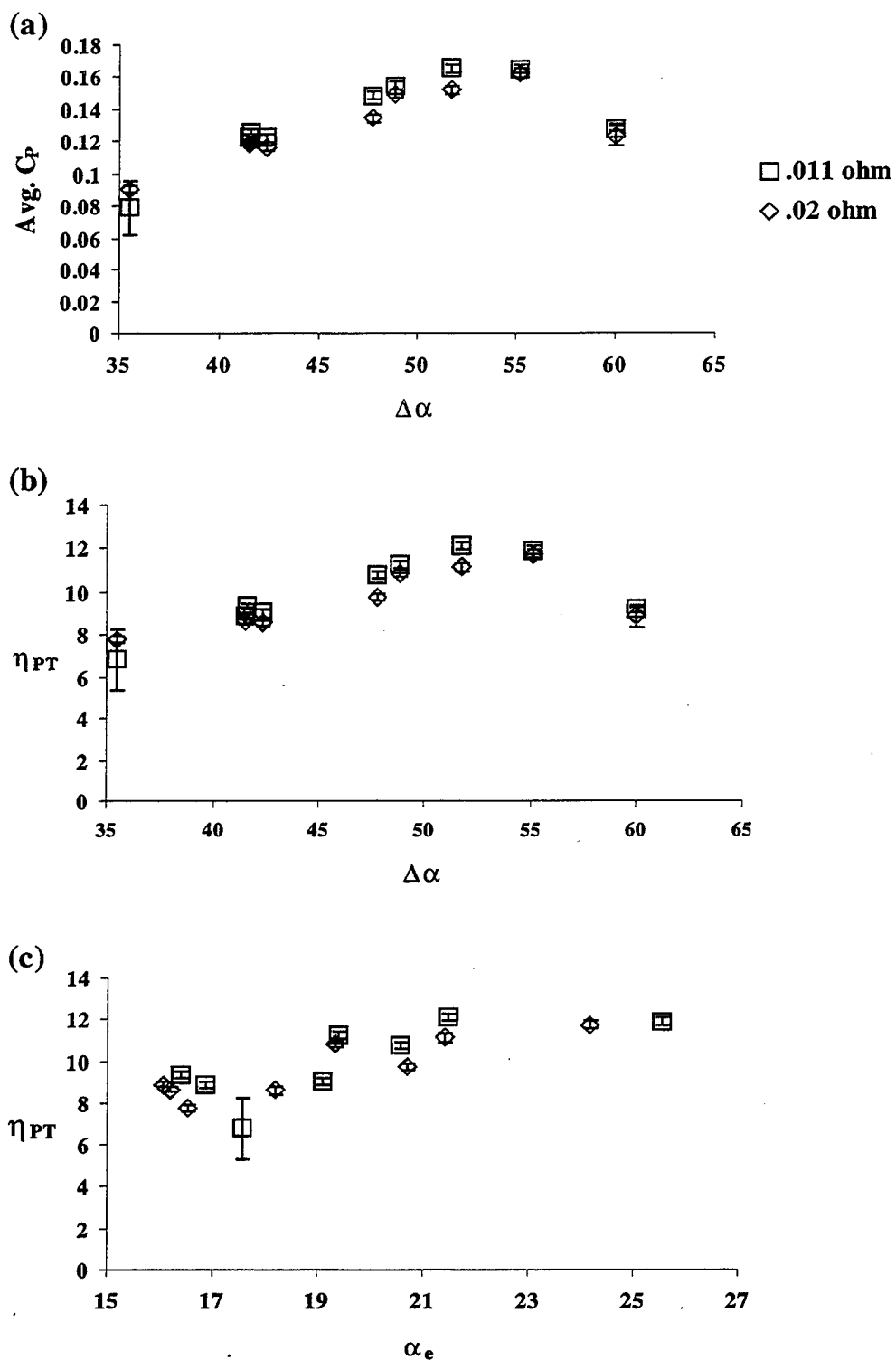
Figure 30. Experimental Results of Wingmill Performance Due to Effective Angle of Attack. $h = 0.526$, $x_p = 0.51$, $\phi = 90°$.

reduction in performance due to dynamic stall as described by Fig. 25, but is impossible to confirm without flow visualization. Reference 14 shows the NACA 0012 airfoil experiences dynamic stall just under $\alpha = 25$ degrees for various reduced frequencies.

The power coefficient and total efficiency plots are similar due to the small change in swept area. The non-linear pitch motion results in the swept area changing very little due to angle of attack variation.

B.   REDUCED FREQUENCY

The reduced frequency of the flutter generator was varied by changing the freestream velocity of the flow and the load on the model. The freestream velocity was easily adjusted with the tunnel motor and measured by the current meter through the digital oscilloscope. As the velocity increased, so did the frequency of the flutter generator. Since the load can only vary between two resistances, 0.011 Ω and 0.02 Ω, the full range of reduced frequencies could not be explored. The model was unable to oscillate at reduced frequencies less than $k \approx 0.8$. This lower limit was due partially to inadequate load on the motor and partially to mechanical friction of the device becoming dominant at low frequencies. As shown in Fig. 31a, performance does not improve with an increase in reduced frequency. As the reduced frequency increases, the geometric angle of attack remains constant while the induced angle of attack increases. Therefore the effective angle of attack decreases with increasing reduced frequency. The decreasing effective angle of attack prevents the wingmill from receiving a performance benefit as would be expected from increasing k. Additionally, inertial losses prevented the wingmill from oscillating at a faster rate. Although the device produced more power through the power stroke with increased frequency as seen in Fig. 31b, it lost a great deal of momentum at the plunge extremes, effectively reducing the frequency of oscillation. As the flow speed was further increased beyond the high frequency limit of the wingmill, the power coefficient decreased (Eq. 11).

(a)

(b)
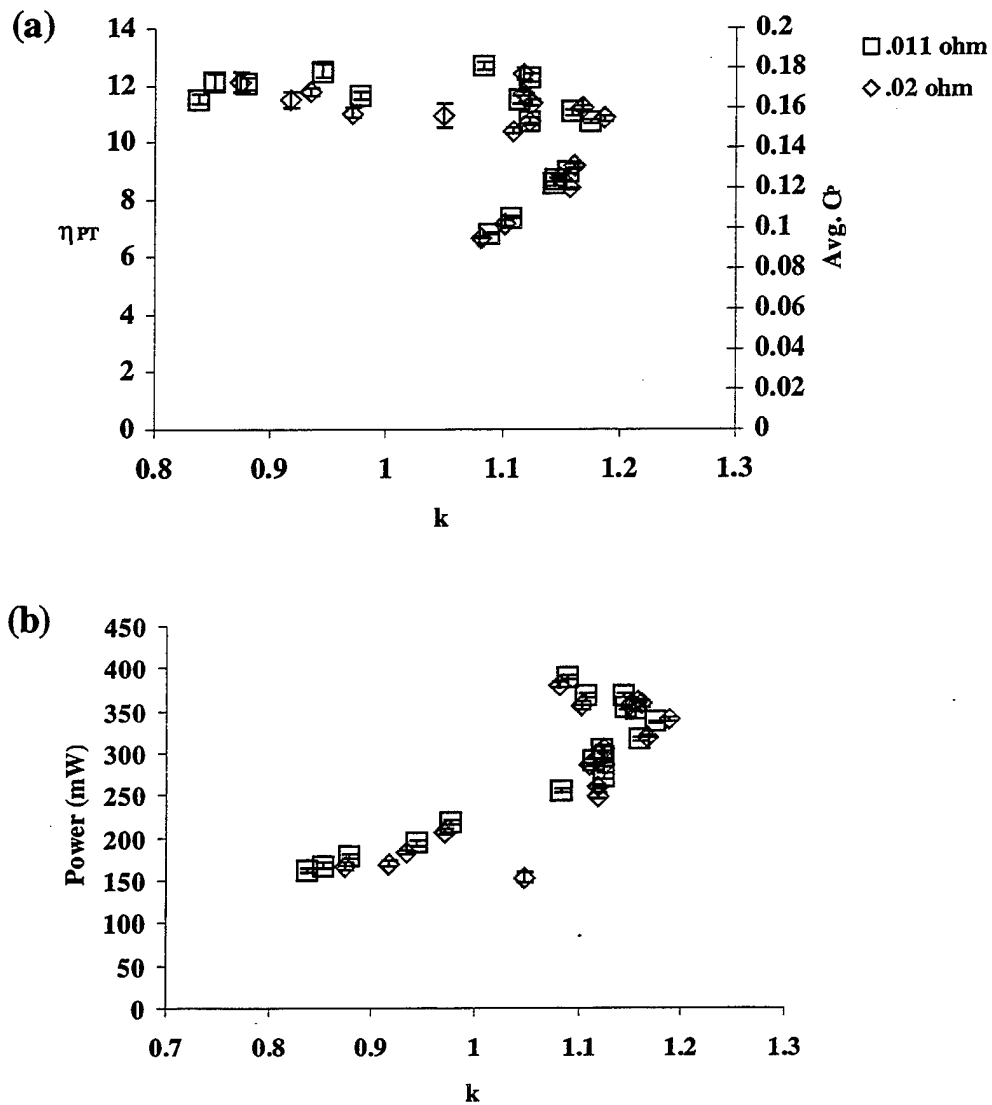
Figure 31. Experimental Results of Wingmill Performance Due to Reduced Frequency.
$h = 0.526$, $x_p = 0.51$, $\phi = 90°$.

C. PLUNGE AMPLITUDE

The non-linear pitching motion of the flutter generator required a modified definition of phase angle. Since a true 90 degree phase difference between pitch and plunge was not possible, 90 degrees phase was defined as existing when the angles of attack were as close to zero as possible at top and bottom dead center. This was done

56

while keeping the maximum pitch amplitude equal for the upstroke and the downstroke. This resulted in a small positive angle of attack at top and bottom dead center for the defined 90 degree phase angle. As the airfoil plunges downward, there is still a positive angle of attack causing lift in the opposite direction of motion. At greater plunge amplitudes this opposing lift exists for a greater distance, therefore the overall negative power in the cycle is increased. Recall the increase of negative power due to phase variation shown in Fig. 18b. During the experiment, the airfoil accelerated rapidly through the mean plunge position, then stopped abruptly for an instant until the momentum of the flywheel pitched the airfoil through top and bottom dead center. When the plunge amplitude was increased further, the negative power requirement grew until the airfoil stalled just past top dead center. Wingmill performance due to change in plunge amplitude is shown in Fig. 32. Since the average power coefficient remains constant for the plunge amplitudes tested (Fig. 32a), there is a steady decrease in performance for increasing plunge amplitudes (Fig. 32b).

(a)

(b)
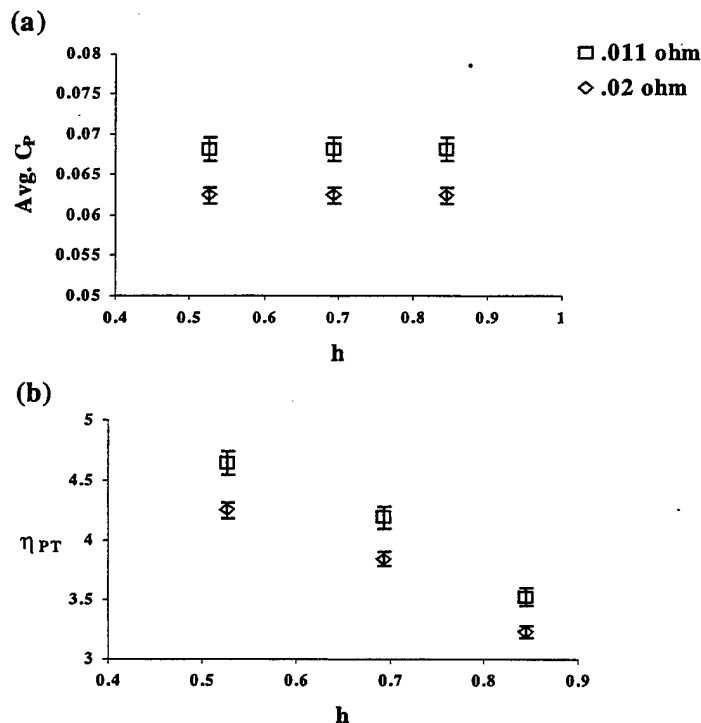
Figure 32. Experimental Results of Wingmill Performance Due to Plunge Amplitude.
$\Delta\alpha = 57^\circ$, $x_p = 0.51$, $\phi = 90^\circ$.

57

D. PHASE RELATION AND PIVOT LOCATION

The phase relationship was varied for two pivot locations, $x_p = 0.41$ and $x_p = 0.51$. As discussed in the previous section, the method of selecting the definition of phase angle was arbitrary and based more on smooth operation of the airfoil than on geometric considerations. The performance effect due to phase angle variation for a pivot location of $x_p = 0.51$ is shown in Fig. 33. The generator appears to perform slightly better at phase angles between 90 and 95 degrees. Once 90 degrees phase was set, adjusting the gear teeth between the phasing gear and the gear on the main shaft varied the phase. As a result, the phase angle at top dead center was not the same as the phase angle at bottom dead center.
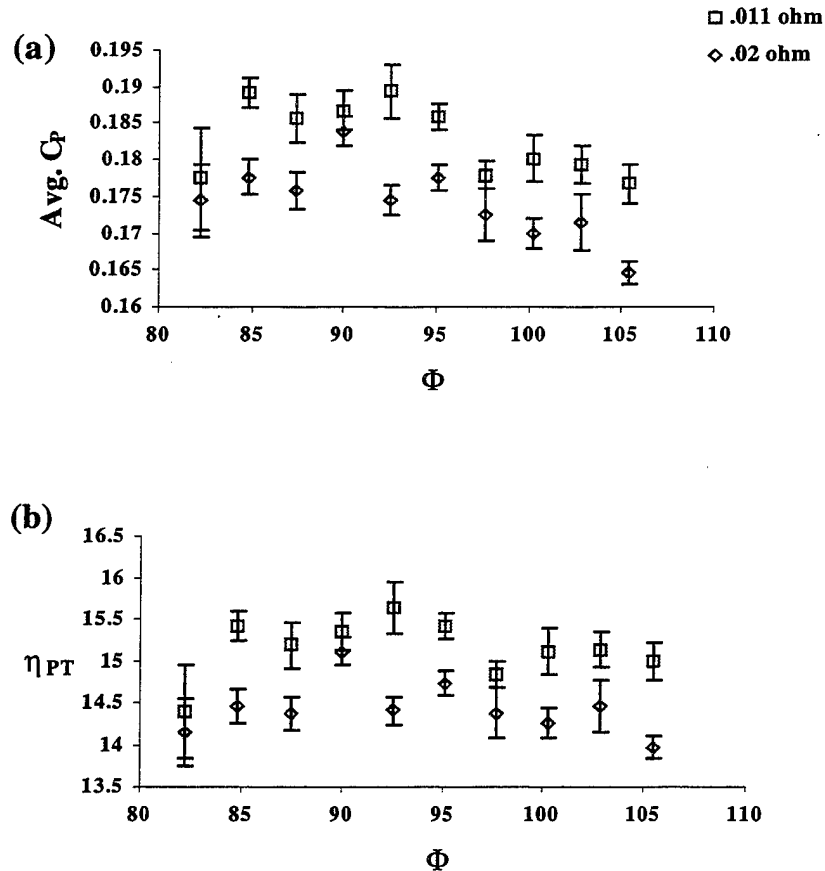
Figure 33. Experimental Results of Wingmill Performance Due to Phase.
$\Delta\alpha = 49°$, $x_p = 0.51$, $\phi = 90°$.

58

The results are consistent with the method the phase angle was defined. When the angle of attack was equal at the zero plunge position on the upstroke and downstroke, the phase angle was considered to be 90 degrees. From this position the teeth of the phasing gear and the main shaft gear were shifted. The resulting phase shift was different for the top and bottom of the cycle. Shifting the mesh of the phasing gear also altered the angle of attack. Although other variables influencing the wingmill's performance are present, the plot does show that the wingmill is responsive to phase variation.
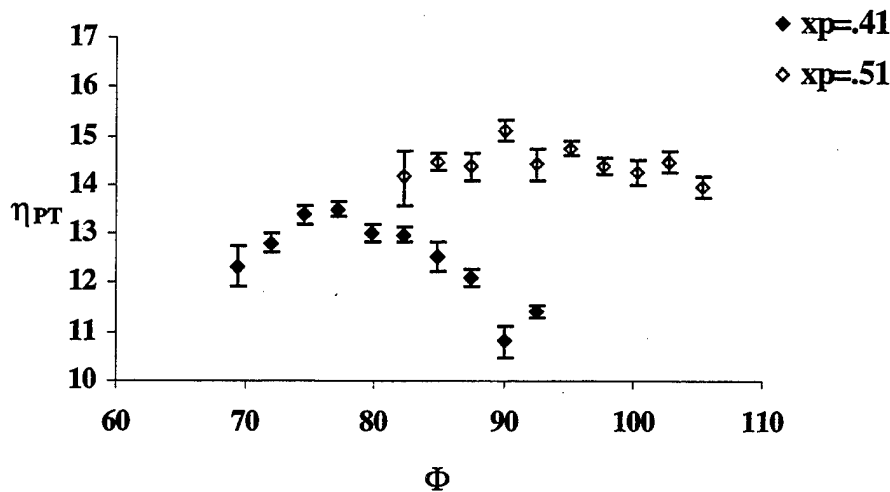
Figure 34. Experimental Results of Wingmill Total Efficiency Due to Phase for Different Pivot Positions. $\Delta\alpha = 49°$, $\phi = 90°$.

This sensitivity to phase angle is more apparent for pivot locations other than at midchord. The performance variation with phase with pivot positions $x_p = 0.41$ and $x_p = 0.51$ are compared in Fig. 34. As expected the pivot location at midchord has a better overall total efficiency than the flutter generator pivoting at $x_p = 0.41$. The wingmill with $x_p = 0.41$ is more sensitive to phase variation, with a peak in performance occurring at $\phi = 78$ degrees.

VIII.   COMPARISON OF EXPERIMENTAL RESULTS TO THEORY

Due to the dissimilar motion between the flutter generator and the panel code, only limited similarity exists when the experiment is compared to UPOT. As described in the previous chapter, the differences arise from the non-sinusoidal velocity and pitch amplitude of the flutter generator. The wingmill is also subject to dynamic stall which further increases the variation from the numerical results. Another factor that exists in the experiment, which is not part of the panel code's solution, is the effect on the wingmill's performance of the mass of the fluid displaced by the oscillating airfoil. This 'apparent mass' can be significant depending on the density of the fluid. Another loss the wingmill experiences that UPOT does not model is the friction of the mechanism. Especially at higher angles of attack, the mechanical friction from the motion of the push-rods and gears of the wingmill restrict its movement. A more significant loss than friction is the mass of the mechanism. The mass of the airfoil, the swing arm, and associated push-rods which must be accelerated through the cycle is not considered by UPOT.
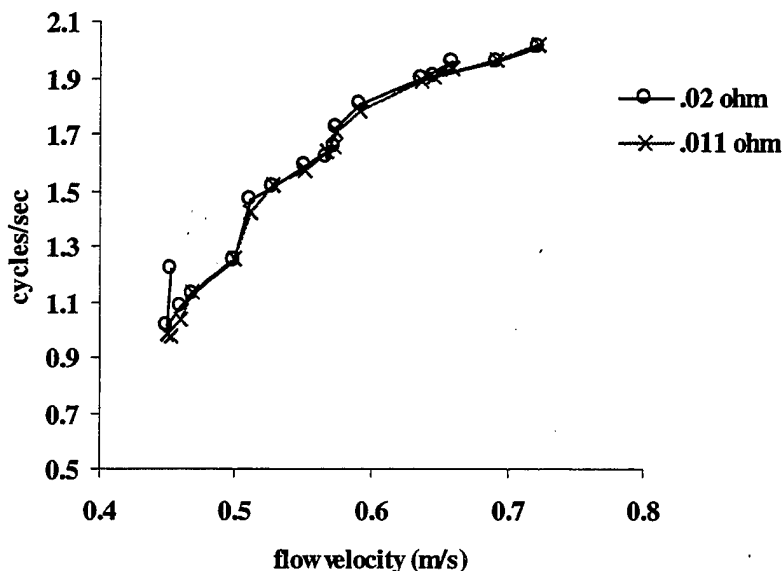
Figure 35. Comparison of the Effect of Different Loads on Wingmill Oscillatory Velocity.

61

In general, the performance measurements obtained from the experiment were significantly lower than the measurements obtained from the panel code. This is because not all the power available to the flutter generator was extracted due to insufficient loads on the motor. Figure 35 is a plot of the oscillation speed of the flutter generator for different flow speeds for resistances 0.011 Ω and 0.02 Ω. When the resistance is switched from 0.02Ω to 0.011Ω, the load on the generator is doubled, yet the frequency does not slow down considerably. The similarity of the plots indicates that the flutter generator is capable of extracting more power from the flow than is currently being extracted.

To compare the panel code with the flutter generator, five parameters variable in UPOT were matched to include the reduced frequency which varied for each experimental point. The comparison between UPOT and experimental results for wingmill performance of varying angles of attack are shown in Figs. 36a and 36b. Both cases experience an increase in performance due to increasing the angle of attack. The total efficiency for UPOT and the experiment is plotted against the effective angle of attack in Fig. 36c. At $\alpha_e \approx 23$ degrees, performance decreases for the experimental model, possibly due to dynamic stall. Since the panel code does not model dynamic stall, its performance continues to increase with the angle of attack until diminishing due to induced camber effects creating a moment in the opposite direction of the pitching motion. The magnitude difference can be attributed to the losses described above and the non-sinusoidal pitch motion of the flutter generator.
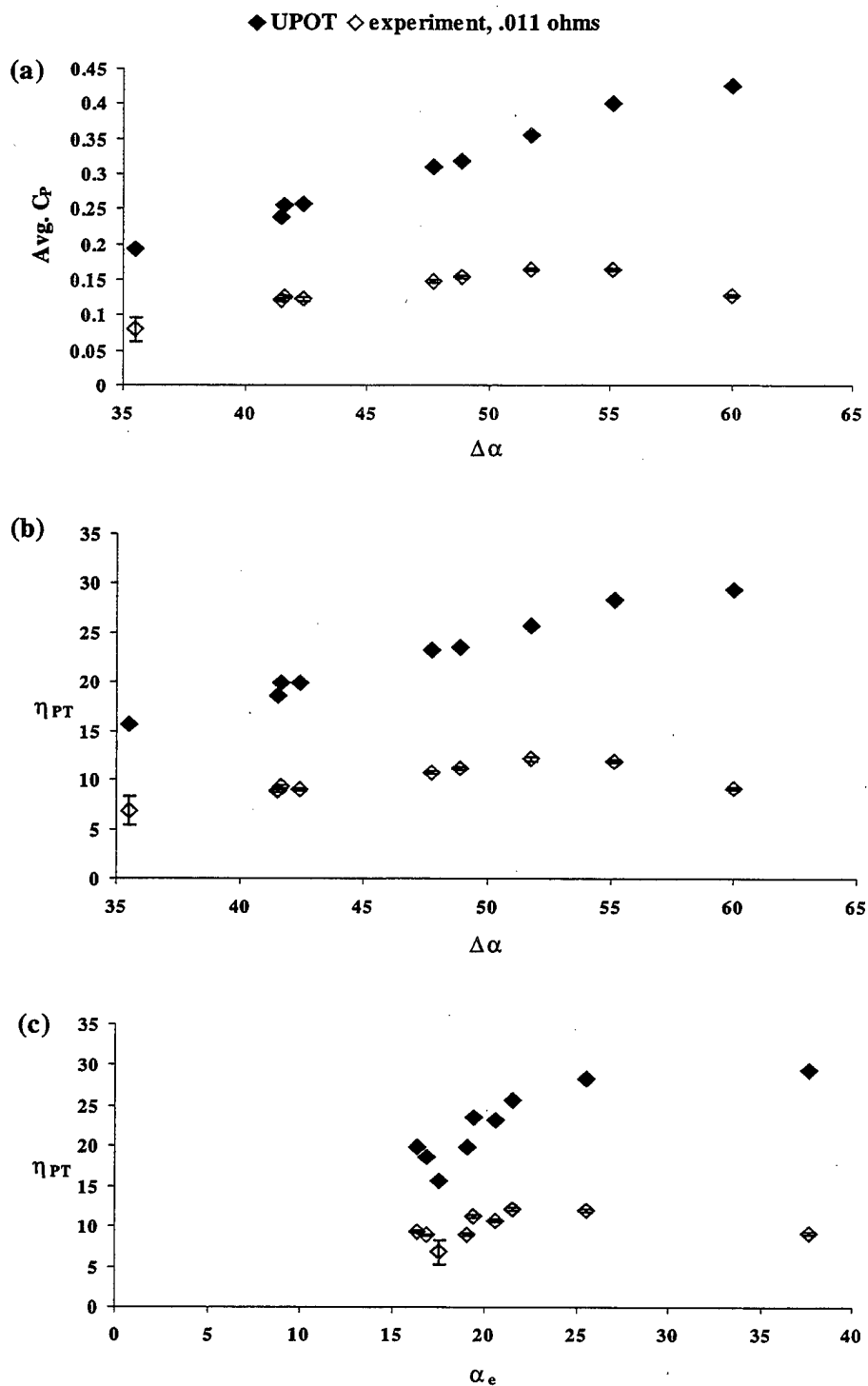
Figure 36. Comparison of the Experimental and Numerical Results of Wingmill Performance Due to Effective Angle of Attack. $h = 0.526$, $\phi = 90°$, $x_p = 0.526$.

The comparison of the measured and computed effect of the reduced frequency variation on wingmill performance is shown in Fig. 37. Previous numerical results demonstrated a performance benefit with increasing reduced frequency. Both the experimental and numerical results indicate a steady performance level for the range of reduced frequencies tested. The group of lower performance values from the experimental model at higher reduced frequencies is due to the mechanical limitations of the flutter generator. These points are the result of the wingmill reaching a limit where it is no longer able to achieve higher frequencies with increasing flow speed. Although the actual power absorbed continues to increase as seen in Fig. 31b, the $\overline{C}_p$, which is dependent on the flow speed, decreases. A large amount of power available to the wingmill is wasted at its endpoints where the airfoil almost comes to a complete stop while it changes plunge direction. The tuning springs were intended to conserve this energy loss, but did not have the desired effect. This was primarily due to the inability of the model to achieve an optimum phase relationship between pitch and plunge. Increasing the flow velocity exacerbated the negative effect of the non-linear phase relationship.
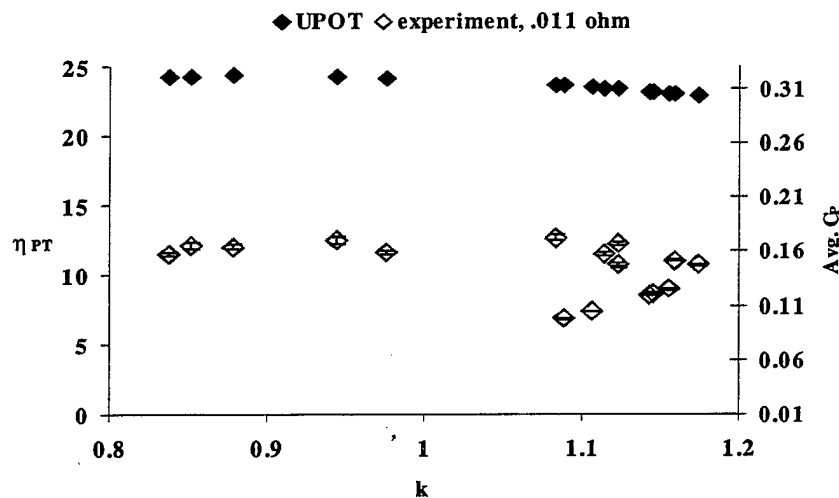
Figure 37. Comparison of the Experimental and Numerical Results of Wingmill Performance Due to Reduced Frequency. $\Delta\alpha = 49°$, $h = .526$, $\phi = 90°$, $x_p = 0.51$.

64

The wingmill may also be reaching a reduced frequency limit aerodynamically. As discussed earlier, higher reduced frequency results in lower effective angles of attack. There will be a reduced frequency where the effective angle of attack becomes too small to further increase the frequency with an increase in flow speed. Provided the wingmill can withstand it structurally, the frequency can be increased by increasing the angle of attack. Since the angle of attack cannot be increased indefinitely, the wingmill has a frequency limit based on angle of attack as well as mechanical limitations.

The comparison of numerical and experimental results of wingmill performance due to plunge amplitude is shown in Fig. 38. The comparison of $\overline{C_P}$ in Fig. 38a shows a large discrepancy in magnitude and trend. The panel code predicts $\overline{C_P}$ to increase with plunge amplitude, whereas the flutter generator shows no change. In the experiment, the wingmill did not operate well at high plunge amplitudes. Once again the difference can be attributed to the non-sinusoidal pitch motion. Additionally, at high plunge amplitudes, the effects of apparent mass will have more of an impact on wingmill performance than at low plunge amplitudes. The trends for total efficiency are similar for the experiment and numerical models as seen in Fig. 38b. However, the magnitudes are much different due the friction, non-linear phase relationships, apparent mass, and momentum loss at the end points.
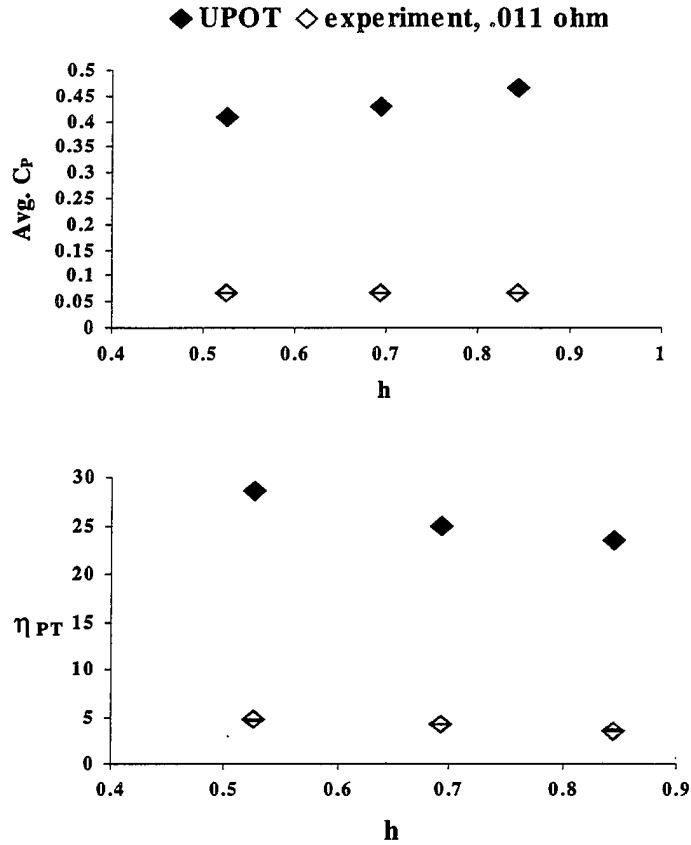
Figure 38. Comparison of Experimental and Numerical Results of Wingmill Performance Due to Plunge Amplitude. $\Delta\alpha = 56.75$, $\phi = 95.14°$, $x_p = 0.51$.

Experimental and numerical results for performance dependent on phase angle are compared in Fig. 39. Since the definition of 90 degrees phase for the experiment as well as the non-linear phase relationship cannot be duplicated by UPOT, the comparison is of limited use. It can be noted, however, that all other parameters being equal, both the numerical and experimental models are relatively insensitive to phase angle variation while pivoting at midchord. This differs from the case where the airfoil pivots at $x_p = 0.41$. Figure 40 is a comparison of experimental and numerical results of wingmill performance with phase variation for $x_p = 0.41$. Although the phase relationship is dissimilar, both the experimental and numerical results show a greater dependency on phase angle if the pivot is away from half-chord.
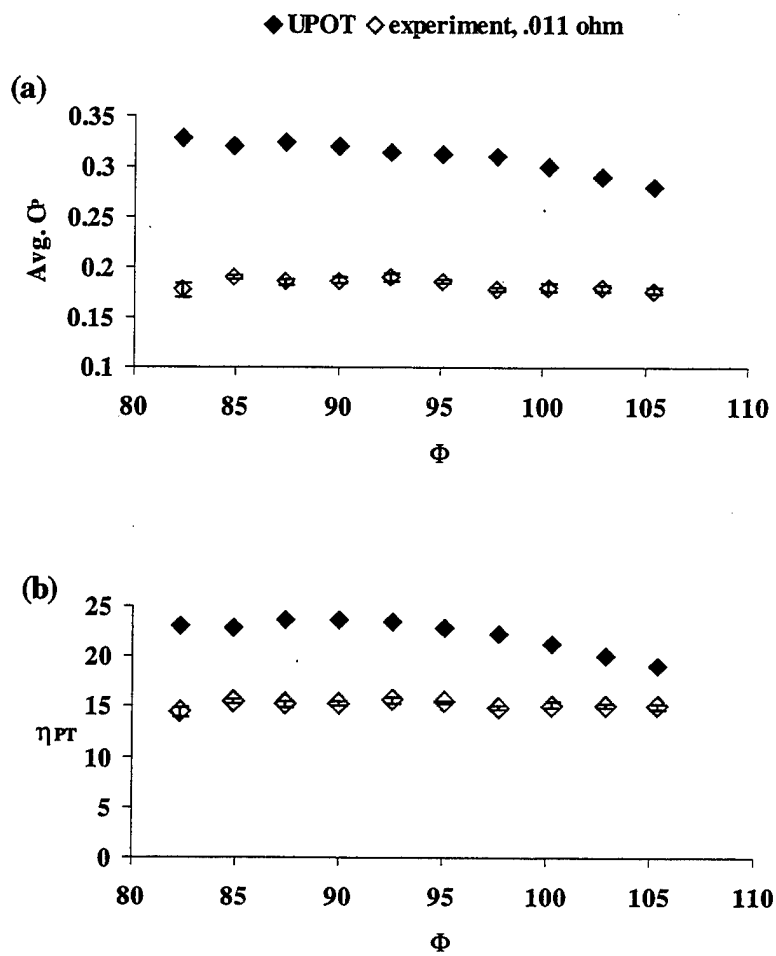
Figure 39. Comparison of Experimental and Numerical Results of Wingmill Performance Due to Phase Angle. $\Delta\alpha = 49°$, $h = 0.526$, $x_p = 0.51$.

♦ UPOT ◇ experiment, .011 ohm
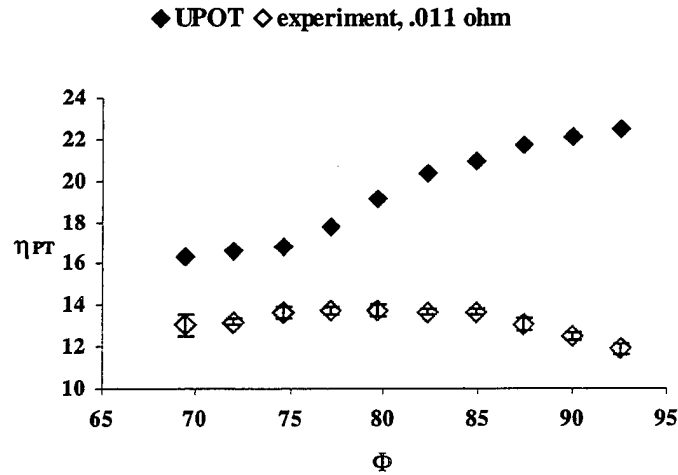
Figure 40. Comparison of Experimental and Numerical Results of Wingmill
Performance Due to Phase Angle. $\Delta\alpha = 49°$, $h = 0.526$, $x_p = 0.41$.

Numerical predictions by UPOT agree more closely with previous experimental
work by McKinney and DeLaurier than with the experiment described here. As with the
experiment in this study, the conditions of the McKinney and DeLaurier experiment were
duplicated by the panel code. The comparison between UPOT and this experiment for
the ideal efficiency, η_{PI}, versus phase angle for $\Delta\alpha = \pm25$ degrees and $\Delta\alpha = \pm30$degrees is
shown in Fig. 41. McKinney and DeLaurier evaluated the performance of their wingmill
in terms of ideal efficiency, η_{PI}. The ideal efficiency is the ratio of the power extracted to
the ideal power available. The ideal power available is based on the theory that at most
16/27 of the power flowing through the control volume can be extracted. Recall the
discussion of the Betz coefficient in Chapter IV. The ideal efficiency is equal to the total
efficiency divided by the Betz coefficient. As expected, the panel code over-predicts the
measured values slightly at lower angles of attack due to flow separation, three-
dimensional effects, and mechanical losses. However, the panel code under-predicts the
performance at the higher angles of attack, particularly at higher phase angles. One
possible explanation for this is the effect of dynamic-stall delay on the lift and moment of
the oscillating airfoil. McKinney and DeLaurier refer to airfoil oscillation experiments
by Johnson and Ham [Ref. 15]. These experiments showed that dynamic stall delay

68

appears to be accompanied by vortices shed from the leading edge of the airfoil which travel in a chord-wise direction. These vortices appear to greatly modify the airfoil's boundary layer. McKinney and DeLaurier concluded that the effect of the altered boundary layer could nullify effective camber thereby improving the performance of the wingmill. Since the panel code accounts for the effective camber, it appears that the dynamic-stall delay has a more substantial effect than merely reducing the effective camber. Referring to Fig. 25, the lift and moment forces on an oscillating airfoil can be much greater than the steady flow lift-curve slope of the airfoil. Since the panel code does not model separated flow, the numerical predictions will continue to show the airfoil producing lift beyond the static stall angle while remaining on the lift curve slope. If the actual airfoil is experiencing normal force above the lift-curve slope due to dynamic stall delay, UPOT will under predict the performance.

Although the flutter generator used in this study was capable of higher plunge and pitch amplitudes, it did not match the performance of the earlier study. This was primarily due to the non-sinusoidal pitch motion that never allowed the flutter generator to operate in an ideal condition. Also, because of the inadequate generator loads, it is not known how much additional power the wingmill was capable of extracting. Even under these non-ideal conditions, total efficiencies of the flutter generator reached 15.5 percent compared with McKinney and DeLaurier's maximum total efficiency of 16.8 percent.
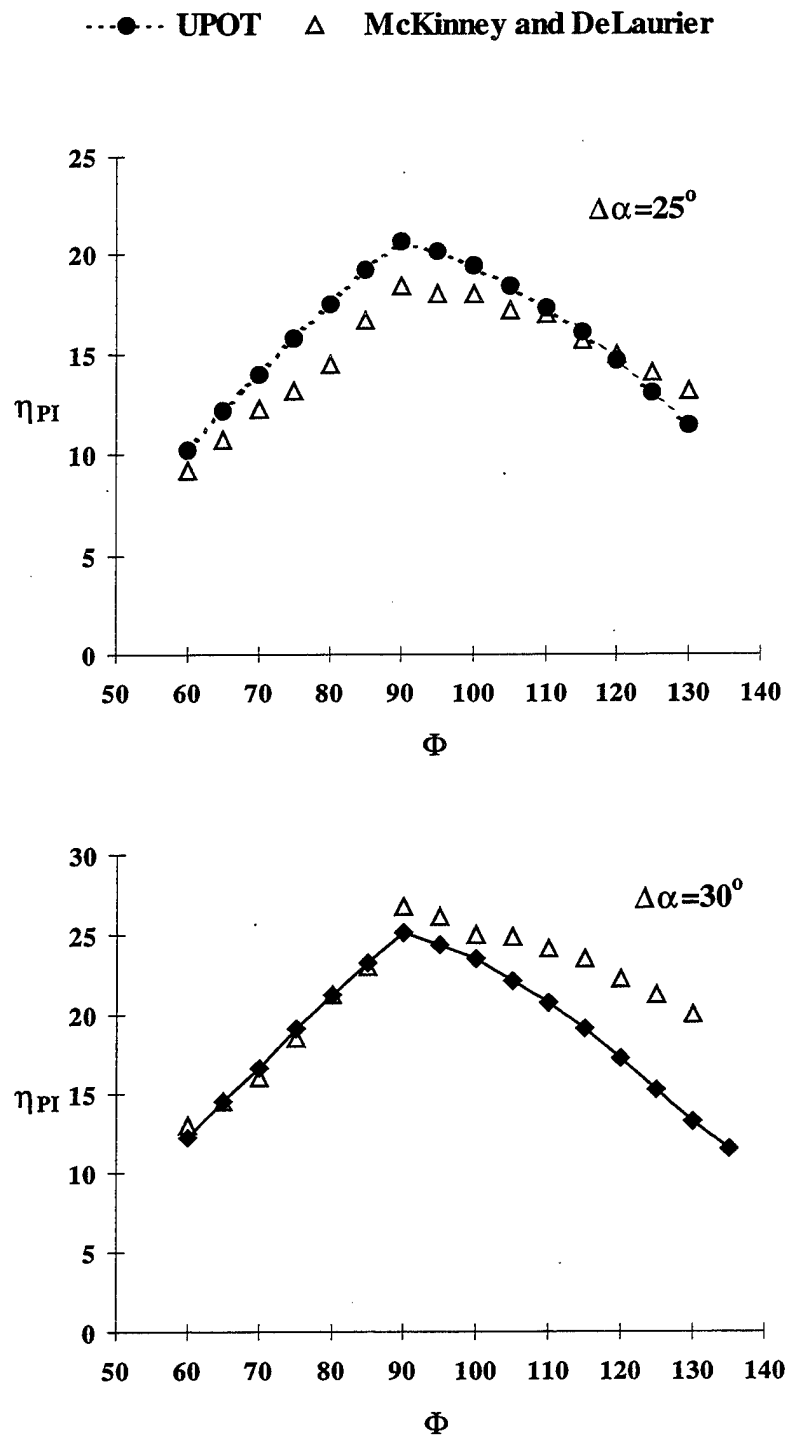
Figure 41. Comparison of UPOT with McKinney and DeLaurier Experiment.

IX. CONCLUSIONS

The numerical study of wingmill performance showed the possibility of achieving total efficiencies of up to 30 percent, a 78 percent increase from earlier experimental studies. Although the experimental model failed to reach this level of performance, its performance trends matched the panel code sufficiently considering its mechanical limitations to suggest that this level of performance may be obtainable. The key to obtaining maximum performance was found from the numerical analysis to be the proper combination of h and k. Optimum values of plunge amplitude and reduced frequencies were found to be h $\approx$ 0.63 and k $\approx$ 2.0, resulting in η_{PT} = 30 percent and $\overline{C}_p$ = 0.52. The experimental results showed that achieving such reduced frequencies might be difficult mechanically and aerodynamically. Mechanically, high reduced frequencies put tremendous stress on the flutter generator components. More important is the fact that as the reduced frequency increases, the geometric angle of attack must also increase to maintain sufficient effective angle of attack to drive the wingmill. This geometric angle of attack reaches its limit with the dynamic stall of the airfoil. This study limited the effective angle of attack to the static stall limit of the airfoil. Even greater total efficiencies may be achievable if the effective angle of attack is increased beyond its static stall limit. Comparison of the numerical study with previous experimental work shows that dynamic stall delay effects may actually increase performance beyond that predicted by the panel code.

Such high efficiencies are capable with the wingmill due to the fact that airfoil normal forces dominate the power production cycle. Typical windmill efficiencies compared to the wingmill efficiencies achieved by DeLaurier and McKinney and predicted by the panel code are shown in Fig. 42. Total efficiencies of various windmills plotted as a function of tip speed. The wingmill data is plotted with total efficiency as a function of maximum plunge velocity in place of tip speed. The wingmill is competitive with the U.S. multiblade and Dutch four-arm type windmills. A large-scale wingmill to capture wind energy would be possible using a counter balance in the form of a weight or an opposing wing. A more likely application would be to use the wingmill in a river

71

channel. The wingmill could be a source of hydroelectric power causing limited environmental damage allowing fish and shipping to pass unhindered. The wingmill could be situated between bridge towers or smaller versions could provide portable power generators for remote areas. The numerical results predict if placed in a river 10 meters wide, flowing 4.5 m/s ($\approx$ 10 mph), a wingmill with a chordlength of 2 meters could produce roughly 10 kilowatts.
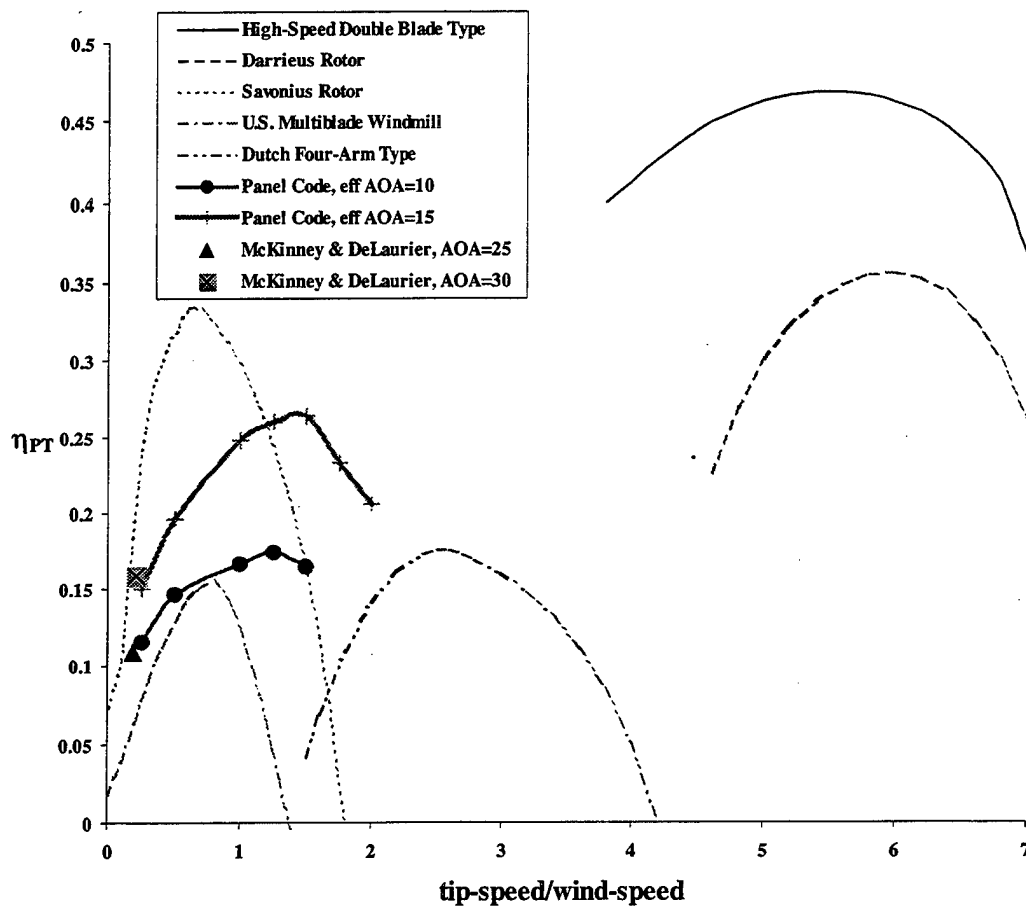
Figure 42. Comparison of Various Windmill Efficiencies with Wingmill Efficiencies. From Ref. 11.

X. RECOMMENDATIONS

The experimental work in this study was constrained by time. Therefore, the effect of parameter variation could not be studied in detail. To prove that the numerical predictions are achievable, further experimental work is necessary. Specifically, more investigation into the limits of reduced frequency and its relationship to effective angle of attack would be useful. Some model modifications could be made to facilitate these studies.

The flutter generator should be reconfigured to achieve a more sinusoidal pitch motion. This will enable the wingmill to operate at optimum phase conditions. A consistent phase relationship may help the airfoil move more smoothly through the extreme plunge positions. This would enable the wingmill to operate at greater plunge amplitudes and possibly greater reduced frequencies. Other model improvements may include a larger flywheel to make the cycle velocity more sinusoidal. Future experiments would benefit from flow visualization from dye injection from the airfoil. This would indicate the nature of the flow and answer questions concerning the existence and effects of flow separations and dynamic stall.

The performance measurement technique with the digital oscilloscope was the best that could be set up in the limited time available. It may be better to use the friction technique used by McKinney and DeLaurier. This method could be implemented with minor modifications of the current flutter generator and would facilitate the ability to adjust the load infinitesimally. This would enable the wingmill to be tested across the full range of reduced frequencies.

Further experiments useful to the study of wingmills would include coupling two oscillating airfoils to the same mechanism so one powers the other through the negative power portion of the cycle. Also of interest would be to consider multiple stages of airfoils optimized for the best efficiency based on drag. In this study the possible benefits of wakes from upstream airfoils could be investigated.

APPENDIX A. MATLAB PROGRAM TO DETERMINE TOTAL SWEPT AREA

```
% Matlab Program to Determine Total Swept Area
% of an Oscillating Airfoil

%Enter Data
xp=.5;
a=50;
h=1;
da=a*2*pi/360;
theta=[0:pi/100:6*pi];
i=0;
j=0;

for phi=60:10:130
    i=i+1;
    phia(i)=phi;
    phir=phi*2*pi/360;

    Yle=h*(cos(theta-phir))+xp*sin(da*cos(theta));

    bump1=max(Yle);
    dent1=min(Yle);

    figure(1)
    subplot(2,1,1), plot(theta,Yle);
    hold on
    title('Leading Edge Position');

    Yte=h*(cos(theta-phir))+(xp-1)*sin(da*cos(theta));

    bump2=max(Yte);
    dent2=min(Yte);

    subplot(2,1,2), plot(theta,Yte);
    hold on
    title('Trailing Edge Position');
    pause

    if bump1>bump2
        peak(i)=bump1
    else peak(i)=bump2
    end

    if dent1<dent2
        valley(i)=dent1
    else valley(i)=dent2
    end
    end
%writes max swept area with corresponding phase angle
a=peak-valley
phia
```

APPENDIX B. NUMERICAL DATA

1. EFFECTIVE ANGLE OF ATTACK

Vary Plunge Amplitude

h=0.1

k	h	Φ	x_p	α_{ind}	α_e	Δα	A	C_T	C_P	max neg C_P	η_{PD}	η_{PT}
0.5	0.1	90	0.5	2.86	2	4.86	0.2172	0.005	0.004	−0.0008	80.64516	1.841621
0.5	0.1	90	0.5	2.86	4	6.86	0.2331	0.011	0.007	−0.002	68.96552	3.003003
0.5	0.1	90	0.5	2.86	6	8.86	0.2527	0.018	0.0107	−0.004	59.88024	4.23427
0.5	0.1	90	0.5	2.86	8	10.86	0.2752	0.026	0.014	−0.0063	52.35602	5.087209
0.5	0.1	90	0.5	2.86	10	12.86	0.3	0.036	0.017	−0.01	46.08295	5.666667
0.5	0.1	90	0.5	2.86	12	14.86	0.3261	0.047	0.019	−0.014	40.98361	5.826434
0.5	0.1	90	0.5	2.86	14	16.86	0.3534	0.059	0.022	−0.018	36.63004	6.225241
0.5	0.1	90	0.5	2.86	16	18.86	0.3816	0.072	0.024	−0.024	32.78689	6.289308
0.5	0.1	90	0.5	2.86	18	20.86	0.4101	0.086	0.026	−0.03	29.67359	6.339917
0.5	0.1	90	0.5	2.86	20	22.86	0.4389	0.102	0.027	−0.038	26.73797	6.151743

h=0.5

k	h	Φ	x_p	α_{ind}	α_e	Δα	A	C_T	C_P	max neg C_P	η_{PD}	η_{PT}
0.5	0.5	90	0.5	14.04	2	16.04	1.0383	0.027	0.024	−0.01	86.05852	2.311471
0.5	0.5	90	0.5	14.04	4	18.04	1.0482	0.049	0.042	−0.011	86.65511	4.006869
0.5	0.5	90	0.5	14.04	6	20.04	1.0591	0.071	0.061	−0.013	85.03401	5.759607
0.5	0.5	90	0.5	14.04	8	22.04	1.0709	0.095	0.079	−0.016	82.64463	7.376973
0.5	0.5	90	0.5	14.04	10	24.04	1.0836	0.12	0.096	−0.021	80.64516	8.859358
0.5	0.5	90	0.5	14.04	12	26.04	1.0972	0.145	0.114	−0.025	78.125	10.39008
0.5	0.5	90	0.5	14.04	14	28.04	1.1117	0.172	0.131	−0.031	76.33588	11.78375
0.5	0.5	90	0.5	14.04	16	30.04	1.1268	0.199	0.147	−0.037	74.07407	13.04579
0.5	0.5	90	0.5	14.04	18	32.04	1.1424	0.226	0.163	−0.044	71.94245	14.26821
0.5	0.5	90	0.5	14.04	20	34.04	1.1586	0.255	0.178	−0.051	69.93007	15.36337

h=1.0

k	h	Φ	x_p	α_{ind}	α_e	Δα	A	C_T	C_P	max neg C_P	η_{PD}	η_{PT}
0.5	1	90	0.5	26.57	2	28.57	2.0608	0.06	0.0477	−0.047	80	2.314635
0.5	1	90	0.5	26.57	4	30.57	2.0694	0.102	0.087	−0.039	85.47009	4.204117
0.5	1	90	0.5	26.57	6	32.57	2.0785	0.144	0.125	−0.038	86.73027	6.013952
0.5	1	90	0.5	26.57	8	34.57	2.0881	0.187	0.162	−0.039	86.73027	7.758249
0.5	1	90	0.5	26.57	10	36.57	2.098	0.231	0.199	−0.043	86.2069	9.485224
0.5	1	90	0.5	26.57	12	38.57	2.1086	0.274	0.234	−0.048	85.47009	11.09741
0.5	1	90	0.5	26.57	14	40.57	2.1193	0.319	0.2698	−0.054	84.74576	12.73062
0.5	1	90	0.5	26.57	16	42.57	2.1308	0.363	0.303	−0.062	83.33333	14.22001
0.5	1	90	0.5	26.57	18	44.57	2.1422	0.407	0.337	−0.07	82.64463	15.73149
0.5	1	90	0.5	26.57	20	46.57	2.1543	0.452	0.369	−0.08	81.30081	17.12853

h=1.5

k	h	Φ	x_p	α_{ind}	α_e	Δα	A	C_T	C_P	max neg C_P	η_{PD}	η_{PT}
0.5	1.5	90	0.5	36.87	2	38.87	3.0752	0.082	0.055	−0.154	67.56757	1.788502
0.5	1.5	90	0.5	36.87	4	40.87	3.0827	0.146	0.117	−0.114	80	3.795374
0.5	1.5	90	0.5	36.87	6	42.87	3.0908	0.211	0.177	−0.09	84.17508	5.726673
0.5	1.5	90	0.5	36.87	8	44.87	3.0993	0.275	0.237	−0.081	86.2069	7.646888
0.5	1.5	90	0.5	36.87	10	46.87	3.1078	0.338	0.293	−0.077	86.95652	9.427891
0.5	1.5	90	0.5	36.87	12	48.87	3.1166	0.402	0.349	−0.078	86.95652	11.1981
0.5	1.5	90	0.5	36.87	14	50.87	3.1261	0.466	0.404	−0.081	86.95652	12.92345
0.5	1.5	90	0.5	36.87	16	52.87	3.1355	0.529	0.458	−0.087	86.2069	14.60692
0.5	1.5	90	0.5	36.87	18	54.87	3.1449	0.592	0.51	−0.095	86.2069	16.21673
0.5	1.5	90	0.5	36.87	20	56.87	3.1551	0.654	0.561	−0.105	86.2069	17.78074

Vary Reduced Frequency

k=.1

k	h	Φ	x_p	α_{ind}	α_e	$\Delta\alpha$	A	C_T	C_P	max neg C_P	η_{PD}	η_{PT}
0.1	1	90	0.5	5.71	2	7.71	2.0045	0.0116	0.0109	-0.00011	93.45794	0.543777
0.1	1	90	0.5	5.71	4	9.71	2.0071	0.02332	0.02157	-0.0003	92.50694	1.074685
0.1	1	90	0.5	5.71	6	11.71	2.0104	0.0355	0.0322	-0.00056	90.66183	1.601671
0.1	1	90	0.5	5.71	8	13.71	2.0142	0.048	0.043	-0.00086	88.80995	2.134843
0.1	1	90	0.5	5.71	10	15.71	2.0186	0.061	0.053	-0.00117	86.88097	2.625582
0.1	1	90	0.5	5.71	12	17.71	2.0237	0.075	0.064	-0.0016	85.10638	3.162524
0.1	1	90	0.5	5.71	14	19.71	2.0292	0.0885	0.0739	-0.002	83.40284	3.641829
0.1	1	90	0.5	5.71	16	21.71	2.0355	0.103	0.084	-0.0024	81.96721	4.12675
0.1	1	90	0.5	5.71	18	23.71	2.042	0.1099	0.089	-0.00272	81.30081	4.358472
0.1	1	90	0.5	5.71	20	25.71	2.0496	0.1244	0.099	-0.00327	79.36508	4.830211

k=.5

k	h	Φ	x_p	α_{ind}	α_e	$\Delta\alpha$	A	C_T	C_P	max neg C_P	η_{PD}	η_{PT}
0.5	1	90	0.5	26.57	2	28.57	2.0608	0.06	0.0477	-0.047	80	2.314635
0.5	1	90	0.5	26.57	4	30.57	2.0694	0.102	0.087	-0.039	85.47009	4.204117
0.5	1	90	0.5	26.57	6	32.57	2.0785	0.144	0.125	-0.038	86.73027	6.013952
0.5	1	90	0.5	26.57	8	34.57	2.0881	0.187	0.162	-0.039	86.73027	7.758249
0.5	1	90	0.5	26.57	10	36.57	2.098	0.231	0.199	-0.043	86.2069	9.485224
0.5	1	90	0.5	26.57	12	38.57	2.1086	0.274	0.234	-0.048	85.47009	11.09741
0.5	1	90	0.5	26.57	14	40.57	·2.1193	0.319	0.2698	-0.054	84.74576	12.73062
0.5	1	90	0.5	26.57	16	42.57	2.1308	0.363	0.303	-0.062	83.33333	14.22001
0.5	1	90	0.5	26.57	18	44.57	2.1422	0.407	0.337	-0.07	82.64463	15.73149
0.5	1	90	0.5	26.57	20	46.57	2.1543	0.452	0.369	-0.08	81.30081	17.12853

k=1.0

k	h	Φ	x_p	α_{ind}	α_e	$\Delta\alpha$	A	C_T	C_P	max neg C_P	η_{PD}	η_{PT}
1	1	90	0.5	45	2	47	2.157	0.13	0.055	-0.57	42.01681	2.549838
1	1	90	0.5	45	4	49	2.1692	0.206	0.127	-0.54	61.7284	5.854693
1	1	90	0.5	45	6	51	2.1817	0.282	0.196	-0.513	69.44444	8.98382
1	1	90	0.5	45	8	53	2.1947	0.356	0.262	-0.51	73.52941	11.93785
1	1	90	0.5	45	10	55	2.2076	0.437	0.33	-0.48	75.75758	14.94836
1	1	90	0.5	45	12	57	2.2207	0.512	0.392	-0.503	76.33588	17.65209
1	1	90	0.5	45	14	59	2.2342	0.588	0.452	-0.523	76.92308	20.23096
1	1	90	0.5	45	16	61	2.2476	0.666	0.511	-0.54	76.92308	22.73536
1	1	90	0.5	45	18	63	2.2609	0.746	0.572	-0.56	76.92308	25.29966
1	1	90	0.5	45	20	65	2.2746	0.822	0.626	-0.58	76.33588	27.52132

k=1.5

k	h	Φ	x_p	α_{ind}	α_e	$\Delta\alpha$	A	C_T	C_P	max neg C_P	η_{PD}	η_{PT}
1.5	1	90	0.5	56.31	4	60.31	2.243	0.336	0.064	-2.18	19.01141	2.853321
1.5	1	90	0.5	56.31	6	62.31	2.2563	0.457	0.174	-2.17	38.02281	7.71174
1.5	1	90	0.5	56.31	8	64.31	2.2698	0.58	0.277	-2.14	47.84689	12.20372
1.5	1	90	0.5	56.31	10	66.31	2.2836	0.702	0.376	-2.13	53.47594	16.46523
1.5	1	90	0.5	56.31	12	68.31	2.2972	0.826	0.473	-2.13	57.14286	20.59028
1.5	1	90	0.5	56.31	14	70.31	2.3107	0.949	0.563	-2.15	59.52381	24.36491
1.5	1	90	0.5	56.31	16	72.31	2.3241	1.07	0.65	-2.16	60.60606	27.96782
1.5	1	90	0.5	56.31	18	74.31	2.3376	1.2	0.73	-2.2	60.97561	31.22861
1.5	1	90	0.5	56.31	20	76.31	2.3511	1.33	0.82	-2.25	61.7284	34.87729

2. REDUCED FREQUENCY

Vary Estimated Effective Angle of Attack

$\alpha_e = 5$

k	h	Φ	x_p	α_{ind}	α_e	Δα	A	C_T	C_P	max neg C_P	η_{PD}	η_{PT}
0.1	1	90	0.5	5.71	5	10.71	2.0087	0.0294	0.027	-0.00042	91.74312	1.344153
0.2	1	90	0.5	11.31	5	16.31	2.0199	0.05403	0.0491	-0.0017	90.90909	2.430813
0.3	1	90	0.5	16.70	5	21.70	2.0355	0.077	0.069	-0.005	89.76661	3.389831
0.4	1	90	0.5	21.80	5	26.80	2.0537	0.0997	0.088	-0.015	88.49558	4.284949
0.5	1	90	0.5	26.57	5	31.57	2.0737	0.123	0.106	-0.037	86.2069	5.111636
0.6	1	90	0.5	30.96	5	35.96	2.0949	0.146	0.122	-0.076	83.54219	5.823667
0.7	1	90	0.5	34.99	5	39.99	2.1161	0.17	0.137	-0.141	80.64516	6.474174
0.8	1	90	0.5	38.66	5	43.66	2.137	0.194	0.148	-0.235	76.33588	6.925597
0.9	1	90	0.5	41.99	5	46.99	2.1569	0.219	0.157	-0.36	71.42857	7.278965
1	1	90	0.5	45.00	5	50.00	2.1753	0.244	0.161	-0.52	66.22517	7.401278
1.1	1	90	0.5	47.73	5	52.73	2.1929	0.27	0.162	-0.731	59.88024	7.387478
1.3	1	90	0.5	52.43	5	57.43	2.2236	0.328	0.15	-1.32	45.6621	6.745818
1.5	1	90	0.5	56.31	5	61.31	2.2497	0.396	0.117	-2.13	29.5858	5.200693

$\alpha_e = 10$

k	h	Φ	x_p	α_{ind}	α_e	Δα	A	C_T	C_P	max neg C_P	η_{PD}	η_{PT}
0.1	1	90	0.5	5.71	10	15.71	2.0186	0.061	0.053	-0.00117	86.88097	2.625582
0.2	1	90	0.5	11.31	10	21.31	2.0342	0.1099	0.096	-0.0039	86.95652	4.7193
0.3	1	90	0.5	16.70	10	26.70	2.0533	0.152	0.133	-0.01	87.26003	6.477378
0.4	1	90	0.5	21.80	10	31.80	2.0748	0.192	0.167	-0.021	86.95652	8.048969
0.5	1	90	0.5	26.57	10	36.57	2.098	0.231	0.199	-0.043	86.2069	9.485224
0.6	1	90	0.5	30.96	10	40.96	2.1216	0.269	0.229	-0.079	84.74576	10.79374
0.7	1	90	0.5	34.99	10	44.99	2.1446	0.306	0.255	-0.135	83.33333	11.89033
0.8	1	90	0.5	38.66	10	48.66	2.1671	0.349	0.284	-0.22	81.30081	13.10507
0.9	1	90	0.5	41.99	10	51.99	2.1881	0.391	0.307	-0.339	78.74016	14.03044
1	1	90	0.5	45.00	10	55.00	2.2076	0.437	0.33	-0.48	75.75758	14.94836
1.1	1	90	0.5	47.73	10	57.73	2.2256	0.481	0.345	-0.7	71.94245	15.50144
1.3	1	90	0.5	52.43	10	62.43	2.2571	0.582	0.368	-1.26	63.29114	16.30411
1.5	1	90	0.5	56.31	10	66.31	2.2836	0.702	0.376	-2.13	53.47594	16.46523

$\alpha_e = 15$

k	h	Φ	x_p	α_{ind}	α_e	Δα	A	C_T	C_P	max neg C_P	η_{PD}	η_{PT}
0.1	1	90	0.5	5.71	15	20.71	2.0323	0.096	0.079	-0.0023	82.64463	3.887221
0.2	1	90	0.5	11.31	15	26.31	2.0518	0.169	0.141	-0.007	83.33333	6.872015
0.3	1	90	0.5	16.70	15	31.70	2.0743	0.231	0.194	-0.017	84.03361	9.352553
0.4	1	90	0.5	21.80	15	36.80	2.0993	0.287	0.241	-0.031	84.03361	11.48002
0.5	1	90	0.5	26.57	15	41.57	2.125	0.34	0.286	-0.057	84.03361	13.45882
0.6	1	90	0.5	30.96	15	45.96	2.1506	0.394	0.329	-0.0297	83.33333	15.29806
0.7	1	90	0.5	34.99	15	49.99	2.1753	0.449	0.37	-0.157	82.64463	17.00915
0.8	1	90	0.5	38.66	15	53.66	2.1989	0.505	0.409	-0.239	80.64516	18.60021
0.9	1	90	0.5	41.99	15	56.99	2.2206	0.564	0.446	-0.358	78.74016	20.08466
1	1	90	0.5	45.00	15	60.00	2.2409	0.627	0.482	-0.52	76.92308	21.50922
1.1	1	90	0.5	47.73	15	62.73	2.2591	0.693	0.513	-0.717	74.07407	22.70816
1.3	1	90	0.5	52.43	15	67.43	2.2913	0.839	0.566	-1.29	67.56757	24.70213
1.5	1	90	0.5	56.31	15	71.31	2.3175	1	0.598	-2.11	59.52381	25.80367

$\alpha_e = 20$

k	h	Φ	x_p	α_{ind}	α_e	Δα	A	C_T	C_P	max neg C_P	η_{PD}	η_{PT}
0.1	1	90	0.5	5.71	15	20.71	2.0496	0.1244	0.099	-0.00327	79.36508	4.830211
0.2	1	90	0.5	11.31	15	26.31	2.0726	0.23	0.184	-0.0012	80	8.877738
0.3	1	90	0.5	16.70	15	31.70	2.0988	0.311	0.252	-0.026	80.64516	12.00686
0.4	1	90	0.5	21.80	15	36.80	2.1264	0.384	0.312	-0.046	81.30081	14.67269
0.5	1	90	0.5	26.57	15	41.57	2.1543	0.452	0.369	-0.08	81.30081	17.12853
0.6	1	90	0.5	30.96	15	45.96	2.1815	0.52	0.423	-0.126	81.30081	19.39033
0.7	1	90	0.5	34.99	15	49.99	2.2075	0.591	0.476	-0.192	80.64516	21.56285
0.8	1	90	0.5	38.66	15	53.66	2.2319	0.663	0.527	-0.284	79.36508	23.61217
0.9	1	90	0.5	41.99	15	56.99	2.2542	0.74	0.576	-0.406	78.125	25.5523
1	1	90	0.5	45.00	15	60.00	2.2746	0.822	0.626	-0.58	76.33588	27.52132
1.1	1	90	0.5	47.73	15	62.73	2.2933	0.908	0.669	-0.778	73.52941	29.17194
1.3	1	90	0.5	52.43	15	67.43	2.3249	1.1	0.746	-1.36	68.02721	32.0874
1.5	1	90	0.5	56.31	15	71.31	2.3511	1.33	0.82	-2.25	61.7284	34.87729

Vary Pivot Location

$x_p=0.4$

k	h	Φ	x_p	α_{ind}	α_e	Δα	A	C_T	C_P	max neg C_P	η_{PD}	η_{PT}
0.1	1	90	0.4	5.71	15	20.71	2.0464	0.096	0.079	0	82.64463	3.860438
0.2	1	90	0.4	11.31	15	26.31	2.0739	0.171	0.143	-0.006	83.33333	6.895222
0.3	1	90	0.4	16.70	15	31.70	2.1063	0.236	0.198	-0.014	84.03361	9.40037
0.4	1	90	0.4	21.80	15	36.80	2.1408	0.296	0.249	-0.03	84.03361	11.63117
0.5	1	90	0.4	26.57	15	41.57	2.1765	0.355	0.296	-0.063	83.33333	13.59982
0.6	1	90	0.4	30.96	15	45.96	2.116	0.415	0.34	-0.117	81.96721	16.06805
0.7	1	90	0.4	34.99	15	49.99	2.2453	0.478	0.382	-0.204	80	17.01332
0.8	1	90	0.4	38.66	15	53.66	2.277	0.544	0.421	-0.332	77.51938	18.48924
0.9	1	90	0.4	41.99	15	56.99	2.3059	0.616	0.456	-0.515	74.07407	19.77536
1	1	90	0.4	45.00	15	60.00	2.3326	0.693	0.486	-0.764	69.93007	20.83512
1.1	1	90	0.4	47.73	15	62.73	2.3566	0.779	0.512	-1.08	65.78947	21.72622
1.3	1	90	0.4	52.43	15	67.43	2.3982	0.974	0.539	-1.99	55.24862	22.47519
1.5	1	90	0.4	56.31	15	71.31	2.4319	1.198	0.517	-3.32	43.10345	21.2591

$x_p=0.5$

k	h	Φ	x_p	α_{ind}	α_e	Δα	A	C_T	C_P	max neg C_P	η_{PD}	η_{PT}
0.1	1	90	0.5	5.71	15	20.71	2.0323	0.096	0.079	-0.002	82.64463	3.887221
0.2	1	90	0.5	11.31	15	26.31	2.0518	0.169	0.141	-0.007	83.33333	6.872015
0.3	1	90	0.5	16.70	15	31.70	2.0743	0.231	0.194	-0.017	84.03361	9.352553
0.4	1	90	0.5	21.80	15	36.80	2.0993	0.287	0.241	-0.031	84.03361	11.48002
0.5	1	90	0.5	26.57	15	41.57	2.125	0.34	0.286	-0.057	84.03361	13.45882
0.6	1	90	0.5	30.96	15	45.96	2.1506	0.394	0.329	-0.0297	83.33333	15.29806
0.7	1	90	0.5	34.99	15	49.99	2.1753	0.449	0.37	-0.157	82.64463	17.00915
0.8	1	90	0.5	38.66	15	53.66	2.1989	0.505	0.409	-0.239	80.64516	18.60021
0.9	1	90	0.5	41.99	15	56.99	2.2206	0.564	0.446	-0.358	78.74016	20.08466
1	1	90	0.5	45.00	15	60.00	2.2409	0.627	0.482	-0.52	76.92308	21.50922
1.1	1	90	0.5	47.73	15	62.73	2.2591	0.693	0.513	-0.717	74.07407	22.70816
1.3	1	90	0.5	52.43	15	67.43	2.2913	0.839	0.566	-1.29	67.56757	24.70213
1.5	1	90	0.5	56.31	15	71.31	2.3175	1	0.598	-2.11	59.52381	25.80367

$x_p=0.6$

k	h	Φ	x_p	α_{ind}	α_e	Δα	A	C_T	C_P	max neg C_P	η_{PD}	η_{PT}
0.1	1	90	0.6	5.71	15	20.71	2.0464	0.095	0.078	-0.003	82.64463	3.811572
0.2	1	90	0.6	11.31	15	26.31	2.0739	0.166	0.138	-0.011	83.33333	6.65413
0.3	1	90	0.6	16.70	15	31.70	2.1063	0.224	0.188	-0.023	84.03361	8.925604
0.4	1	90	0.6	21.80	15	36.80	2.1408	0.275	0.231	0	84.03361	10.79036
0.5	1	90	0.6	26.57	15	41.57	2.1765	0.322	0.271	-0.067	84.03361	12.45118
0.6	1	90	0.6	30.96	15	45.96	2.2116	0.368	0.309	-0.104	84.03361	13.97179
0.7	1	90	0.6	34.99	15	49.99	2.2453	0.412	0.345	-0.153	83.33333	15.36543
0.8	1	90	0.6	38.66	15	53.66	2.277	0.457	0.379	-0.214	82.64463	16.64471
0.9	1	90	0.6	41.99	15	56.99	2.3059	0.502	0.412	-0.29	81.96721	17.86721
1	1	90	0.6	45.00	15	60.00	2.3326	0.548	0.444	-0.383	81.30081	19.03455
1.1	1	90	0.6	47.73	15	62.73	2.3566	0.594	0.474	-0.5	80	20.11372
1.3	1	90	0.6	52.43	15	67.43	2.3982	0.691	0.53	-0.826	76.92308	22.09991
1.5	1	90	0.6	56.31	15	71.31	2.4319	0.791	0.575	-1.29	72.46377	23.64406

3. PLUNGE AMPLITUDE

Vary Estimated Effective Angle of Attack

$\alpha_e=5$

k	h	Φ	x_p	α_{ind}	α_e	Δα	A	C_T	C_P	max neg C_P	η_{PD}	η_{PT}
0.5	0.2	90	0.5	5.71	5	10.71	0.4414	0.0248	0.0192	-0.0041	77.51938	4.349796
0.5	0.4	90	0.5	11.31	5	16.31	0.849	0.0478	0.0406	-0.0087	84.81764	4.782097
0.5	0.6	90	0.5	16.70	5	21.70	1.258	0.0725	0.0628	-0.015	86.58009	4.992051
0.5	0.8	90	0.5	21.80	5	26.80	1.667	0.0978	0.0849	-0.024	86.73027	5.092981
0.5	1	90	0.5	26.57	5	31.57	2.0737	0.123	0.106	-0.037	86.2069	5.111636
0.5	1.2	90	0.5	30.96	5	35.96	2.4801	0.147	0.125	-0.055	85.10638	5.040119
0.5	1.4	90	0.5	34.99	5	39.99	2.885	0.168	0.141	-0.075	83.54219	4.887348
0.5	1.6	90	0.5	38.66	5	43.66	3.288	0.188	0.153	-0.117	81.30081	4.653285
0.5	1.8	90	0.5	41.99	5	46.99	3.6912	0.204	0.16	-0.168	78.74016	4.334634
0.5	2	90	0.5	45.00	5	50.00	4.0929	0.216	0.162	-0.24	75.18797	3.958074

$\alpha_e=10$

k	h	Φ	x_p	α_{ind}	α_e	Δα	A	C_T	C_P	max neg C_P	η_{PD}	η_{PT}
0.5	0.2	90	0.5	5.71	10	15.71	0.4843	0.056	0.036	-0.011	64.51613	7.433409
0.5	0.4	90	0.5	11.31	10	21.31	0.8816	0.098	0.076	-0.017	77.51938	8.62069
0.5	0.6	90	0.5	16.70	10	26.70	1.2864	0.142	0.117	-0.023	82.64463	9.095149
0.5	0.8	90	0.5	21.80	10	31.80	1.6924	0.186	0.158	-0.032	84.74576	9.335854
0.5	1	90	0.5	26.57	10	36.57	2.098	0.23	0.199	-0.042	86.2069	9.485224
0.5	1.2	90	0.5	30.96	10	40.96	2.503	0.274	0.238	-0.054	86.95652	9.50859
0.5	1.3	90	0.5	33.02	10	43.02	2.7047	0.2962	0.257	-0.061	86.76037	9.501978
0.5	1.35	90	0.5	34.02	10	44.02	2.8055	0.3069	0.26617	-0.0637	86.73027	9.487435
0.5	1.4	90	0.5	34.99	10	44.99	2.906	0.317	0.275	-0.068	86.73027	9.46318
0.5	1.45	90	0.5	35.94	10	45.94	3.007	0.328	0.285	-0.073	86.73027	9.477885
0.5	1.5	90	0.5	36.87	10	46.87	3.1078	0.338	0.293	-0.077	86.95652	9.427891
0.5	1.6	90	0.5	38.66	10	48.66	3.309	0.359	0.31	-0.083	86.43042	9.368389
0.5	1.8	90	0.5	41.99	10	51.99	3.711	0.4	0.343	-0.107	85.47009	9.242792
0.5	2	90	0.5	45.00	10	55.00	4.112	0.438	0.372	-0.14	84.74576	9.046693

$\alpha_e=15$

k	h	Φ	x_p	α_{ind}	α_e	Δα	A	C_T	C_P	max neg C_P	η_{PD}	η_{PT}
0.5	0.2	90	0.5	5.71	15	20.71	0.5368	0.095	0.051	-0.023	54.34783	9.500745
0.5	0.4	90	0.5	11.31	15	26.31	0.9205	0.154	0.109	-0.03	70.77141	11.84139
0.5	0.6	90	0.5	16.70	15	31.70	1.3193	0.216	0.168	-0.038	78.125	12.73403
0.5	0.8	90	0.5	21.80	15	36.80	1.7219	0.278	0.227	-0.048	81.96721	13.18311
0.5	1	90	0.5	26.57	15	41.57	2.125	0.34	0.286	-0.057	84.03361	13.45882
0.5	1.2	90	0.5	30.96	15	45.96	2.528	0.403	0.345	-0.068	85.47009	13.64715
0.5	1.4	90	0.5	34.99	15	49.99	2.93	0.466	0.403	-0.08	86.35579	13.75427
0.5	1.6	90	0.5	38.66	15	53.66	3.331	0.528	0.459	-0.089	86.95652	13.77965
0.5	1.8	90	0.5	41.99	15	56.99	3.732	0.591	0.514	-0.102	86.95652	13.77278
0.5	2	90	0.5	45.00	15	60.00	4.132	0.653	0.568	-0.115	86.95652	13.74637

$\alpha_e=20$

k	h	Φ	x_p	α_{ind}	α_e	Δα	A	C_T	C_P	max neg C_P	η_{PD}	η_{PT}
0.5	0.2	90	0.5	5.71	20	25.71	0.5951	0.14	0.065	-0.038	46.51163	10.92253
0.5	0.4	90	0.5	11.31	20	31.31	0.9641	0.216	0.14	-0.046	64.93506	14.52132
0.5	0.6	90	0.5	16.70	20	36.70	1.356	0.294	0.216	-0.056	73.52941	15.9292
0.5	0.8	90	0.5	21.80	20	41.80	1.7541	0.373	0.292	-0.067	78.125	16.64671
0.5	1	90	0.5	26.57	20	46.57	2.154	0.452	0.369	-0.078	81.30081	17.13092
0.5	1.2	90	0.5	30.96	20	50.96	2.555	0.525	0.44	-0.088	84.03361	17.22114
0.5	1.4	90	0.5	34.99	20	54.99	2.955	0.613	0.5222	-0.098	85.47009	17.67174
0.5	1.6	90	0.5	38.66	20	58.66	3.355	0.694	0.6	-0.109	86.2069	17.88376
0.5	1.8	90	0.5	41.99	20	61.99	3.754	0.777	0.677	-0.119	86.95652	18.0341
0.5	2	90	0.5	45.00	20	65.00	4.153	0.86	0.754	-0.129	87.7193	18.15555

4. PHASE ANGLE

Vary Reduced Frequency

k=.25

k	h	Φ	x_p	α_{ind}	α_e	$\Delta\alpha$	A	C_T	C_P	max neg C_P	η_{PD}	η_{PT}
0.25	1	65	0.5	14.04	15	29.04	2.2568	0.211	0.166	-0.04	78.74016	7.355548
0.25	1	70	0.5	14.04	15	29.04	2.2216	0.213	0.172	-0.025	81.30081	7.742168
0.25	1	75	0.5	14.04	15	29.04	2.1844	0.213	0.175	-0.015	82.64463	8.011353
0.25	1	80	0.5	14.04	15	29.04	2.1455	0.211	0.176	-0.009	83.33333	8.203216
0.25	1	85	0.5	14.04	15	29.04	2.1047	0.207	0.173	-0.0078	84.03361	8.219699
0.25	1	90	0.5	14.04	15	29.04	2.0629	0.201	0.168	-0.011	84.03361	8.143875
0.25	1	95	0.5	14.04	15	29.04	2.1047	0.193	0.161	-0.02	83.33333	7.649546
0.25	1	100	0.5	14.04	15	29.04	2.1455	0.184	0.151	-0.034	81.96721	7.037986
0.25	1	105	0.5	14.04	15	29.04	2.1844	0.173	0.138	-0.053	80	6.317524
0.25	1	110	0.5	14.04	15	29.04	2.2216	0.16	0.123	-0.077	76.92308	5.53655
0.25	1	115	0.5	14.04	15	29.04	2.2568	0.146	0.106	-0.105	72.46377	4.696916
0.25	1	120	0.5	14.04	15	29.04	2.2895	0.131	0.087	-0.136	66.66667	3.799956
0.25	1	125	0.5	14.04	15	29.04	2.3204	0.114	0.066	-0.171	57.80347	2.844337

k=.50

k	h	Φ	x_p	α_{ind}	α_e	$\Delta\alpha$	A	C_T	C_P	max neg C_P	η_{PD}	η_{PT}
0.5	1	65	0.5	26.57	15	41.57	2.3815	0.383	0.272	-0.244	70.92199	11.42137
0.5	1	70	0.5	26.57	15	41.57	2.3361	0.383	0.289	-0.182	75.75758	12.37105
0.5	1	75	0.5	26.57	15	41.57	2.2874	0.378	0.298	-0.129	79.36508	13.02789
0.5	1	80	0.5	26.57	15	41.57	2.236	0.37	0.301	-0.088	81.30081	13.46154
0.5	1	85	0.5	26.57	15	41.57	2.1819	0.357	0.297	-0.065	83.33333	13.61199
0.5	1	90	0.5	26.57	15	41.57	2.125	0.341	0.287	-0.058	84.03361	13.50588
0.5	1	95	0.5	26.57	15	41.57	2.1819	0.32	0.269	-0.071	84.03361	12.3287
0.5	1	100	0.5	26.57	15	41.57	2.236	0.297	0.245	-0.103	82.64463	10.95707
0.5	1	105	0.5	26.57	15	41.57	2.2874	0.27	0.216	-0.154	80	9.443036
0.5	1	110	0.5	26.57	15	41.57	2.3361	0.241	0.182	-0.221	75.18797	7.790762
0.5	1	115	0.5	26.57	15	41.57	2.3215	0.21	0.142	-0.303	67.56757	6.116735
0.5	1	120	0.5	26.57	15	41.57	2.4235	0.176	0.097	-0.391	55.24862	4.002476
0.5	1	125	0.5	26.57	15	41.57	2.4622	0.14	0.048	-0.492	34.36426	1.949476

k=1.0

k	h	Φ	x_p	α_{ind}	α_e	$\Delta\alpha$	A	C_T	C_P	max neg C_P	η_{PD}	η_{PT}
1	1	65	0.5	45	15	60	2.5571	0.769	0.302	-1.99	39.21569	11.81025
1	1	70	0.5	45	15	60	2.5031	0.761	0.383	-1.6	50.25126	15.30103
1	1	75	0.5	45	15	60	2.4445	0.741	0.44	-1.25	59.1716	17.99959
1	1	80	0.5	45	15	60	2.3811	0.711	0.473	-0.938	66.66667	19.86477
1	1	85	0.5	45	15	60	2.3132	0.673	0.487	-0.712	72.46377	21.05309
1	1	90	0.5	45	15	60	2.2409	0.627	0.481	-0.518	76.92308	21.46459
1	1	95	0.5	45	15	60	2.3132	0.575	0.458	-0.392	80	19.79941
1	1	100	0.5	45	15	60	2.3811	0.5189	0.42	-0.435	81.30081	17.63891
1	1	105	0.5	45.	15	60	2.4445	0.458	0.368	-0.587	80.64516	15.0542
1	1	110	0.5	45	15	60	2.5031	0.395	0.304	-0.793	76.92308	12.14494
1	1	115	0.5	45	15	60	2.5571	0.329	0.228	-1.04	68.96552	8.916351
1	1	120	0.5	45	15	60	2.6065	0.262	0.141	-1.3	53.76344	5.409553
1	1	125	0.5	45	15	60	2.6511	0.194	0.043	-1.59	22.37136	1.621968

k=1.25

k	h	Φ	x_p	α_{ind}	α_e	$\Delta\alpha$	A	C_T	C_P	max neg C_P	η_{PD}	η_{PT}
1.25	1	65	0.5	51.34	15	66.34	2.6122	1.041	0.207	-3.99	19.88072	7.924355
1.25	1	70	0.5	51.34	15	66.34	2.5569	1.02	0.347	-3.27	34.01361	13.57112
1.25	1	75	0.5	51.34	15	66.34	2.4964	0.985	0.447	-2.62	45.45455	17.90578
1.25	1	80	0.5	51.34	15	66.34	2.4306	0.932	0.511	-2.01	54.94505	21.02362
1.25	1	85	0.5	51.34	15	66.34	2.3597	0.871	0.547	-1.54	62.89308	23.18091
1.25	1	90	0.5	51.34	15	66.34	2.2838	0.805	0.558	-1.14	69.44444	24.43296
1.25	1	95	0.5	51.34	15	66.34	2.3597	0.723	0.538	-0.806	74.62687	22.79951
1.25	1	100	0.5	51.34	15	66.34	2.4306	0.643	0.5	-0.736	78.125	20.57105
1.25	1	105	0.5	51.34	15	66.34	2.4964	0.561	0.445	-0.998	79.36508	17.82567
1.25	1	110	0.5	51.34	15	66.34	2.5569	0.478	0.372	-1.33	78.125	14.54887
1.25	1	115	0.5	51.34	15	66.34	2.6122	0.396	0.285	-1.71	71.94245	10.91034
1.25	1	120	0.5	51.34	15	66.34	2.6623	0.314	0.183	-2.1	58.13953	6.873756
1.25	1	125	0.5	51.34	15	66.34	2.7073	0.231	0.066	-2.55	28.40909	2.437853

k=1.50

k	h	Φ	x_p	α_{ind}	α_e	$\Delta\alpha$	A	C_T	C_P	max neg C_P	η_{PD}	η_{PT}
1.5	1	65	0.5	56.31	15	71.31	2.6525	1.38	0.006	-7.27	4.166667	0.226202
1.5	1	70	0.5	56.31	15	71.31	2.5967	1.33	0.216	-5.93	16.15509	8.31825
1.5	1	75	0.5	56.31	15	71.31	2.5353	1.27	0.373	-4.74	31.84713	14.71226
1.5	1	80	0.5	56.31	15	71.31	2.4682	1.19	0.481	-3.71	40.48583	19.48789
1.5	1	85	0.5	56.31	15	71.31	2.3955	1.1	0.554	-2.82	50.50505	23.1267
1.5	1	90	0.5	56.31	15	71.31	2.3175	0.998	0.591	-2.06	59.1716	25.50162
1.5	1	95	0.5	56.31	15	71.31	2.3955	0.892	0.596	-1.52	66.66667	24.87998
1.5	1	100	0.5	56.31	15	71.31	2.4682	0.783	0.571	-1.21	72.9927	23.13427
1.5	1	105	0.5	56.31	15	71.31	2.5353	0.674	0.518	-1.62	76.92308	20.43151
1.5	1	110	0.5	56.31	15	71.31	2.5967	0.567	0.442	-2.11	78.125	17.0216
1.5	1	115	0.5	56.31	15	71.31	2.6525	0.466	0.348	-2.67	74.62687	13.1197

Vary Estimated Effective Angle of Attack
eff AOA=5

k	h	Φ	x_p	α_{ind}	α_e	Δα	A	C_T	C_P	max neg C_P	η_{PD}	η_{PT}
1.25	1	80	0.5	51.34019	5	56.34019	2.3523	0.384	0.074	-2.02	19.34236	3.145857
1.25	1	85	0.5	51.34019	5	56.34019	2.2863	0.352	0.127	-1.56	36.23188	5.554827
1.25	1	90	0.5	51.34019	5	56.34019	2.2162	0.313	0.155	-1.1	49.50495	6.993954
1.25	1	95	0.5	51.34019	5	56.34019	2.2863	0.267	0.158	-0.794	59.52381	6.910729
1.25	1	100	0.5	51.34019	5	56.34019	2.3523	0.215	0.141	-0.559	65.35948	5.994133
1.25	1	105	0.5	51.34019	5	56.34019	2.414	0.16	0.104	-0.808	64.93506	4.308202
1.25	1	110	0.5	51.34019	5	56.34019	2.4712	0.101	0.049	-1.17	48.78049	1.982842

Phase angles below 80 and above 110 required work to drive wingmill

eff AOA=10

k	h	Φ	x_p	α_{ind}	α_e	Δα	A	C_T	C_P	max neg C_P	η_{PD}	η_{PT}
1.25	1	70	0.5	51.34019	10	61.34019	2.5147	0.714	0.12	-3.21	16.77852	4.771941
1.25	1	75	0.5	51.34019	10	61.34019	2.4554	0.692	0.228	-2.51	32.89474	9.285656
1.25	1	80	0.5	51.34019	10	61.34019	2.3916	0.656	0.302	-2	46.08295	12.62753
1.25	1	85	0.5	51.34019	10	61.34019	2.323	0.61	0.346	-1.51	56.81818	14.89453
1.25	1	88	0.5	51.34019	10	61.34019	2.2797	0.579	0.361	-1.27	62.5	15.83542
1.25	1	90	0.5	51.34019	10	61.34019	2.2499	0.556	0.364	-1.11	65.35948	16.1785
1.25	1	92	0.5	51.34019	10	61.34019	2.2797	0.532	0.364	-0.96	68.49315	15.96701
1.25	1	95	0.5	51.34019	10	61.34019	2.323	0.496	0.358	-0.769	72.46377	15.41111
1.25	1	100	0.5	51.34019	10	61.34019	2.3916	0.431	0.331	-0.635	76.92308	13.84011
1.25	1	105	0.5	51.34019	10	61.34019	2.4554	0.363	0.285	-0.916	78.74016	11.60707
1.25	1	110	0.5	51.34019	10	61.34019	2.5147	0.293	0.222	-1.26	75.75758	8.828091
1.25	1	115	0.5	51.34019	10	61.34019	2.5691	0.22	0.142	-1.62	64.51613	5.527227
1.25	1	120	0.5	51.34019	10	61.34019	2.6187	0.147	0.047	-2.02	32.05128	1.794784

eff AOA=15

k	h	Φ	x_p	α_{ind}	α_e	Δα	A	C_T	C_P	max neg C_P	η_{PD}	η_{PT}
1.25	1	65	0.5	51.34019	15	66.34019	2.6122	1.04	0.021	-4.04	19.88072	0.80392
1.25	1	70	0.5	51.34019	15	66.34019	2.5569	1.02	0.347	-3.28	34.01361	13.57112
1.25	1	75	0.5	51.34019	15	66.34019	2.4964	0.985	0.447	-2.61	45.45455	17.90578
1.25	1	80	0.5	51.34019	15	66.34019	2.4306	0.932	0.511	-1.99	54.94505	21.02362
1.25	1	85	0.5	51.34019	15	66.34019	2.3597	0.871	0.547	-1.53	62.89308	23.18091
1.25	1	90	0.5	51.34019	15	66.34019	2.2838	0.8	0.554	-1.12	69.44444	24.25782
1.25	1	95	0.5	51.34019	15	66.34019	2.3597	0.723	0.538	-0.803	74.62687	22.79951
1.25	1	100	0.5	51.34019	15	66.34019	2.4306	0.643	0.501	-0.738	78.125	20.61219
1.25	1	105	0.5	51.34019	15	66.34019	2.4964	0.561	0.445	-0.998	79.36508	17.82567
1.25	1	110	0.5	51.34019	15	66.34019	2.5569	0.479	0.373	-1.34	78.125	14.58798
1.25	1	115	0.5	51.34019	15	66.34019	2.6122	0.396	0.285	-1.71	71.94245	10.91034
1.25	1	120	0.5	51.34019	15	66.34019	2.6623	0.313	0.182	-2.13	58.13953	6.836194
1.25	1	125	0.5	51.34019	15	66.34019	2.7073	0.231	0.066	-2.56	28.49003	2.437853

Vary Pivot Location

xp=0

k	h	Φ	x_p	α_{ind}	α_e	$\Delta\alpha$	A	C_T	C_P	max neg C_P	η_{PD}	η_{PT}
Phase angle 60 required work to drive wingmill										0		
0.5	1	65	0	26.56505	10	36.56505	2	0.181	0.022	-0.717	12.34568	1.1
0.5	1	70	0	26.56505	10	36.56505	2	0.203	0.07	-0.59	34.36426	3.5
0.5	1	75	0	26.56505	10	36.56505	2.0713	0.221	0.11	-0.473	50	5.310674
0.5	1	80	0	26.56505	10	36.56505	2.1713	0.236	0.145	-0.368	60.97561	6.678027
0.5	1	85	0	26.56505	10	36.56505	2.2676	0.247	0.171	-0.27	69.44444	7.541013
0.5	1	90	0	26.56505	10	36.56505	2.36	0.254	0.192	-0.192	75.18797	8.135593
0.5	1	95	0	26.56505	10	36.56505	2.4481	0.258	0.206	-0.128	80	8.414689
0.5	1	100	0	26.56505	10	36.56505	2.5318	0.257	0.213	-0.079	82.64463	8.412987
0.5	1	105	0	26.56505	10	36.56505	2.611	0.253	0.214	-0.051	84.45946	8.196093
0.5	1	110	0	26.56505	10	36.56505	2.685	0.246	0.209	-0.043	84.96177	7.783985
0.5	1	115	0	26.56505	10	36.56505	2.754	0.236	0.1986	-0.06	84.03361	7.211329
0.5	1	120	0	26.56505	10	36.56505	2.819	0.223	0.182	-0.092	81.96721	6.45619
0.5	1	125	0	26.56505	10	36.56505	2.879	0.2071	0.161	-0.137	77.51938	5.59222
0.5	1	130	0	26.56505	10	36.56505	2.933	0.189	0.134	-0.195	70.92199	4.568701

xp=0.3

k	h	Φ	x_p	α_{ind}	α_e	$\Delta\alpha$	A	C_T	C_P	max neg C_P	η_{PD}	η_{PT}
0.5	1	60	0.3	26.56505	10	36.56505	2.21	0.228	0.098	-0.51	42.91845	4.434389
0.5	1	65	0.3	26.56505	10	36.56505	2.185	0.241	0.133	-0.412	55.24862	6.086957
0.5	1	70	0.3	26.56505	10	36.56505	2.158	0.251	0.161	-0.321	64.51613	7.460612
0.5	1	75	0.3	26.56505	10	36.56505	2.129	0.256	0.183	-0.24	71.42857	8.595585
0.5	1	80	0.3	26.56505	10	36.56505	2.0995	0.257	0.198	-0.18	76.92308	9.430817
0.5	1	85	0.3	26.56505	10	36.56505	2.116	0.256	0.206	-0.12	80.64516	9.73535
0.5	1	90	0.3	26.56505	10	36.56505	2.187	0.249	0.209	-0.074	84.03361	9.55647
0.5	1	95	0.3	26.56505	10	36.56505	2.254	0.24	0.205	-0.048	85.47009	9.094942
0.5	1	100	0.3	26.56505	10	36.56505	2.319	0.228	0.196	-0.043	86.2069	8.451919
0.5	1	105	0.3	26.56505	10	36.56505	2.3803	0.212	0.181	-0.065	85.47009	7.604084
0.5	1	110	0.3	26.56505	10	36.56505	2.4381	0.194	0.16	-0.103	82.64463	6.562487
0.5	1	115	0.3	26.56505	10	36.56505	2.4924	0.173	0.135	-0.161	78.125	5.416466
0.5	1	120	0.3	26.56505	10	36.56505	2.5428	0.15	0.104	-0.229	69.44444	4.08998
0.5	1	125	0.3	26.56505	10	36.56505	2.5893	0.125	0.0695	-0.31	55.86592	2.684123
0.5	1	130	0.3	26.56505	10	36.56505	2.6318	0.099	0.0311	-0.39	32.25806	1.181701

xp=0.5

k	h	Φ	x_p	α_{ind}	α_e	$\Delta\alpha$	A	C_T	C_P	max neg C_P	η_{PD}	η_{PT}
0.5	1	60	0.5	26.56505	10	36.56505	2.37	0.26	0.159	-0.334	61.34969	6.708861
0.5	1	65	0.5	26.56505	10	36.56505	2.332	0.264	0.182	-0.26	68.49315	7.80446
0.5	1	70	0.5	26.56505	10	36.56505	2.29	0.265	0.198	-0.195	74.62687	8.646288
0.5	1	75	0.5	26.56505	10	36.56505	2.246	0.262	0.207	-0.139	79.36508	9.216385
0.5	1	80	0.5	26.56505	10	36.56505	2.199	0.255	0.21	-0.092	82.64463	9.549795
0.5	1	85	0.5	26.56505	10	36.56505	2.15	0.244	0.207	-0.059	84.74576	9.627907
0.5	1	90	0.5	26.56505	10	36.56505	2.098	0.231	0.199	-0.043	86.2069	9.485224
0.5	1	95	0.5	26.56505	10	36.56505	2.15	0.214	0.184	-0.05	86.2069	8.55814
0.5	1	100	0.5	26.56505	10	36.56505	2.199	0.194	0.164	-0.081	84.81764	7.457935
0.5	1	105	0.5	26.56505	10	36.56505	2.246	0.171	0.139	-0.131	81.30081	6.18878
0.5	1	110	0.5	26.56505	10	36.56505	2.29	0.145	0.108	-0.197	74.62687	4.716157
0.5	1	115	0.5	26.56505	10	36.56505	2.332	0.118	0.073	-0.277	62.03474	3.13036
0.5	1	120	0.5	26.56505	10	36.56505	2.37	0.088	0.033	-0.362	37.87879	1.392405

xp=0.7

k	h	Φ	x_p	α_{ind}	α_e	$\Delta\alpha$	A	C_T	C_P	max neg C_P	η_{PD}	η_{PT}
0.5	1	60	0.7	26.56505	10	36.56505	2.5428	0.278	0.2	-0.2	71.94245	7.865345
0.5	1	65	0.7	26.56505	10	36.56505	2.4924	0.274	0.211	-0.151	76.92308	8.465736
0.5	1	70	0.7	26.56505	10	36.56505	2.4381	0.266	0.215	-0.102	80.64516	8.818342
0.5	1	75	0.7	26.56505	10	36.56505	2.3803	0.255	0.214	-0.071	84.03361	8.990463
0.5	1	80	0.7	26.56505	10	36.56505	2.319	0.241	0.206	-0.049	85.47009	8.883139
0.5	1	85	0.7	26.56505	10	36.56505	2.2544	0.222	0.192	-0.043	86.50519	8.516678
0.5	1	90	0.7	26.56505	10	36.56505	2.1866	0.2005	0.1722	-0.06	85.91065	7.87524
0.5	1	95	0.7	26.56505	10	36.56505	2.1159	0.1758	0.1469	-0.099	83.54219	6.942672
0.5	1	100	0.7	26.56505	10	36.56505	2.0995	0.148	0.116	-0.161	78.49294	5.525125
0.5	1	105	0.7	26.56505	10	36.56505	2.1294	0.118	0.081	-0.239	68.49315	3.803888
0.5	1	110	0.7	26.56505	10	36.56505	2.1581	0.085	0.0397	-0.321	46.72897	1.839581

Phase angles above 115 required work to drive wingmill

xp=1.0

k	h	Φ	x_p	α_{ind}	α_e	$\Delta\alpha$	A	C_T	C_P	max neg C_P	η_{PD}	η_{PT}
0.5	1	60	0.3	26.56505	10	36.56505	2.819	0.28	0.227	-0.0803	81.03728	8.052501
0.5	1	65	0.3	26.56505	10	36.56505	2.7543	0.265	0.222	-0.058	83.68201	8.060124
0.5	1	70	0.3	26.56505	10	36.56505	2.685	0.246	0.21	-0.044	85.3971	7.821229
0.5	1	75	0.3	26.56505	10	36.56505	2.611	0.224	0.1924	-0.046	86.05852	7.368824
0.5	1	80	0.3	26.56505	10	36.56505	2.532	0.1972	0.168	-0.067	85.3971	6.635071
0.5	1	85	0.3	26.56505	10	36.56505	2.448	0.167	0.138	-0.112	82.64463	5.637255
0.5	1	90	0.3	26.56505	10	36.56505	2.3599	0.1342	0.1026	-0.177	76.33588	4.347642
0.5	1	95	0.3	26.56505	10	36.56505	2.2676	0.0977	0.0611	-0.262	62.5	2.694479
0.5	1	100	0.3	26.56505	10	36.56505	2.1713	0.0588	0.0147	-0.362	24.93766	0.677014

Phase angles above 100 required work to drive wingmill

84

5.   PIVOT LOCATION

Vary Phase
Φ=80

k	h	Φ	x_p	α_{ind}	α_0	$\Delta\alpha$	A	C_T	C_P	max neg C_P	η_{PD}	η_{PT}
0.5	1	80	-0.3	26.57	10	36.57	2.349	0.185	0.047	-0.644	25.38071	2.000851
0.5	1	80	-0.2	26.57	10	36.57	2.2852	0.206	0.084	-0.537	41.15226	3.675827
0.5	1	80	-0.1	26.57	10	36.57	2.2256	0.223	0.117	-0.449	52.35602	5.257009
0.5	1	80	0	26.57	10	36.57	2.1715	0.236	0.145	-0.368	60.97561	6.677412
0.5	1	80	0.1	26.57	10	36.57	2.1223	0.246	0.166	-0.293	67.56757	7.821703
0.5	1	80	0.2	26.57	10	36.57	2.0794	0.253	0.184	-0.227	72.46377	8.848706
0.5	1	80	0.3	26.57	10	36.57	2.0995	0.257	0.198	-0.18	76.92308	9.430817
0.5	1	80	0.4	26.57	10	36.57	2.1461	0.257	0.206	-0.128	80.64516	9.598807
0.5	1	80	0.5	26.57	10	36.57	2.199	0.255	0.21	-0.092	82.64463	9.549795
0.5	1	80	0.6	26.57	10	36.57	2.2563	0.249	0.21	-0.065	84.03361	9.307273
0.5	1	80	0.7	26.57	10	36.57	2.319	0.241	0.206	-0.049	85.47009	8.883139
0.5	1	80	0.8	26.57	10	36.57	2.3862	0.229	0.197	-0.041	86.2069	8.255804
0.5	1	80	0.9	26.57	10	36.57	2.4571	0.2145	0.185	-0.05	86.2069	7.529201
0.5	1	80	1	26.57	10	36.57	2.532	0.1972	0.168	-0.067	85.3971	6.635071
0.5	1	80	1.1	26.57	10	36.57	2.6092	0.177	0.148	-0.0999	83.47245	5.672237
0.5	1	80	1.2	26.57	10	36.57	2.69	0.154	0.1231	-0.1449	79.93605	4.576208
0.5	1	80	1.3	26.57	10	36.57	2.7734	0.128	0.095	-0.199	73.90983	3.425398

Φ=90

k	h	Φ	x_p	α_{ind}	α_0	$\Delta\alpha$	A	C_T	C_P	max neg C_P	η_{PD}	η_{PT}
0.5	1	90	-0.3	26.57	10	36.57	2.5717	0.231	0.134	-0.394	58.13953	5.210561
0.5	1	90	-0.2	26.57	10	36.57	2.4975	0.2423	0.158	-0.317	65.35948	6.326326
0.5	1	90	-0.1	26.57	10	36.57	2.4266	0.25	0.178	-0.25	70.92199	7.335366
0.5	1	90	0	26.57	10	36.57	2.36	0.254	0.192	-0.192	75.18797	8.135593
0.5	1	90	0.1	26.57	10	36.57	2.2974	0.255	0.202	-0.145	78.74016	8.792548
0.5	1	90	0.2	26.57	10	36.57	2.2392	0.254	0.208	-0.104	81.96721	9.289032
0.5	1	90	0.3	26.57	10	36.57	2.187	0.249	0.209	-0.074	84.03361	9.55647
0.5	1	90	0.4	26.57	10	36.57	2.1392	0.241	0.206	-0.054	85.25149	9.629768
0.5	1	90	0.5	26.57	10	36.57	2.098	0.231	0.199	-0.043	86.2069	9.485224
0.5	1	90	0.6	26.57	10	36.57	2.1392	0.217	0.187	-0.044	86.43042	8.741586
0.5	1	90	0.7	26.57	10	36.57	2.1866	0.2005	0.1722	-0.06	85.91065	7.87524
0.5	1	90	0.8	26.57	10	36.57	2.2392	0.1813	0.1531	-0.087	84.45946	6.837263
0.5	1	90	0.9	26.57	10	36.57	2.2974	0.159	0.1297	-0.127	81.56607	5.645512
0.5	1	90	1	26.57	10	36.57	2.3599	0.134	0.102	-0.18	76.33588	4.322217
0.5	1	90	1.1	26.57	10	36.57	2.4266	0.106	0.071	-0.24	67.11409	2.925905
0.5	1	90	1.2	26.57	10	36.57	2.4975	0.075	0.036	-0.305	47.61905	1.441441

Φ=100

k	h	Φ	x_p	α_{ind}	α_0	$\Delta\alpha$	A	C_T	C_P	max neg C_P	η_{PD}	η_{PT}
0.5	1	100	-0.3	26.57	10	36.57	2.7734	0.26	0.1921	-0.2	74.07407	6.926516
0.5	1	100	-0.2	26.57	10	36.57	2.69	0.2622	0.2034	-0.149	77.57952	7.561338
0.5	1	100	-0.1	26.57	10	36.57	2.6092	0.2611	0.2103	-0.111	80.5153	8.059942
0.5	1	100	0	26.57	10	36.57	2.5318	0.257	0.213	-0.079	82.64463	8.412987
0.5	1	100	0.1	26.57	10	36.57	2.4571	0.257	0.213	-0.065	82.78146	8.668756
0.5	1	100	0.2	26.57	10	36.57	2.3862	0.24	0.206	-0.0436	85.5432	8.632973
0.5	1	100	0.3	26.57	10	36.57	2.319	0.228	0.196	-0.043	86.2069	8.451919
0.5	1	100	0.4	26.57	10	36.57	2.2563	0.212	0.182	-0.0546	85.76329	8.066303
0.5	1	100	0.5	26.57	10	36.57	2.199	0.194	0.164	-0.081	84.81764	7.457935
0.5	1	100	0.6	26.57	10	36.57	2.1461	0.172	0.1421	-0.114	82.50825	6.621313
0.5	1	100	0.7	26.57	10	36.57	2.0995	0.148	0.116	-0.161	78.49294	5.525125
0.5	1	100	0.8	26.57	10	36.57	2.0794	0.121	0.086	-0.218	71.42857	4.135808
0.5	1	100	0.9	26.57	10	36.57	2.1223	0.0914	0.0525	-0.284	57.47126	2.473731
0.5	1	100	1	26.57	10	36.57	2.1715	0.0588	0.0147	-0.362	24.93766	0.676951

APPENDIX C. EXPERIMENTAL DATA

1. ANGLE OF ATTACK

.011 ohm

AOA	phase	Pout	Pout avg dev	Pin	pts/cyc	freq (Hz)	k	Vel (m/s)	C_P	d	η_{PT}
35.5	90	2.52	1.56	112.264	1247	0.801925	0.615818	0.507286	0.07926	0.0721	6.815669
41.5	90	6.87	0.134	172.7078	881	1.135074	0.871651	0.507286	0.121934	0.085	8.893983
41.625	90	7.28	0.123	178.0876	856.8	1.167134	0.896271	0.507286	0.125732	0.0836	9.324613
42.375	90	6.91	0.174	173.235	938	1.066098	0.818683	0.507286	0.122306	0.08401	9.026265
47.75	90	9.84	0.172	210.4435	787	1.270648	0.975762	0.507286	0.148575	0.0857	10.74875
48.875	90	10.56	0.169	219.1598	714.3	1.399972	1.075073	0.507286	0.154729	0.08554	11.21489
51.75	90	11.81	0.177	233.8921	692	1.445087	1.109718	0.507286	0.16513	0.08441	12.129
55.125	90	11.76	0.23	233.3126	711	1.40647	1.080063	0.507286	0.164721	0.08592	11.88632
60	90	7.53	0.119	181.3412	981	1.019368	0.782798	0.507286	0.128029	0.08655	9.17134

.02 ohm

AOA	phase	power out	Po avg dev	power in	pts/cyc	freq (Hz)	k	Vel (m/s)	C_P	d	η_{PT}
35.5	90	4.351	0.1008	128.0172	1176	0.85034	0.652997	0.507286	0.090382	0.0721	7.772062
41.5	90	7.466	0.141	167.9211	854	1.17096	0.899209	0.507286	0.118554	0.085	8.64748
41.625	90	7.58	0.0954	169.3351	845	1.183432	0.908787	0.507286	0.119552	0.0836	8.866332
42.375	90	7.21	0.214	164.7338	899	1.112347	0.854199	0.507286	0.116304	0.08401	8.583314
47.75	90	9.322	0.201	190.5353	792	1.262626	0.969602	0.507286	0.13452	0.0857	9.731906
48.875	90	11.122	0.202	211.6387	712	1.404494	1.078546	0.507286	0.149419	0.08554	10.83002
51.75	90	11.412	0.24	214.9623	690	1.449275	1.112934	0.507286	0.151766	0.08441	11.14735
55.125	90	12.777	0.263	230.3222	674	1.48368	1.139354	0.507286	0.16261	0.08592	11.73396
60	90	8.0798	0.729	175.4958	919	1.088139	0.835609	0.507286	0.123902	0.08655	8.875709

2. REDUCED FREQUENCY

.02 ohm

Vi (m/s)	Vi avg dev	Vo	Vel (m/s)	Pout	Pout (mW)	Pout avg dev	Pin (mW)	pts/cyc	freq (Hz)	k	C$_P$	d	η$_{PT}$
0.48987	0.0757	0.037055	0.452815	0.00629	6.29	0.369	153.1433	819.9	1.219661	1.049276	0.152022	0.08622	10.93175
0.48741	0.076573	0.037055	0.450355	0.00738	7.38	0.312	166.8522	989.9	1.010203	0.873827	0.168359	0.08622	12.10656
0.49766	0.070549	0.037055	0.460605	0.00758	7.58	0.231	169.3351	921.9	1.084716	0.917401	0.15971	0.08622	11.48457
0.50602	0.070106	0.037055	0.468965	0.00871	8.71	0.069	183.1743	889.8	1.123848	0.933552	0.163687	0.08622	11.77056
0.53646	0.075082	0.037055	0.499405	0.01072	10.72	0.23	206.9963	803.5	1.244555	0.970807	0.15317	0.08622	11.01433
0.54801	0.0771	0.037055	0.510955	0.01455	14.55	0.278	249.5726	681.6	1.467136	1.11856	0.172433	0.08622	12.39946
0.56489	0.071336	0.037055	0.527835	0.01548	15.48	0.121	259.3536	660.5	1.514005	1.117379	0.162543	0.08622	11.68831
0.5879	0.07268	0.037055	0.550845	0.01815	18.15	0.1798	286.2244	629.11	1.589547	1.124127	0.15783	0.08622	11.34939
0.6106	0.070569	0.037055	0.573545	0.02007	20.07	0.362	304.4377	604.6	1.653986	1.123404	0.148719	0.08622	10.69424
0.60463	0.073548	0.037055	0.567575	0.01817	18.17	0.173	286.4189	618.54	1.61671	1.109636	0.144378	0.08622	10.38212
0.61145	0.077686	0.037055	0.574395	0.02178	21.78	0.153	319.8775	581.19	1.720608	1.166925	0.155569	0.08622	11.18679
0.62918	0.066077	0.037055	0.592125	0.02407	24.07	0.291	339.4008	554.11	1.804696	1.187305	0.150676	0.08622	10.83494
0.67442	0.076212	0.037055	0.637365	0.02638	26.38	0.3228	357.7569	526.64	1.89883	1.160565	0.127348	0.08622	9.157508
0.69614	0.075522	0.037055	0.659085	0.02691	26.91	0.257	361.7789	510.64	1.958327	1.157485	0.116463	0.08622	8.374771
0.68349	0.06264	0.037055	0.646435	0.02628	26.28	0.328	356.9901	524.72	1.905778	1.148468	0.121801	0.08622	8.758616
0.72856	0.06867	0.037055	0.691505	0.02629	26.29	0.522	357.0669	510.67	1.958212	1.103153	0.099525	0.08622	7.156777
0.75983	0.076175	0.037055	0.722775	0.02956	29.56	0.385	380.8283	498.14	2.007468	1.081974	0.092959	0.08622	6.684574

.011 ohm

Vi (m/s)	Vi avg dev	Vo	Vel (m/s)	Pout	Pout (mW)	Pout avg dev	Pin (mW)	pts/cyc	freq (Hz)	k	C$_P$	d	η$_{PT}$
0.48987	0.0757	0.037055	0.452815	0.006	6	0.0842	161.111	1027	0.97371	0.837684	0.159931	0.08622	11.5005
0.48741	0.076573	0.037055	0.450355	0.00642	6.42	0.173	166.7402	1015	0.985222	0.852218	0.168246	0.08622	12.09843
0.49766	0.070549	0.037055	0.460605	0.00726	7.26	0.148	177.8265	963	1.038422	0.878247	0.167718	0.08622	12.06047
0.50602	0.070106	0.037055	0.468965	0.00853	8.53	0.194	194.1525	880	1.136364	0.943949	0.173497	0.08622	12.47601
0.53646	0.075082	0.037055	0.499405	0.01051	10.51	0.109	218.5599	799	1.251564	0.976274	0.161727	0.08622	11.62963
0.54801	0.0771	0.037055	0.510955	0.01371	13.71	0.179	255.3127	704	1.420455	1.08297	0.176398	0.08622	12.68465
0.56489	0.071336	0.037055	0.527835	0.01529	15.29	0.221	272.2322	657	1.52207	1.123332	0.170614	0.08622	12.26871
0.5879	0.07268	0.037055	0.550845	0.01699	16.99	0.237	289.5305	635	1.574803	1.113701	0.159653	0.08622	11.48048
0.6106	0.070569	0.037055	0.573545	0.01867	18.67	0.22	305.7026	605	1.652893	1.122661	0.149337	0.08622	10.73867
0.60463	0.073548	0.037055	0.567575	0.01759	17.59	0.343	295.4116	611	1.636661	1.123329	0.148911	0.08622	10.70808
0.61145	0.077686	0.037055	0.574395	0.0198	19.8	0.236	316.0643	585	1.709402	1.159325	0.153714	0.08622	11.05344
0.62918	0.066077	0.037055	0.592125	0.02216	22.16	0.2009	336.3662	560	1.785714	1.174817	0.149328	0.08622	10.73807
0.67442	0.076212	0.037055	0.637365	0.024	24	0.2488	350.939	529	1.890359	1.155388	0.124922	0.08622	8.98299
0.69614	0.075522	0.037055	0.659085	0.02634	26.34	0.387	367.8824	517	1.934236	1.143246	0.118428	0.08622	8.516058
0.68349	0.06264	0.037055	0.646435	0.02435	24.35	0.253	353.5864	526	1.901141	1.145674	0.12064	0.08622	8.675109
0.72856	0.06867	0.037055	0.691505	0.02627	26.27	0.2283	367.4013	509	1.964637	1.106773	0.102406	0.08622	7.363913
0.75983	0.076175	0.037055	0.722775	0.02963	29.63	0.346	388.6945	495	2.020202	1.088838	0.094879	0.08622	6.822648

3. PLUNGE AMPLITUDE

.011 ohm

AOA	phase	h	Pout	Po avg dev	Pin	pts/cyc	freq (Hz)	k	Vel (m/s)	C_P	d	η_{PT}
56.6	90	0.5264	0.01106	0.000243	74.605536	738	1.355014	0.180535	0.465344	0.068237	0.09115	4.641453
56.6	90	0.6924	0.01117	0.000282	74.607232	775	1.290323	0.171916	0.465344	0.068238	0.10098	4.189722
56.6	90	0.8439	0.007041	0.0000458	74.543571	1105	0.904977	0.120574	0.465344	0.06818	0.1198	3.528523

.02 ohm

AOA	phase	h	Pout	Po avg dev	Pin	pts/cyc	freq (Hz)	k	Vel (m/s)	C_P	d	η_{PT}
56.6	90	0.5264	0.01039	0.000146	68.338543	772	1.295337	0.172584	0.465344	0.062505	0.09115	4.251563
56.6	90	0.6924	0.01022	0.000115	68.336112	783	1.277139	0.170159	0.465344	0.062503	0.10098	3.837554
56.6	90	0.8439	0.00659	0.000083	68.284218	1159	0.862813	0.114957	0.465344	0.062455	0.1198	3.232236

4. PHASE AND PIVOT

Phase Comparison at $x_p=.41$

.02 ohm

phase	Pout	Pout avg dev	Pin	steps/cyc	k	Vel (m/s)	C_P	d	η_{PT}
69.43	16.1	0.564	265.7533	745	0.946067	0.552705	0.145067	0.072919	12.33448
72	17.05	0.441	275.3715	705	0.999745	0.552705	0.150317	0.072769	12.80714
74.57	18.25	0.181	287.1959	666	1.058288	0.552705	0.156772	0.072609	13.38657
77.14	18.43	0.151	288.9383	656	1.074421	0.552705	0.157723	0.072439	13.49949
79.71	17.32	0.195	278.0636	661	1.066293	0.552705	0.151787	0.072258	13.02382
82.29	17.14	0.119	276.2709	662	1.064683	0.552705	0.150808	0.072068	12.97399
84.86	16.15	0.227	266.2651	663	1.063077	0.552705	0.145346	0.07187	12.53856
87.43	15.26	0.262	257.0594	684	1.030438	0.552705	0.140321	0.071774	12.12121
90	12.7	0.504	229.4682	716	0.984385	0.552705	0.12526	0.071841	10.81019
92.57	13.89	0.1797	242.4991	724	0.973508	0.552705	0.132373	0.0719	11.41463

.011 ohm

phase	Pout	Pout std dev	Pin	steps/cyc	k	Vel (m/s)	C_P	d	η_{PT}
69.43	16.1	0.344	280.5915	751	0.938509	0.552705	0.153167	0.072919	13.02317
72	16.42	0.147	283.8352	714	0.987143	0.552705	0.154937	0.072769	13.20078
74.57	17.28	0.204	292.3876	677	1.041093	0.552705	0.159606	0.072609	13.62856
77.14	17.48	0.181	294.3421	661	1.066293	0.552705	0.160673	0.072439	13.75196
79.71	17.42	0.172	293.7572	652	1.081012	0.552705	0.160354	0.072258	13.75887
82.29	17.11	0.149	290.7161	655	1.076061	0.552705	0.158694	0.072068	13.65236
84.86	17.11	0.266	290.7161	658	1.071155	0.552705	0.158694	0.07187	13.68997
87.43	15.82	0.187	277.726	673	1.047281	0.552705	0.151603	0.071774	13.0957
90	14.6	0.193	264.9431	694	1.015591	0.552705	0.144625	0.071841	12.4814
92.57	13.46	0.277	252.5613	743	0.948614	0.552705	0.137866	0.0719	11.88827

Phase comparison at $x_p=.51$

.02 ohm

phase	Pout	Pout std dev	Pin	steps/cyc	k	Vel (m/s)	C_P	d	η_{PT}
82.29	12.36	0.487	225.6796	800	0.989317	0.492205	0.174431	0.076434	14.14906
84.86	12.73	0.2052	229.8011	757	1.045514	0.492205	0.177617	0.076138	14.46363
87.43	12.51	0.198	227.3546	745	1.062354	0.492205	0.175726	0.075818	14.37003
90	13.47	0.155	237.9407	726	1.090157	0.492205	0.183908	0.075476	15.10715
92.57	12.37	0.156	225.7914	750	1.055272	0.492205	0.174518	0.075115	14.40473
95.14	12.72	0.118	229.6901	730	1.084183	0.492205	0.177531	0.074735	14.72788
97.71	12.12	0.326	222.9878	752	1.052465	0.492205	0.172351	0.074339	14.37431
100.29	11.85	0.147	219.9421	758	1.044134	0.492205	0.169997	0.073927	14.25712
102.86	12.01	0.347	221.7492	761	1.040018	0.492205	0.171393	0.073502	14.45722
105.43	11.23	0.088	212.8789	847	0.93442	0.492205	0.164537	0.073067	13.96167

.011 ohm

phase	Pout	Pout std dev	Pin	steps/cyc	k	Vel (m/s)	C_P	d	η_{PT}
82.29	11.44	0.671	229.5843	820	0.965187	0.492205	0.177449	0.076434	14.39386
84.86	12.77	0.15	244.8618	744	1.063782	0.492205	0.189258	0.076138	15.41155
87.43	12.36	0.292	240.2135	764	1.035934	0.492205	0.185665	0.075818	15.18278
90	12.48	0.222	241.5796	726	1.090157	0.492205	0.186721	0.075476	15.33819
92.57	12.78	0.341	244.9745	710	1.114724	0.492205	0.189345	0.075115	15.62855
95.14	12.38	0.1178	240.4415	723	1.09468	0.492205	0.185841	0.074735	15.41726
97.71	11.48	0.123	230.0521	761	1.040018	0.492205	0.177811	0.074339	14.8297
100.29	11.74	0.275	233.0806	750	1.055272	0.492205	0.180152	0.073927	15.10879
102.86	11.65	0.1925	232.0347	763	1.037292	0.492205	0.179343	0.073502	15.12781
105.43	11.35	0.1925	228.5297	826	0.958176	0.492205	0.176634	0.073067	14.98812

LIST OF REFERENCES

1. McKinney, W. and DeLaurier, J., "The Wingmill: An Oscillating-Wing Windmill," Journal of Energy, Vol. 5, No. 2, March-April 1981, pp. 109-115.

2. Jones, K. D. and Platzer, M. F., "Numerical Computation of Flapping-Wing Propulsion and Power Extraction," AIAA Paper No. 97-0826, Reno, Nevada, January 1997.

3. Platzer, M. F., Class Lecture Notes, Naval Postgraduate School, Monterey, California, September 1998.

4. Bertin, J. J., Smith, M. L., *Aerodynamics for Engineers*, 3d edition, Prentice Hall, 1998.

5. Fung, Y.C., *The Theory of Aeroelasticity*, Dover Publications, Inc., New York, 1969

6. Teng, N. H., "The Development of a Computer Code for the Numerical Solution of Unsteady, Inviscid and Incompressible Flow over an Airfoil," Master's Thesis, Naval Postgraduate School, Monterey, California, June 1987.

7. Jones, K. D. and Center, K. B., "Numerical Wake Visualization for Airfoils Undergoing Forced and Aeroelastic Motions," AIAA Paper No. 96-0055, January 1996.

8. Hess, J.L. and Smith, A.M.O. "Calculation of Potential Flow about Arbitrary Bodies," *Progress in Aeronautical Sciences*, Vol. 8, Pergamon Press, Oxford, 1966, pp. 1-138.

9. Basu, B. C. and Hancock, G. J., "The Unsteady Motion of a Two –Dimensional Aerofoil in Incompressible Inviscid Flow," *Journal of Fluid Mechanics*, Vol. 87, 1978, pp. 159-168.

10. Riester, Peter J., "A Computational and Experimental Investigation of Incompressible Oscillatory Airfoil Flow and Flutter Problems," Master's Thesis, Naval Postgraduate School, Monterey, California, June 1993.

11. Jones, K. D., Davids, S. T., Platzer, M. F., "Oscillating-Wing Power Generation," ASME Paper No. FEDSM 99-7050, San Francisco, California, July 1999.

12. Eggleston, D.M. and Stoddard, F.S. "Wind Turbine Engineering Design," Van Nostrand Reinhold Company, New York, 1987, pp. 20-23.

13. Birnbaum, W. "Das ebene Problem des schlagenden Flüels," Zeitschrift für Angewandte Mathematik und Mechanik, Vol. 4, No. 4, August, 1924, pp. 277-292.

14. Carr, L. W.; McAlister, K. W.; and McCroskey, W. J. "Analysis of the Development of Dynamic Stall Based on Oscillating Airfoil Experiments," NASA TN-D-8382, NASA Ames Research Center, Moffet Field, California, January 1977.

15. Johnson, W., and Ham, N., "On the Mechanism of Dynamic Stall," *Journal of the American Helicopter Society*, Vol. 17, No. 4, October 1972, pp. 36-45.

INITIAL DISTRIBUTION LIST

1. Defense Technical Information Center 2
    8725 John J. Kingman Rd., Suite 0944
    Ft. Belvoir, VA 22060-6218

2. Dudley Knox Library 2
    Naval Postgraduate School
    411 Dyer Rd.
    Monterey, CA 93943-5101

3. Director, Training and Education 1
    MCCDC, Code C46
    1019 Elliot Rd.
    Quantico, Virginia 22134-5027

4. Director, Marine Corps Research Center 2
    MCCDC, Code C40RC
    2040 Broadway Street
    Quantico, Virginia 22134-5107

5. Director, Studies and Analysis Division 1
    MCCDC, Code C45
    300 Russell Road
    Quantico, Virginia 22134-5130

6. Marine Corps Representative 1
    Naval Postgraduate School
    Code 037
    699 Dyer Road
    Monterey, CA 93940

7. Marine Corps Tactical Systems Support Activity 1
    Technical Advisory Branch
    Attn: Maj J.C. Cummiskey
    Box 555171
    Camp Pendleton, CA 92055-5080

8. Dr. Wolfgang Send 1
    DLR – Institute of Aeroelasticity
    Bunsenstr. 10
    D-37073 Göttingen Germany